MARMARA UNIVERSITY
INSTITUTE FOR GRADUATE STUDIES IN PURE AND APPLIED SCIENCES

THERMOECONOMIC AND EXERGETIC ANALYSIS OF MULTIGENERATION HYBRID ORC SYSTEM DESIGN IN GONEN

ÖZLEM BOYDAK

(724611007)

Ph.D. THESIS

Department of Mechanical Engineering

Thesis Supervisor
Assoc. Prof. Mustafa YILMAZ

Thesis CO- Supervisor
Prof. Dr. İsmail EKMEKÇİ

ISTANBUL, 2024

MARMARA UNIVERSITY
INSTITUTE FOR GRADUATE STUDIES IN PURE AND APPLIED SCIENCES

Ozlem BOYDAK, a Doctor of Philosophy student of Marmara University Institute for Graduate Studies in Pure and Applied Sciences, defended her thesis entitled "Thermoeconomic And Exergetic Analysis Of Multigeneration Hybrid ORC System Design In Gonen", on December 20, 2024 and has been found to be satisfactory by the jury members.

Jury Members

Assoc.Prof. Mustafa YILMAZ (Advisor)
Marmara University .....(SIGN) .....

Prof.Dr. Mesut GÜR (Jury Member)
Istanbul Technical University.....(SIGN) .....

Prof.Dr. Ahmet Korhan BİNARK (Jury Member)
Istanbul Sabahattin Zaim University.....(SIGN) .....

Prof.Dr. Ayhan ONAT (Jury Member)
Marmara University .....(SIGN) .....

Assoc.Prof. Hasan KÖTEN (Jury Member)
Istanbul Medeniyet University .....(SIGN) .....

APPROVAL

Marmara University Institute for Graduate Studies in Pure and Applied Sciences Executive Committee approves that Özlem BOYDAK be granted the degree of Doctor of Philosophy in Department of Mechanical Engineering, Energy Program on December 25, 2024. (Resolution no: 2024/02-29).

Director of the Institute

Prof. Dr. Bülent MERTOĞLU

ACKNOWLEDGMENTS

My deep gratitude goes first to my thesis advisors Prof. Dr. Ismail Ekmekci and Assoc. Prof. Mustafa Yılmaz for their help, advice, and encouragement during this research. Their expertise, knowledge and support to overcome difficulties during the study were priceless.

I would like thank to all esteemed thesis committee members Prof. Dr. Mesut Gur, Prof. Dr. Ahmet Korhan Binark, Prof. Dr. Ayhan Onat, and Assoc. Prof. Hasan Koten for their encouragement and valuable comments.

I wish to express my sincere gratitude to Dr. Tugrul Başaran and Dr. Erman Ozen for their help, support and guidance during my learning of the simulation programme. Moreover, I also thank to Ebsilon Professional simulation programme company for providing the last version of this comprehensive useful software, which is supportive for this academic study. Last but not the least I would like to thank my caring family for their infinite supports, encouragements and priceless motivations, besides I would like to remercie Cenk and Ece Nur.

I would like to express my sincere gratitude and appreciation to all those who have contributed to the successful completion of this research on the "Thermoeconomic And Exergetic Analysis Of Multigeneration Hybrid ORC System Design In Gonen". This working would not have been possible without the support, guidance, and encouragement. Thank you to everyone who played a role, big or small, in making this study.

Özlem Boydak

December 2024

CONTENTS

ABSTRACT ix

CLAIM OF ORGINALITY x

SYMBOLS xi

ABBREVIATIONS xii

LIST OF FIGURES xiii

LIST OF TABLES xvi

1 INTRODUCTION 1

1.1 ORC Energy Recovery System Overview 3

1.1.1 Selection of working fluids 4

1.2 Thermodynamic Analysis And Modeling Of ORC 8

1.2.1 Exergy efficiency 9

1.2.1.1 Pump phase 11

1.2.1.2 Evaporator phase 11

1.2.1.3 Turbine Phase 11

1.2.1.4 Condenser Phase 11

1.2.1.5 Cycle Efficiency 12

1.3 ORC Power Plant Design And Testing 12

2 LITERATURE REVIEW 14

2.1 Multigeneration Systems Overview 14

2.1.1 Advantages of multigenerational systems 18

2.2 Turkey’s Geothermal And Solar Energy Potential 19

2.2.1 Turkey’s Geothermal Energy Potential 21

2.2.1.1 Geothermal heat pump 24

2.2.2 Turkey’s Solar Energy Potential 26

2.2.2.1 Solar water heating and energy storage 30

2.2.2.2 Solar drying 32

2.2.2.3. Solar heat pump combination 33

2.3 Gonen's Geothermal And Solar Energy Potential 35
2.3.1 Gonen's geothermal energy potential 35
2.3.2 Gonen's solar energy potential 39
3 THERMODYNAMIC MODELING OF MULTIGENERATION SYSTEM WITH ORC 41
3.1 Working Fluids Selection Parameters 44
4 ANALYSES OF STUDIED MULTIGENERATION SYSTEM WITH ORC 47
4.1 Analysis Of Multigeneration System With R507A Via Ebsilon 51
4.2 Analysis Of Multigeneration System With R507A Via EES 52
4.2.1 Energetic thermodynamic analysis of multigeneration system with R507A via EES 52
4.2.2 Exergetic thermodynamic analysis of multigeneration system with R507A via EES 53
4.3 Analysis Of Multigeneration System With R1234yf Via Ebsilon 55
4.4 Analysis Of Multigeneration System With R1234yf Via EES 57
4.4.1 Energetic thermodynamic analysis of multigeneration system with R1234yf via EES 57
4.4.2 Exergetic thermodynamic analysis of multigeneration system with R1234yf via EES 58
4.5 Analysis Of Multigeneration System With R245fa Via Ebsilon 60
4.6 Analysis Of Multigeneration System With R245fa Via EES 62
4.6.1 Energetic thermodynamic analysis of multigeneration system with R245fa via EES 62
4.6.2 Exergetic thermodynamic analysis of multigeneration system with R245fa via EES 63
4.7 Analysis Of Multigeneration System With R1233zd Via Ebsilon 64
4.8 Analysis Of Multigeneration System With R1233zd Via EES 66
4.8.1 Energetic thermodynamic analysis of multigeneration system with R1233zd via EES 66
4.8.2 Exergetic thermodynamic analysis of multigeneration system with R1233zd via EES 67

4.9 Analysis Of Multigeneration System With R1234ze Via Ebsilon 68

4.10 Analysis Of Multigeneration System With R1234ze Via EES 70

4.10.1 Energetic thermodynamic analysis of multigeneration system with R1234ze via EES 70

4.10.2 Exergetic thermodynamic analysis of multigeneration system with R1234ze via EES 71

4.11 Analysis Of Multigeneration System With R152A Via Ebsilon 71

4.12 Analysis Of Multigeneration System With R152A Via EES 73

4.12.1 Energetic thermodynamic analysis of multigeneration system with R152A via EES 73

4.12.2 Exergetic thermodynamic analysis of multigeneration system with R152A via EES 74

4.13 Analysis Of Multigeneration System With R245CA Via Ebsilon 74

4.14 Analysis Of Multigeneration System With R245CA Via EES 76

4.14.1 Energetic thermodynamic analysis of multigeneration system with R245CA via EES 76

4.14.2 Exergetic thermodynamic analysis of multigeneration system with R245CA via EES 77

4.15 Second Law Efficiency Analyses Of Multigeneration System 77

4.16 Cost Analyses 81

4.16.1 Equipment investment 81

4.16.2 Working fluid investment 83

4.16.3 Total cost of ORC system 83

4.16.4 Net Earnings (NE) of ORC 83

4.16.5 Payback Period (PP) of the ORC 84

4.16.6 Return on Investment (ROI) 84

4.16.7 Levelized Energy Cost (LEC) 84

4.16.8 Present value of total profit in system service life 85

4.16.9 R245fa cost analysis 85

4.16.10 R1234yf cost analysis 86

4.16.11 R507A cost analysis 86

4.16.12 R1233zd cost analysis 87
4.16.13 R152A cost analysis 87
4.16.14 R245CA cost analysis 88
4.16.15 R1234ze cost analysis 88
4.16.16 Cost analyses with respect to engineering economy 91
5 RESULTS AND DISCUSSION 106
6 CONCLUSIONS AND RECOMMENDATIONS 109
REFERENCES 115
APPENDIX A 127

ÖZET

GÖNEN'DE MULTİJENERASYON HİBRİD ORC SİSTEMİNİN TERMOEKONOMİK VE EKSERJETİK ANALİZİ

Bu çalışmada, Balıkesir Gönen jeotermali ve parabolik oluklu panellerden oluşan güneş enerji sistemi ile çalışan organik rankin çevrimi komplesinin yedi farklı organik sıvı ile çalıştırılıp, enerji ekserji hesaplamaları yapılarak, sistem verimliliği irdelenmiştir. Jeotermal sistem, Gönen dokuzuncu sondaj kuyusunun değerleri olan 94°C sıcaklığında, 2.13 bar basıncında ve 8.3 kg/s debisindedir. Yine, güneş sistemi değerleri için de Gönen'in güneş ışınım değerleri, direkt normal radyasyonu 1000 W/m^2, rüzgar hızı 5 m/s, ortam sıcaklığı 20° ile enlem 40.1049° ve boylam 27.654° değerleri ile birlikte Therminol VP1 kullanılan yağ akışkan olarak Ebsilon proffesional simülasyon programında girilerek hesaplamalar yapılmıştır. Organik rankin çevriminde kullanılan yedi farklı organik sıvı ise; R245FA, R245CA, R152A, R507A ve yeni nesil akışkanlar R1233zd, R1234yf, R1234ze'dir. Bu akışkanlar ile birlikte gereken basınç, sıcaklık ve debi değerleri de simülasyonda girilerek, bu çoklu sistemin verimliliği ve üretilen elektrik enerjisi ile birlikte güç çıktıları, ekserji analizleri ve maliyet hesapları irdelenmiştir. Hesaplamalar Engineering Equation Solver (EES) ile birlikte Ebsilon Professional programında da yapılarak, sonuçların uyumluluğuna binaen, hesapların doğruluğu teyit edilmiştir. Bu çalışmamızda da görüldüğü gibi; yenilenebilir enerji kaynaklarının kullanıldığı çoklu enerji sistemleri, enerji verimliliği ve doğa dostu özellikleri ile avantajlı sistemlerdir.

ABSTRACT

THERMOECONOMIC AND EXERGETIC ANALYSIS OF MULTIGENERATION HYBRID ORC SYSTEM DESIGN IN GONEN

In this study, the multigenerational system with Balıkesir Gonen geothermal, solar energy system consisting of solar panels with parabolic trough collectors and Organic Rankine Cycle (ORC) was simulated with seven different organic fluids and the system efficiency was examined by doing energy and exergy calculations. The geothermal system has temperature of 94°C, pressure of 2.13 bar and mass flow rate of 8.3 kg/s, which are the values of the nineth sondage well of Gonen. Moreover, for the solar system, Gonen's solar radiation values, direct normal irradiance (DNI) 1000 W/m^2, wind speed 5 m/s, ambient temperature 20°C, latitude 40.1049° and longitude 27.654° values, with Therminol VP1 oil fluid were used in the calculations by entering the Ebsilon professional simulation program. The seven different organic liquids used in the organic rankine cycle are; R245FA, R245CA, R152A, R507A and new generation fluids are R1233zd, R1234yf, R1234ze. The required related pressure, temperature and mass flow values, along with these fluids, were entered in the simulation and thermal efficiency and power outputs with generated electric energy, cost, exergy and second law efficiency analyses of this multigenerational system were examined. The calculations were made in the Engineering Equation Solver (EES) program as well as the Ebsilon Professional program, and the accuracy of the calculations was confirmed based on the compatibility of the results. As observed in this study; multigenerational energy systems using renewable energy sources are advantageous systems with their energy efficiency and nature-friendly features.

CLAIM OF ORGINALITY

The orginality of this doctoral thesis is to perform comprehensive modeling, analysis and optimization of the novel renewable energy based multigeneration system which have not been studied on past research as having specific design with the particular values and seven different working fluids which were not utilized together, previously. Thus, unlike the existing literature, which lacks specific investigations for this particular region, the solar radiation and geothermal sondage well values in Gonen serve as the fundamental novel basis for designing a multigenerational energy system using an ORC with seven different particular working fluids. So, solar radiation and geothermal sondage well values play a critical role in this study. And, this innovative research aims to seamlessly integrate renewable energy sources and optimize their performance.

Moreover, analyses of this novel multigeneration system demonstrate the best organic working fluid to select among these seven organic fluids not used together in previous literature, which is the originality of this doctorate thesis. Thus, this thesis study can be taken as a guideline to choose the best efficient working fluid.

This phD thesis consists of some main novel objectives as follows:

1. To design an efficient model for the novel solar, geothermal and ORC based multigeneration energy system via thermodynamic modeling of a solar and geothermal based multigeneration system with seven different organic fluided ORC.
2. To calculate energy and exergy analyses of the designed multigeneration system.
3. To perform optimization of this multigeneration energy system to find the best design parameters by finding the best decision variables and maximizing energy output while minimizing losses, which identifies optimal design parameters by optimizing decision variables.
4. To conduct cost analyses for the multigeneration system. Calculation of purchase cost of components, total costs and not only present values in terms of bare module calculations but also future values in terms of engineering economics.

To summarize, this thesis not only fills a research void but also conducts a thorough examination and enhancement of an innovative multigeneration energy system. By addressing the absence of previous investigations, it offers valuable perspectives on sustainable energy solutions for the specified region, emphasizing their practical feasibility.

SYMBOLS

°C or K : Degree celsius or kelvin
C **:** Heat capacity [kJ/Kg K]
$\dot{E}$**x** **:** Exergy rate (kW)
Ex **:** Specific exergy (kJ/kg)
F **:** Future value ($)
g **:** Acceleration due to gravity [m/s^2]
h **:** Specific enthalpy (kJ/kg)
i **:** Interest rate
$\dot{m}$ **:** Mass flow rate (kg/s)
P **:** Present value ($)
$\dot{Q}$ **:** Heat rate (kW)
Rg **:** Gas constant
s **:** Specific entropy (kJ/kgK)
T **:** Temperature [°C]
$\dot{W}$ **:** Work rate (kW)
x **:** Vapour quality
V **:** Velocity [m/s]
t **:** Time (s)
t_{op} **:** Annual operation time of system (h)
η **:** System efficiency
η_t **:** Turbine efficiency
η_p **:** Pump efficiency
η_g **:** Generator efficiency
η_{col} **:** Collector efficiency
Qeva **:** Evaporator heat capacity
Qcol **:** Collector heat capacity
$\dot{W}t$ **:** Turbine work
$\dot{W}p$ **:** Pump work
MWe **:** Megawatt-electric
MWh **:** Megawatt-hour
kWe **:** Kilowatt-electric
kWh **:** Kilowatt-hour

Greek symbols
η **:** Energy efficiency
ψ **:** Exergy efficiency

Subscripts
T **:** Turbine
1, 2. . .46: State numbers
0 **:** Ambient (or reference environment) condition

ABBREVIATIONS

DFE : Difluoroethane

DNI : Direct Normal Irradiance

EES : Engineering Equation Solver

ETA : Thermal Efficiency of Multigenerational System

GC-MS : Gas Chromatography–Mass Spectrometry Systems

GWP : Global Warming Potential

HFC : Hydrofluorocarbon

HFO : Hydrofluoroolefin

HVAC : Heating, Ventilating and Air Conditioning

LEC : Levelized Energy Cost

MTA : Mineral Research and Exploration

NE : Net Earning

ODP : Ozone Depletion Potential

ORC : Organic Rankine Cycle

PP : Payback Period

ROI : Return On Investment

LIST OF FIGURES

Figure 1.1. (ORC) Organic rankine cycle overview 2

Figure 1.2. Pie chart of percentage of ORC energy sources [6] 3

Figure 1.3. General system layout: a typical T–s process diagram for the ORC system utilizing organic fluid [16] 4

Figure 1.4. Illustration of ORC power plant [40] 13

Figure 2.1. Sketches of solar energy, solar thermal collectors, wind energy, geothermal energy, biomass energy and multigeneration [64] 15

Figure 2.2. Energy sources and commodious properties of multigeneration systems[65] 16

Figure 2.3. Schematic of input and outputs of multigeneration systems [66] 16

Figure 2.4. Sketch of multigeneration application for a community [67] 17

Figure 2.5. Schematic of advantages of multigenerational systems [68] 18

Figure 2.6. Sketch of geothermal and solar resources [69] 20

Figure 2.7. Sketch of the multigenerational hybrid system with basic part [69] 21

Figure 2.8. Geothermal resources and applications map of Turkey (MTA 2019) [57] 22

Figure 2.9. Geothermal power generation capacity in Turkey (MW) 1976-2020 (source: ThinkGeoEnergy) [71] 23

Figure 2.10. Horizontal, vertical and pond/lake closed loop systems [72] 25

Figure 2.11. Open loop systems [72] 25

Figure 2.12. Working principle of geothermal heat pump [73] 26

Figure 2.13. Turkey's total solar radiation map [74] 27

Figure 2.14. Turkey's solar energy map [74] 28

Figure 2.15. Solar power plant distribution map of Turkey [58] 28

Figure 2.16. Turkish solar energy capacity from 2008 to 2023 [77] 29

Figure 2.17. Solar heating water system with the termal energy storage, investigated by Mahfuz et al. [55] 30

Figure 2.18. (a) Active type solar water heater system; (b) Passive type solar water heater system [78] 31

Figure 2.19. Classification of solar dryers [79] 32

Figure 2.20. Solar drying application [80] 33

Figure 2.21. Simplified scheme of a solar assisted heat pump in parallel mode (Buker and Riffat, 2016) [81] 34

Figure 2.22. Parabolic concentrated solar collector system integrated with heat pump [82] 35

Figure 2.23. Geothermal and hot wellspring resources map of Balıkesir city and Gonen region [84] 36

Figure 2.24. Gonen geothermal well layout plan [84] 39

Figure 2.25. Map of Balıkesir city's solar energy potential [85] 40

Figure 2.26. Diagrams of Balıkesir global radiation values (kWh/m2-day), Balıkesir sunshine durations (hour), Balıkesir solar energy values (Wh/m2) respectively [85] 40

Figure 3.1. Schematic of the multigenerational system with solar, geothermal and ORC 42

Figure 3.2. Basic t-s diagram of the multigenerational system 42

Figure 3.3. Ebsilon proffesional programme display image of the multigenerational system 43

Figure 4.1. T-s diyagram of the ORC side of the multigenerational system with R507A via Ebsilon Professional programme. 52

Figure 4.2. T-s diyagram of the ORC side of the multigenerational system with R507A via EES. 53

Figure 4.3. Ebsilon display image of the multigenerational system with R1234yf. 55

Figure 4.4. T-s diyagram of the ORC side of the multigenerational system with R1234yf via Ebsilon Professional programme. 57

Figure 4.5. T-s diyagram of the ORC side of the multigenerational system with R1234yf via EES. 58

Figure 4.6. Ebsilon display image of the multigenerational system with R245fa. 60

Figure 4.7. T-s diyagram of the ORC side of the multigenerational system with R245fa via Ebsilon Professional programme. 61

Figure 4.8. T-s diyagram of the ORC side of the multigenerational system with R245fa via EES. 62

Figure 4.9. Ebsilon display image of the multigenerational system with R1233zd. 64

Figure 4.10. T-s diyagram of the ORC side of the multigenerational system with R1233zd via Ebsilon. 65

Figure 4.11. T-s diyagram of the ORC side of the multigenerational system with R1233zd via EES. 66

Figure 4.12. Ebsilon display image of the multigenerational system with R1234ze. 68

Figure 4.13. T-s diyagram of the ORC side of the multigenerational system with R1234ze via Ebsilon. 69

Figure 4.14. T-s diyagram of the ORC side of the multigenerational system with R1234ze via EES. 70

Figure 4.15. Ebsilon display image of the multigenerational system with R152A. 71

Figure 4.16. T-s diyagram of the ORC side of the multigenerational system with R152A via Ebsilon. 72

Figure 4.17. T-s diyagram of the ORC side of the multigenerational system with R152A via EES. 73

Figure 4.18. Ebsilon display image of the multigeneration system with R245CA. 74

Figure 4.19. T-s diyagram of the ORC side of the multigeneration system with R245CA via Ebsilon. 75

Figure 4.20. T-s diyagram of the ORC side of the multigeneration system with R245CA via EES. 76

Figure 4.21. Diagrams of second law efficiency vs. geothermal source mass flow rate 78

Figure 4.22. Diagrams of second law efficiency vs. geothermal source temperature 79

Figure 4.23. Diagrams of second law efficiency vs. solar energy source temperature 80

Figure 4.24. (a) Inlet temperature vs purchased cost of turbine. **(b)** Thermal efficiency vs purchased cost of turbine. **(c)** Thermal efficiency vs net earning 89

Figure 4.25. Solar energy input vs. total cost 90

Figure 4.26. Cost flow diagram of R245fa fluided system for service life of 20 years 92

Figure 4.27. Diagram of present value of cumulative investment cost (Seri2) vs. present value of net earnings (Seri1) for R245fa fluided system 93

Figure 4.28. Cost flow diagram of R1234yf fluided system for service life of 20 years 94

Figure 4.29. Diagram of present value of cumulative investment cost (Seri2) vs. present value of net earnings (Seri1) for R1234yf fluided system 95

Figure 4.28. Cost flow diagram of R507A fluided system for service life of 20 years 96

Figure 4.29. Diagram of present value of cumulative investment cost (Seri2) vs. present value of net earnings (Seri1) for R507A fluided system 97

Figure 4.28. Cost flow diagram of R1233zd fluided system for service life of 20 years 98

Figure 4.29. Diagram of present value of cumulative investment cost (Seri2) vs. present value of net earnings (Seri1) for R1233zd fluided system 99

Figure 4.28. Cost flow diagram of R152A fluided system for service life of 20 years 100

Figure 4.29. Diagram of present value of cumulative investment cost (Seri2) vs. present value of net earnings (Seri1) for R152A fluided system 101

Figure 4.28. Cost flow diagram of R245CA fluided system for service life of 20 years 102

Figure 4.29. Diagram of present value of cumulative investment cost (Seri2) vs. present value of net earnings (Seri1) for R245CA fluided system 103

Figure 4.28. Cost flow diagram of R1234ze fluided system for service life of 20 years 104

Figure 4.29. Diagram of present value of cumulative investment cost (Seri2) vs. present value of net earnings (Seri1) for R1234ze fluided system 104

Figure 6.1. t-s diagrams of all working fluids used in this thesis 113

Figure 6.2. p-v diagrams of all working fluids used in this thesis 113

LIST OF TABLES

Table 1.1. Properties of some common ORC working fluids [17] 6

Table 2.1. Specific values of Gonen geothermal wells [84] 37

Table 3.1. Environmental properties of each fluid [121] 46

Table 4.1. Thermo-physical properties of the selected fluids [120] 50

Table 4.2. Results of energy and exergy analyses via EES for R507A fluided hybrid system [120] 54

Table 4.3. Output parameters for R507A fluided hybrid system. 55

Table 4.4. Results of energy and exergy analyses via EES for R1234yf fluided hybrid system. 59

Table 4.5. Output parameters for R1234yf fluided hybrid system. 59

Table 4.6. Results of energy and exergy analyses via EES for R245FA fluided hybrid system. 63

Table 4.7. Output parameters for R245FA fluided hybrid system. 63

Table 4.8. Results of energy and exergy analyses via EES for R1233zd fluided hybrid system. 67

Table 4.9. Output parameters for R1233zd fluided hybrid system. 68

Table 4.10. Results of energy and exergy analyses via EES for R1234ze fluided hybrid system. 71

Table 4.11. Results of energy and exergy analyses via EES for R152A fluided hybrid system. 74

Table 4.12. Results of energy and exergy analyses via EES for R245CA fluided hybrid system 77

Table 4.13. Correction factors for purchased cost of heat exchanger[131] 82

Table 4.14. Correction factors for purchased cost of pump and expander[131] 82

Table 4.15. Calculation of future values of R245fa fluided system for ten years (half of service life) 92

Table 4.16. Calculation of future values of R1234yf fluided system for ten years (half of service life) 94
Table 4.17. Calculation of future values of R507A fluided system for ten years (half of service life) 96
Table 4.18. Calculation of future cost values of R1233zd fluided system for ten years (half of service life) 98
Table 4.19. Calculation of future cost values of R152A fluided system for ten years (half of service life) 100
Table 4.20. Calculation of future cost values of R245CA fluided system for ten years (half of service life) 102
Table 4.21. Calculation of future cost values of R1234ze fluided system for ten years (half of service life) 103
Table 5.1. Total output parameters for each fluided system 107
Table 5.2. Outputs of each cycle 108
Table 6.1. The outputs evaluated for the same heat energy input for each working fluid 111

1 INTRODUCTION

Energy requisition is increasing with the technological advancements and population growth. Energy utilization, which is a veiled proxy for prosperity and financial standing, is typically seen as a gauge of a nation's degree of progress. Turkey-based sources claim that the installed capacity based on Ministry of Energy and Natural Resources data as of the year 2023 of the 106668 MW is the total installed capacity, 11315.6 MW is solar, 384.5 MW is waste heat, and 1691.3 MW is geothermal.

Not only considering their potential for transformation as primary and secondary but also renewable and non-renewable are types of energy resources. Non-renewable energy sources are expected to run out soon, based on historical resource supply and demand data. Because of this, renewable energy resources that never run out or need to be replenished, are intensified for research and development.

On the other hand, technology development aimed at supplying to maximize the power output from the energy sources employed, and to boost cycle efficiency with research of material optimization and working fluids selection.

The heat that has accumulated underground is the geothermal energy that is concentrated substances, the temperatures of which differ according to the locale. It is present in all forms, including hot water, rock, and gas. There are several applications for this form arriving on Earth. Utilizing these resources, whether directly or indirectly, is actually the definition of geothermal energy. It will enable the production of power from these geothermal fields with ORC. The low waste heat recovery characteristics enable the creation of energy from industrial waste, geothermal heat, solar energy, and more effectively available oil and gas resources, that is not profitable.

Furthermore, we will also employ sun data to assist the system. The latitude and the longitude of populated areas, solar time, and seasons determine how sunlight affects our planet. Sun descends to Earth in many pieces after traversing the atmosphere.

Solar radiation can be transformed into useful form through the use of collectors. The placement and angle of the collectors greatly influence the performance of the solar system. Solar collectors should be placed where they receive the best solar radiation in order to benefit solar radiation, mostly. The optimal inclination angle of collectors depends on the geographical location of the country and the season.

Organic Rankine Cycle (ORC) is the recent type of an environmentally friendly leading technological system, applying the principle of the steam Rankine cycle, but can utilize

relatively low-grade heat sources below 150°C. This system uses an organic substance as a working fluid; therefore it is named as 'Organic' Rankine. Thus, the system utilizes low-grade heat sources for economic energy production and consists of an evaporator (heating area), a turbine and a condenser (cooling area). Utilizing different kinds of working fluid instead of water/steam provides the opportunity of constructing miniature, compact and portable thermal power plants. The selection of the architecture will rely on heat source temperature stage and also sort of working fluid, dry or wet. ORC based new type of power plant system is designed to use low and mid temperature waste heat sources and to convert them into electric energy– efficiently, economically and CO2 free. ORC systems are typically used for four major applications: waste heat recovery, geothermal power plants, biomass combustion plants and solar thermal plants [1,2,3].

The most developed application for an ORC system is the so-called "waste heat recovery". The term "waste heat recovery" may be utilized to express the use of any heat overall ejected to the environment. Thus, the ORC system is a useful way of heat recovery in the temperature range between 150 to 200 °C; especially if no other utilization for the waste heat is present on the site [4,5,6].

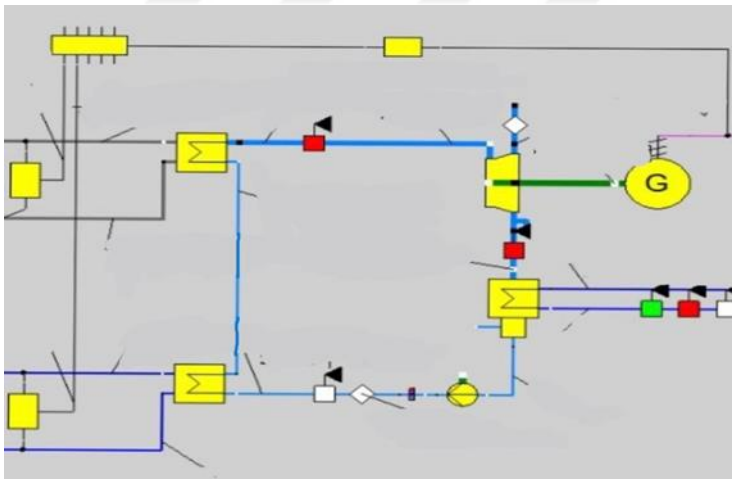


Figure 1.1. Organic rankine cycle (ORC) overview

ORC is simplier and economically more feasible than the steam Rankine cycle. Thus, many commercial and test plants can be made by using organic Rankine cycle due to its advantages. The ORC system exhibits great flexibility, high safety and low maintenance requirements in recovering this grade of waste heat. Integrating the ORC to the energy system, such as power plants, could achieve using low grade energy (waste heat) to generate high grade energy

(power), easing the power burden and enhancing system efficiency. Since the ORC consumes virtually no additional fuel, for the same added power, the emission of environmental pollutants such as carbon dioxide (CO2), sulphur dioxide (SO2) and so on would be decreased. What's more, according to the local demand, the exhaust heat exiting from the ORC could be further utilized to drive chillers such as absorption chillers to supply cooling capacity. The ORC technology is a newly emerged technology since 1961. Thus, its usage is not so common in our country [6,7].

The Organic Rankine Cycle transforms thermal energy into mechanical shaft power. The advantage of ORC systems is the return of useful energy, often as electrical turnout, from low-energy resources such as the low-pressure steam affiliated with steam-driven turbines used for electricity generation [8].

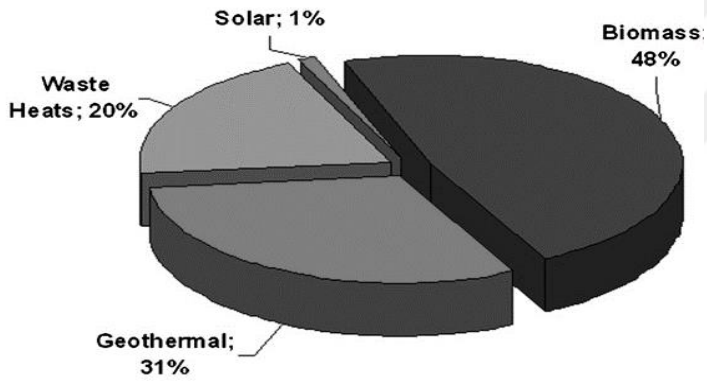


Figure 1.2. Pie chart of percentage of ORC energy sources [6]

Figure 1.2 is an approximate sketch of proportion of energy sources for ORC systems. According to the pie chart seen in the Figure 1.2, the percentage of biomass energy source is 48%, the percentage of geothermal energy source is 31%, the percentage of waste heats energy source is 20% and the percentage of solar energy source is 1%.

1.1 ORC Energy Recovery System Overview

An Organic Rankine Cycle (ORC) is energy recovery system shown in Figure 1.1, like a traditional rankine steam system, except the organic working fluid, which is high molecular mass fluid with a liquid-vapor phase change, or boiling point at a lower temperature than the water-steam phase transition [8,9].

The low-temperature heat is transformed into useful work to be transformed into electricity. Selection of the fluid of ORC system relies on the temperatures of the thermal sink and also the thermal source [9,10].

ORC energy recovery system is a closed loop consisting four fundamental functions:

• 1–2 Pump Compression: A feed pump make liquid working fluid being pressurized.

• 2–3 Boiler Vaporization: The liquid working fluid takes thermal energy in and vaporizes to the steam phase. Evaporators provide the heat transfer from the heat carrier fluid to the working fluid.

• 3–4 Expansion by an expander: An expander transforms the heat energy of the working fluid into mechanical energy, which is the power generating operation. Then, an alternator makes this mechanical energy to be transformed into electricity.

• 4–1 Condensation by a condenser: The steam fluid condenses into the liquid phase, which is the heat-refusing operation [10,11]. In Figure 1.1 general system layout is given.

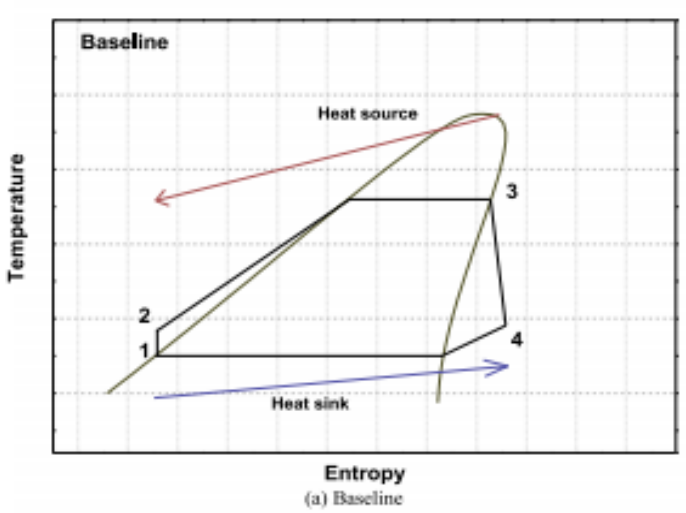


Figure 1.3. General system layout: a typical T–s process diagram for the ORC system utilizing organic fluid [16]

1.1.1 Selection of working fluids

Working fluid selection is the significant concept in order to further develop the design of the ORC system. Since the working fluid selection involves the thermodynamic design and effectiveness of all parts in an ORC, it is a restricting aspect in ORC system design. Additionally, the required pressure grade and material class of all components within the system is also affected by the refrigerant [11,12].

The common specifications which the working fluid should ideally suit are various and significant. Some of the preferred physical and chemical properties are non-flammability, stability, non-corrosiveness, non-fouling, and non-toxicity. Moreover, low boiling point of the working fluid is another property to be used in a binary power cycle as involving with low temperature geothermal waters [13,14].

Considering working fluids that are appropriate for a binary geothermal power cycle, it can be expressed that: Ammonia is toxic with exposures of more than 500 ppm presenting an immediate hazard to life and health. N-Pentane is highly flammable. HCFC has ozone depletion characteristics. PF5050 is non-toxic, non-flammable and it has zero ozone depletion capability [14,15].

Features of various organic fluids can be inspected. Accordingly, the amount of thermal decomposition of toluene in oil-free circumstances is very low up to about 400°C. In terms of low-temperature applications, isobutane (C4H10) is found to be rather appropriate. In that circumstances, it follows better than toluene to be cooled. Common refrigerants utilized within ORC systems were outlined and summarized in Table 1.1 [15,16,17].

R134A is readily accessible, low costed and widely used through the refrigeration industry as a working fluid. But, it will be replaced in near future due to its high GWP. The thermodynamic efficiency of R-134a at temperatures higher than 50°C was detected to be amazingly deficient. Higher process pressures also declined the safety factor of experimental components. Therefore, a more profitable refrigerant can be selected. A refrigerant mix called HFC-M1 can be chosen for utilization with the ORC test bed. HFC-M1 is a mix of 50% R-245fa and 50% R-365mfc. [17,18].

Lower boiling point and dry saturation curve are some of the various advantages of the refrigerant offers over water which is advantageous for the system efficiency since the steam flowing through the turbine is not a wet mixture [18,19].

Table 1.1. Properties of some common ORC working fluids [17]

SHRAE number	Name	Molecular weight	T_c (K)	P_c (MPa)	Vapor C_p (J/kg K)	Latent heat L (kJ/kg)	ξ (J/kg K^2)
R-21	Dichlorofluoromethane	102.92	451.48	5.18	339.85	216.17	−0.78
R-22	Chlorodifluoromethane	86.47	369.30	4.99	1069.13	158.46	−1.33
R-23[a]	Trifluoromethane	70.01	299.29	4.83	3884.02	89.69	−6.49
R-32	Difluoromethane	52.02	351.26	5.78	2301.61	218.59	−4.33
R-41[a]	Fluoromethane	34.03	317.28	5.90	3384.66	270.04	−7.20
R-116[a]	Hexafluoroethane	138.01	293.03	3.05	4877.91	30.69	−5.54
R-123	2,2-Dichloro-1,1,1-trifluoroethane	152.93	456.83	3.66	738.51	161.82	0.26
R-124	2-Chloro-1,1,1,2-tetrafluoroethane	136.48	395.43	3.62	908.70	132.97	0.26
R-125	Pentafluoroethane	120.02	339.17	3.62	1643.89	81.49	−1.08
R-134a	1,1,1,2-Tetrafluoroethane	102.03	374.21	4.06	1211.51	155.42	−0.39
R-141b	1,1-Dichloro-1-fluoroethane	116.95	477.50	4.21	848.37	215.13	0.00
R-142b	1-Chloro-1,1-difluoroethane	100.50	410.26	4.06	1036.52	185.69	0.00
R-143a	1,1,1-Trifluoroethane	84.04	345.86	3.76	1913.97	124.81	−1.49
R-152a	1,1-Difluoroethane	66.05	386.41	4.52	1456.02	249.67	−1.14
R-170[a]	Ethane	30.07	305.33	4.87	5264.72	223.43	−8.28
R-218	Octafluoropropane	188.02	345.02	2.64	1244.87	58.29	0.45
R-227ea	1,1,1,2,3,3,3-Heptafluoropropane	170.03	375.95	3.00	1013.00	97.14	0.76
R-236ea	1,1,1,2,3,3-Hexafluoropropane	152.04	412.44	3.50	973.69	142.98	0.76
R-245ca	1,1,2,2,3-Pentafluoropropane	134.05	447.57	3.93	1011.26	188.64	0.60
R-245fa	1,1,1,3,3-Pentafluoropropane	134.05	427.20	3.64	980.90	177.08	0.19
HC-270	Cyclopropane	42.08	398.30	5.58	1911.81	366.18	−1.54
R-290	Propane	44.10	369.83	4.25	2395.46	292.13	−0.79
R-C318	Octafluorocyclobutane	200.03	388.38	2.78	896.82	93.95	1.05
R-3-1-10	Decafluorobutane	238.03	386.33	2.32	928.83	77.95	1.32
FC-4-1-12	Dodecafluoropentane	288.03	420.56	2.05	884.25	86.11	1.56
R-600	Butane	58.12	425.13	3.80	1965.59	336.82	1.03
R-600a	Isobutane	58.12	407.81	3.63	1981.42	303.44	1.03
R-601	Pentane	72.15	469.70	3.37	1824.12	349.00	1.51
R-717	Ammonia	17.03	405.40	11.33	3730.71	1064.38	−10.48
R-718	Water	18.00	647.10	22.06	1943.17	2391.79	−17.78
R-744[a]	Carbon dioxide	44.01	304.13	7.38	3643.72	167.53	−8.27
R-1270	Propene	42.08	365.57	4.66	2387.36	284.34	−1.77
	Propyne	40.06	402.38	5.63	2100.54	431.61	−1.87
	Benzene	78.11	562.05	4.89	1146.72	418.22	−0.70
	Toluene	92.14	591.75	4.13	1223.90	399.52	−0.21

[a] The critical temperature of the fluid is below 320 K, and the data is given based on 290 K.

Thus, high density and low latent heat are the properties which the organic substance chosen for working fluid must have. In order to boost the turbine inlet mass flow rate, such properties are favored. The thermal properties of these working fluids can be observed from Table 1.1. Accordingly, the utilized organic fluids in this study have favorable properties. For instance, R245fa is one of the mostly used and well known organic fluids in ORC systems [19,20]. R245fa, an HFC refrigerant, boasts several advantages. Firstly, it is environmentally friendly due to its low global warming potential (GWP). Secondly, it is considered safe for use, with no known toxicity risks. Thirdly, R245fa demonstrates good compatibility with commonly used materials in heat exchangers and other components. These positive attributes position R245fa as a suitable choice for applications involving heat recovery and power generation. For example, in ORC systems, R245fa efficiently converts waste heat into electricity, especially under medium-temperature conditions. However, factors such as pressure, temperature, and system design significantly impact its performance. Optimizing operating conditions ensures reliable function and effective energy recovery. R-245fa, which has favorable thermodynamic properties for medium-temperature heat sources and is considered

safe with low toxicity, is a non-flammable hydrofluorocarbon with a critical temperature of 154.0°C and a critical pressure of 5.29 bar.

R245CA, also known as 1,1,1,3,3-pentafluoropropane, serves as an organic fluid in ORC systems since it is designed for low-temperature heat recovery and it offers slightly higher ORC cycle efficiency compared to other working fluids. It also has non-toxic, non-flammable and a favorable toxicological profile which minimizes investment costs and reduces CO2 emissions providing CO2-free power without fuel consumption. Leak-tight systems avoid direct chemical contributions to global warming. R245CA balances performance, safety, and environmental considerations, making it a versatile choice for various ORC applications.

R507A is a mixture of R-125 (pentafluoroethane) and R-143a (1,1,1-trifluoroethane) in a 50/50 weight ratio. R507A as a working fluid is favorable for the ORC. Yet it has a moderately high GWP. This might not make it a good choice for the future applications as regulations change more focus on switching to environmentally friendly options. When choosing a refrigerant for an ORC system, it's important to consider about how well it works, if it follows the regulations, its impact to the environment and its safety.

R152A, also known as 1,1-difluoroethane (DFE), serves as a refrigerant (often listed as R-152A or HFC-152A) and is used in refrigeration systems and aerosol sprays. Despite its flammability, it has similar operating pressures and cooling capacity to R134A, making it suitable for large chillers and specific applications. Environmentally, R152A has a low GWP compared to other HFCs and no ozone depletion potential. Additionally, it finds use in gas dusters and as a molecular weight marker in Gas Chromatography–Mass Spectrometry (GC-MS) systems [20,21].

The new generation fluids R1233zd, R1234yf and R1234ze are also utilized in this study due to their promising properties. R1233zd, recognized for its effective performance, environmental friendliness, and safety, has garnered attention as a refrigerant. However, like any refrigerant, its suitability hinges on context. Its thermodynamic properties facilitate efficient heat recovery and power generation, especially under medium-temperature conditions. As an HFO (hydrofluoroolefin), R1233zd boasts a low GWP, aligning with environmental goals by minimizing greenhouse gas emissions. While R1233zd (E) is deemed safe for use, adherence to safety protocols during handling, storage, and operation is crucial. Understanding its toxicity risks and exposure limits is essential. Assessing the specific system’s needs and requirements is vital. Factors like pressure, temperature, and system

design significantly impact performance of R1233zd. Rigorous checks and tests help determine its suitability.

R1234ze, an organic fluid, has garnered attention as a refrigerant and it is also suitable for heat pumps. R1234ze falls into the category of HFOs, the unsaturated organic molecules composed of hydrogen, carbon, and fluorine. Honeywell developed R1234ze as a replacement for the commonly used refrigerant R-134a. R1234ze boasts a low GWP, aligning with environmental goals and it is considered safe for use. While similar to R-134a, R1234ze has slightly lower refrigerating capacity. R1234ze strikes a balance between performance, safety, and environmental considerations, making it a viable choice for various applications.

R1234yf, as a refrigerant it is expected to have low GWP, and has smaller impact to environment compared to R-134a. With low flammability, R-1234yf is generally more efficient than R-134a and in cooling systems it leads lower energy consumption. In ORC systems, it is crucial to have balance between efficiency, environmental impact and safety. Thus, R-1234yf is a suitable choice as a working fluid.

Although it is thermodynamically suitable to use R134a in ORC systems, it should not be used due to the damage it causes to the environment. Therefore, in this thesis, fluids that can replace R134a were investigated remembering that informed decision-making involves considering all aspects to optimize system performance and reliability [21,22,23].

1.2 Thermodynamic Analysis And Modeling Of ORC

A thermodynamic model of the conceptual design can be developed in Engineering Equation Solver (EES) and validated against experimental data. Then, the model can be adapted to utilize both the convenient resource temperatures and prospected performance characteristics of the system components. Assessments could then be performed for the function of each of the four major components within the system [24,25]. The system efficiency for an ORC system is a key performance parameter and is defined as:

$$\eta_t = \frac{\dot{W}_{gen} - \dot{W}_{input}}{Q_{in}} \quad (1)$$

The thermal efficiency can be evaluated as 5.7%. The efficiency of an ORC system is typically very low due to the low resource temperatures used. The theoretical maximum efficiency for a thermodynamic cycle is the Carnot efficiency of a cycle:

$$\eta_t = \frac{T_h - T_c}{T_h} \quad (2)$$

Thermodynamic efficiency is often utilized as a gauge for ORC system design, yet is not the only concern. Maintenance, facility of manufacture, essential costs and environmental effect all need to be estimated when optimizing the system design. These concerns are equalized with thermal efficiency during the design operation and concluded in the design efficiency of 5.7% [26,27].

The organic working fluid is in its liquid state at the pump phase of the ORC. The pump increases the pressure of the fluid which raises its energy level to prepare for the following phases. The pump work can be calculated with the equations:

$$W_{pump,in} = m(h_{out} - h_{in}) = v(P_{out} - P_{in})$$

After pump phase, the high-pressurized liquid organic working fluid is heated and vaporized utilizing an external heat source (e.g. solar) at the evaporator phase. This phase commonly becomes at constant pressure and temperature. The required heat input can be calculated as:

$$Q_{in} = m(h_{out} - h_{in})$$

After evaporator phase, the high-pressurized vapor expands through the turbine, producing mechanical work that drives a generator at the turbine phase. The work output of the turbine can be calculated as: $W_{turb,out} = m(h_{in} - h_{out})$

After turbine phase, the low-pressure vapor out of the turbine is condensed back into a liquid by emitting heat to a cooling medium (e.g. water) at the condenser phase. The heat emitted can be calculated with this equation: $Q_{out} = m(h_{in} - h_{out})$

The efficiency of the ORC can be defined as the ratio of the net work output to the heat input: $\mu_{cycle} = \frac{W_{turbine} - W_{pump}}{Q_{in}}$

The ORC system can be designed and optimized for various applications, such as waste heat recovery, geothermal power generation, and solar power plants, by analyzing each phase and carrying out required thermodynamic formulas [27,28].

1.2.1 Exergy efficiency

Exergy efficiency for the binary geothermal power plants is described as the rate of exergy output to the exergy input. In binary geothermal cycles, the geothermal fluid leaving the evaporator is reinjected in to the ground and its exergy is lost [48,49]. Thus, efficiency is formed on the primary heat source exergy as given by Eq. (3):

$$\eta_{ex} = \frac{E_{out}}{E_{heat\ source}} \quad (3)$$

where

$$E_{heat\ source} = (h_{HWI} - h_0) - T_0(s_{HWI} - s_0) \quad (4)$$

and

$$E_{out} = (h_{HWI} - h_{HWO}) - \frac{\dot{m}_{HW}}{\dot{m}_{CW}}\left\{273.15 c_p exp\left[\frac{\dot{m}_{HW}}{m_{CW}} x\ (s_{HWI} - s_{HWO}) - s_{CWI}\right] - h_{CWI}\right\} \quad (5)$$

Eq. (5) is evolved utilizing energy and entropy balances for the whole cycle.

The thermal efficiency of the ORC is the ratio of the net power output to the heat inclusion. However, this definition could be deceptive when considering various working fluids under particular operating conditions if the heat source of the inlet temperature and the pinch point are set. Nevertheless, the diversities of the thermal efficiency is straightly related to the variations of Wnet since the inlet, outlet temperatures and the flow rate of the heat source are set. Furthermore, the exergy efficiency is analyzed herein, which can be utilized to gauge the efficiency for waste heat recovery since the thermal efficiency can not indicate the capability to transform energy from low grade waste heat into functional work [28,29,30]. Regarding P0 and T0 to be the ambient pressure and temperature as the particular dead reference state, the exergy of the state point can be expressed as:

$$\dot{E}_i = \dot{m}[(h_i - h_0) - T_0(s_i - s_0)] \quad (6)$$

The exergy efficiency of ORC system can be considered as:

$$\eta_{exg} = \frac{\dot{W}_{net}}{\dot{E}_{input}} \quad (7)$$

In terms of exergy analysis, we quantify the efficiency and performance of a system depends on the destruction and usage of exergy, which is the maximum theoretical work that can be acquired from a system as it is correlated with its ambiance. The basic formula for exergy analysis is:

$$\sum \dot{Ex}_{in} - \sum \dot{Ex}_{out} - \dot{Ex}_{dest} = \Delta \dot{E}x_s$$

In terms of steady state system, exergy difference is: $\Delta \dot{Ex}_s = 0$.

$$\sum \dot{Ex}_{in} - \sum \dot{Ex}_{out} = I$$

Thus, in and out exergy is equivalent to exergy destruction which is *I*, irreversibility.

$$\mathrm{Ex}_{dest} = T_0 \Delta \mathrm{S}_{\mathrm{gen}}$$

In terms of isentropic processes, there is no entropy difference, thus, $Ex_{dest} = 0$.

1.2.1.1 Pump phase

The exergy input to the pump can be calculated in the manner that the product of the mass flow rate and the variance in specific exergy between the inlet and outlet of the pump, because there is no exergy destruction due to the isentropic compression:

$Ex_{pump} = \dot{m}\ (e_{out} - e_{in})$.

Where *e* are the specific exergy of the organic working fluid entering and exiting the pump:

$e_i = h_i - h_0 - [T_0(s_i - s_0)]$.

1.2.1.2. Evaporator phase

The exergy input to the evaporator is the heat transfer into the system, which can be calculated resembling to the energy input. Thus, the related evaporator phase exergy equations are:

$Ex_{dest} = Ex_{mass} + Ex_{heat}$

$Ex_{mass_{eva}} = (h_{in} - h_{out}) - T_0(s_{in} - s_{out})$

$Ex_{heat_{eva}} = Q_{in}(1 - \frac{T_0}{T_H})$

$Ex_{dest_{eva}} = (h_{in} - h_{out}) - T_0(s_{in} - s_{out}) + Q_{in}(1 - \frac{T_0}{T_H})$

$Ex_{dest_{eva}} = T_0(s_{out} - s_{in}) - (\frac{Q_{in}}{T_H})$

1.2.1.3. Turbine phase

Since there is no exergy destruction due to the isentropic compression, the exergy output from the turbine is the work output of the turbine. Thus, the related turbine phase exergy equations are: $Ex_{turbine} = \dot{m}\ (e_{in} - e_{out})$

where *e* for each step, $e_i = h_i - h_0 - [T_0(s_i - s_0)]$.

1.2.1.4. Condenser phase

The exergy output from the condenser is the heat transfer out of the system. Thus, the related condenser phase exergy equations are: $Ex_{dest} = Ex_{mass} - Ex_{heat}$ and

$$Ex_{mass_{eva}} = (h_{in} - h_{out}) - T_0(s_{in} - s_{out})$$

$$Ex_{heat_{eva}} = Q_{out}(1 - \frac{T_0}{T_L})$$

$$Ex_{dest_{eva}} = (h_{in} - h_{out}) - T_0(s_{in} - s_{out}) - Q_{out}(1 - \frac{T_0}{T_L})$$

1.2.1.5. Cycle efficiency

How well a system utilizes energy compared to how much work could be performed with that energy is evaluated with the second law efficiency. In the Organic Rankine Cycle, the second law efficiency evaluates how effectively the cycle transmute heat into usable work, taking cognizance of any inefficiencies.

$$\mu_{II,cycle} = \frac{Ex_{recovered}}{Ex_{expended}} = 1 - \frac{Ex_{destroyed}}{Ex_{expended}}$$

$$Ex_{expended} = Ex_{heat_{in}} + W_{pump_{in}}$$

$$Ex_{recovered} = W_{turbine_{out}}$$

The second law efficiency focuses on to the irreversibilities and losses within the system. A higher second law efficiency implies that energy is utilized more efficiently and there are less energy losses. Enhancing the second law efficiency means providing ways to decrease wasted energy by designing superior, optimization of operating conditions, and selection of valid components [30,31,32].

1.3. ORC Power Plant Design And Testing

The major modules can be designed as standard modules, which constitute the ORC energy plant, which means the power plant can simply be conformed to any waste heat origin by only transforming the central cycle to the particular industry plant. The switch module is designed for stable operating process circumstances. Furthermore, the power plant can be designed to only utilize a limited surface area, due to a rather compact constitution [33,34]. Temperature, pressure and flow rate data is obtained throughout the system to permit the utilizer to process the system and attain a steady state at the requested process conditions. A CompacDAQ can be utilized for data acquisition and also permits the system performance to be calculated. Presently, the system will required to be commanded by the utilizer, however as the system dynamics are comprehended better PID control will able to be

enabled. Constitution of the system can be accomplished throughout nearly one year and then the system can be prompt for testing. Most of the components chosen are readily accessible which shortened the fabrication time plan. Extra caution should be taken throughout the constitution and assembly operations in order to assure no leakage in the system, which avoids deficit of refrigerant [34,35,36].

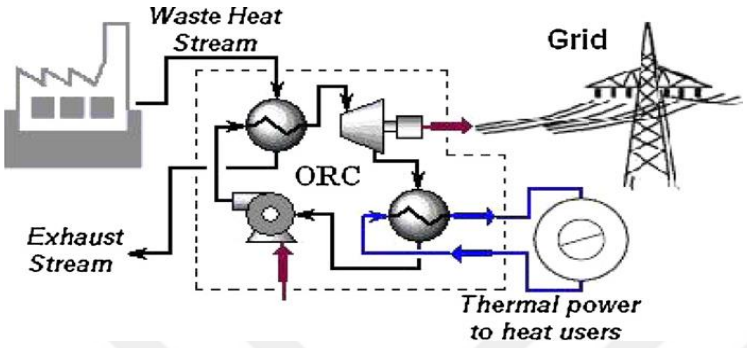


Figure 1.4. Illustration of ORC power plant [40]

The compact and modular design of the power plant is demonstrated in the Figure 1.4; all components requiring monitoring or maintenance (electro-mechanical parts such as turbine, pumps, generator, valves etc.) are fixed at the lowest stage. The median floor stage includes every static systematic components as process heat exchangers, piping. Additionally, the condensers are beared by the top of the steel body. The system can be merged in almost any industrial processes due to its modular design. The two cycle system provides an adaptable integration in current plants. The flexibility in its function permits for economic utilization of waste heat with temperatures beginning from 150°C to produce power from 500 kW to double digit MW [36,37,38].

The ORC power plant is -from the cement maker's perspective- an installation of secondary significance, thus it must not intervene in or even disrupt the main process of cement manufacturing. This requirement is performed by fixing the heat exchangers in a bypass mode. If the ORC power plant should somehow be out of service, while the kiln is under full operation, the waste gas bypasses the heat exchanger and takes the regular path through the cooling tower. In bypass mode, the clinker cooler air is cooled in the existing cooler before it arrives the dust precipitator [38,39,40].

The organic rankine cycle (ORC) is generally recognized as an applicable technology to transform low temperature heat into electricity. Moreover, ORCs are designed for unmanned process with a small amount of maintenance. Industrial waste heat, solar heat,

geothermal energy and biomass combustion heat are recoverable energy resources. Organic rankine cycle (ORC) energy recovery system was modeled and reviewed. In addition, a comprehensive literature survey is carried out. Thus, many recent papers about ORC were studied over accordingly in the literature section. Then, they were expressed within this paper in order to sum up. A thermodynamic analysis was also carried out for an ORC system throughout this paper. Binary fluid cycles utilize a blend of water/ammonia, yet are rather complicated compared to rankine cycles. Additionally, the organic substance chosen for the working fluid must have low latent heat and high density to boost the turbine inlet mass flow rate. Typical features of a ORC module are indicated as heat source temperature, power output, thermal efficiency, etc. The maximum thermal efficiency of a module is about 25%. The choice of a module is basically founded upon operation, heat source temperature and aimed power output. The selection of the sort of organic rankine cycle machine is commonly affected by the nature, condition and temperature of the heat source. Thus, the temperature is a critical property during selection in case studies. According to results, the system varies according to technology, size and cost aspects. Moreover, machine, engineering, system integration, capital costs are contained in the investment cost of an ORC Project and also the investment cost is closely related to the application [40,41,42].

Since the ORC consumes virtually no additional fuel, the emission of environmental pollutants such as carbon dioxide (CO2), sulphur dioxide (SO2) and etc. would be decreased. Moreover, the exhaust heat exiting from the ORC could be further used to drive chillers such as absorption chillers to supply cooling capacity if required by the local demand. Moreover, further work is needed to enhance the ORC's performance, such as decreasing the heat and pressure losses in the whole system and developing the performance of the common parts such as the turbine, generator, and heat exchangers [42,43].

2 LITERATURE REVIEW

2.1 Multigenerational Systems Overview

As the world turns toward sustainability, the energy sector stands at the forefront of this transformation, along with the evolution of multi-generational renewable energy systems. The energy sector stands at the forefront of this transformation, along with the evolution of multigenerational renewable energy systems. These innovative systems not only utilize natural resources such as wind, solar, hydropower, geothermal and biomass but also integrate technological advances and multi-generational planning to ensure energy resiliency and sustainability over decades as observed in Figure 2.1 [44,45].

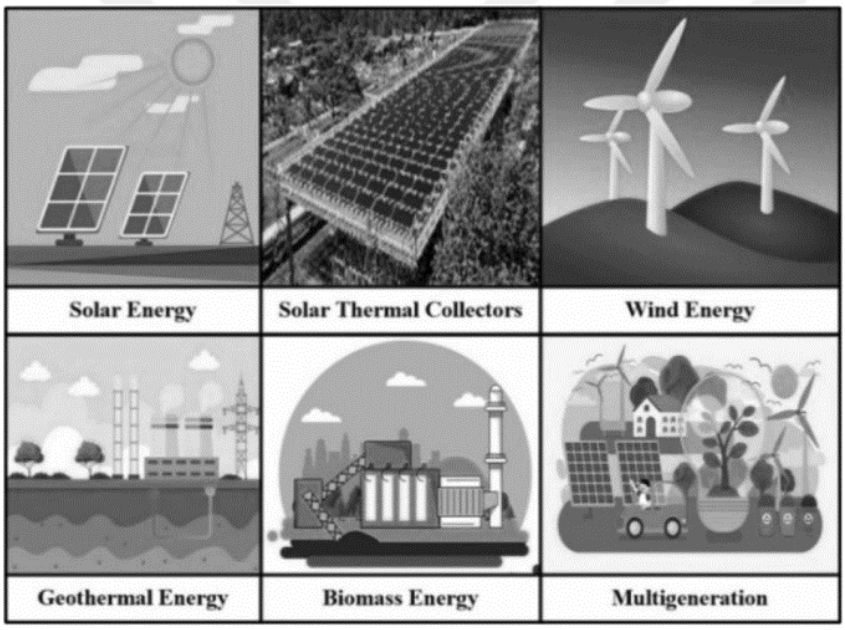


Figure 2.1. Sketches of solar energy, solar thermal collectors, wind energy, geothermal energy, biomass energy and multigeneration [64]

Multigenerational renewable energy systems are designed to remain adaptable over extended time frames, often with a vision spanning 50 to 100 years. This long-term perspective allows for the integration of both existing renewable technologies and those still under development. These systems may initially rely on solar and wind technologies, which can later be complemented by newer forms such as marine or geothermal energy as they become viable. The key strength of these systems lies in their adaptability. As technology evolves and energy demands shift, they can incorporate innovations

like improved battery storage, advanced solar panels, or efficient wind turbine designs. This flexibility is crucial for addressing the changing climate and its impact on energy resources.

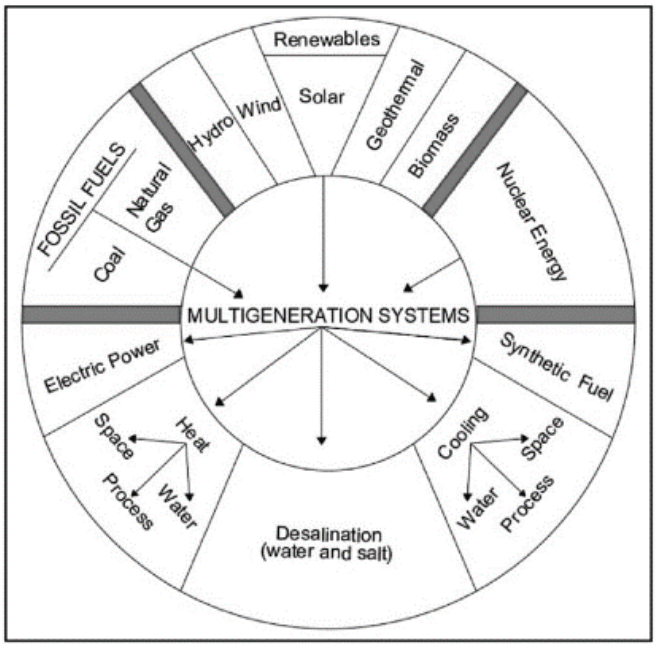


Figure 2.2. Energy sources and commodious properties of multigeneration systems [65]

From an environmental perspective, multigenerational renewable energy systems represent a significant step forward in reducing carbon footprints. By maximizing the use of renewable sources, these systems minimize reliance on fossil fuels, thereby decreasing greenhouse gas emissions and promoting biodiversity through less intrusive energy production methods [45,46,47].

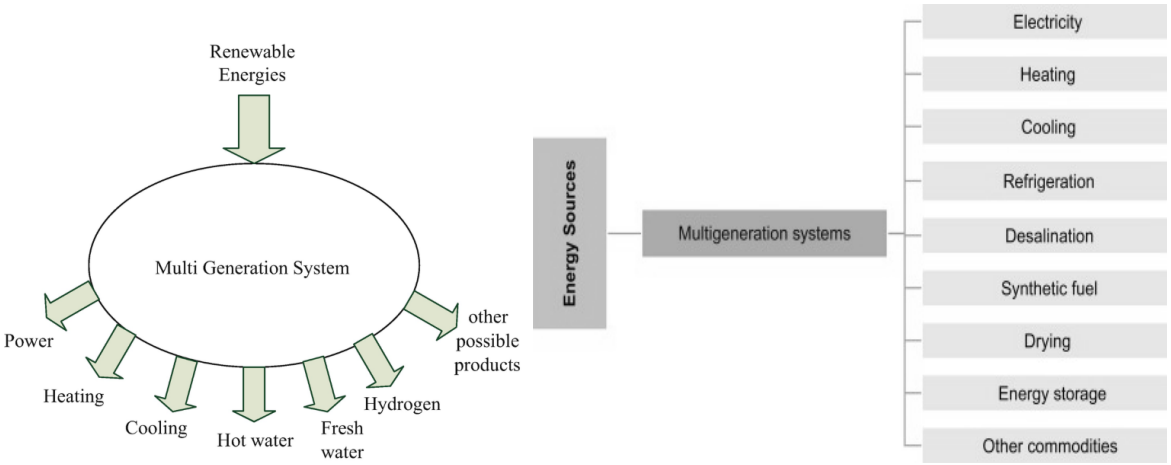


Figure 2.3. Schematic of input and outputs of multigeneration systems [66]

Despite their benefits, multigenerational systems face challenges, particularly related to initial capital outlay, technological integration, and regulatory environments. However, with supportive policy frameworks and continued technological innovation, these hurdles can be overcome.

The expansion of multigenerational renewable energy systems is likely to play a pivotal role in global efforts to combat climate change. As communities and nations increasingly recognize the importance of sustainable energy practices, these systems will become integral to achieving long-term environmental, economic, and social goals.

Multigenerational systems also prioritize the community aspect. They are often developed with local input and designed to provide energy security for multiple generations within a region. This community-based approach ensures that the infrastructure supports not only present needs but also future demands, fostering a sense of ownership and responsibility among residents. Economically, these systems aim to stabilize energy costs by reducing dependence on imported fuels and minimizing exposure to volatile fossil fuel markets. By investing in renewable energy infrastructure, communities can lock in lower and more predictable energy costs over the long term [47,48,49].

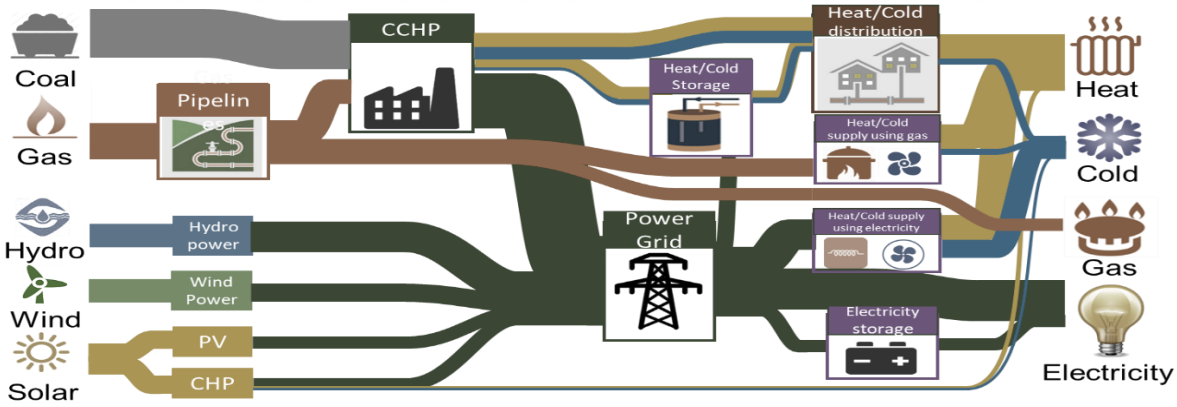


Figure 2.4. Sketch of multigeneration application for a community [77]

Multigenerational renewable energy systems exemplify a commitment to future generations. They offer a blueprint for sustainable development, blending innovative technology with forward-thinking energy policies to create resilient, efficient, and environmentally friendly energy solutions for today and tomorrow [50,51,52].

2.1.**1** Advantages of multigenerational systems

Considering advantages of multigeneration systems, as observed from the Figure 2.5, multiple perspectives are one of the advantages. As different generations bring unique viewpoints to job responsibilities. When these perspectives are shared within and across teams, they contribute a diverse range of knowledge and abilities, fostering innovation. Problem-solving abilities are another advantage of multigeneration systems. As combining various perspectives and diverse skills leads to creative solutions [53,54].

In terms of improved productivity, the other advantage of multigeneration systems, the collaboration of fresh innovation with wisdom from experience enhances productivity. Younger employees adapt to rapidly changing technology, while mature employees contribute decision-making insights [54,55,56].

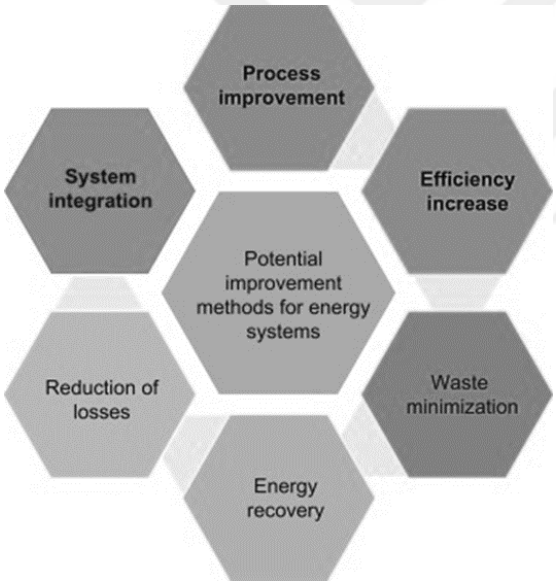


Figure 2.5. Schematic of advantages of multigenerational systems [68]

Observing the Figure 2.5, potential improvement methods for multigeneration energy systems are efficiency increase, waste minimization, high energy recovery, reduction of losses and process improvement with the integration of the subsystems.

Employing multigenerational workforces creates a competitive advantage by improving workforce continuity, stability, and knowledge retention. It strengthens the talent pipeline and contributes to overall economic growth. Employing a diverse range of ages strengthens

the talent pipeline. Organizations can tap into the skills and perspectives of different generations, fostering innovation and adaptability [57,58].

A study conducted by the World Economic Forum, AARP, and the OECD revealed that investing in multigenerational workforces can lead to an almost 19% increase in GDP per capita over a span of three decades. By embracing employees from all life stages, companies can create a thriving workforce that significantly contributes to economic growth and cost savings.

In conclusion, multigenerational systems contribute not only to economic growth but also to a more resilient and sustainable workforce. By recognizing and leveraging the strengths of each generation, companies gain a significant competitive advantage. Multigenerational systems offer a sustainable development blueprint, combining innovative technology with forward-thinking practices to create resilient, efficient, and environmentally friendly solutions for today and future work of tomorrow [58,59].

2.2 Turkey's Geothermal And Solar Energy Potential

In Turkey, a variety of low-carbon and renewable energy sources play a significant role in the energy structure of the country. These sources are essential for reducing greenhouse gas emissions and decreasing dependence on fossil fuels. Some key low-heat resources are geothermal energy, solar power, hydropower, wind power and biofuels.

As the largest low-carbon energy source in Turkey, hydropower generates about 20% of the nation's electricity. The country's numerous rivers and water bodies make hydroelectric power a crucial component of the national energy strategy.

Wind energy is another major renewable resource, contributing around 10% of Turkey's electricity. The Aegean and Marmara regions, known for their high wind potential, host many wind farms that efficiently capture this energy.

Solar energy accounts for nearly 6% of Turkey's electricity. The country's geographical location provides abundant sunlight, particularly in the southern and central regions, leading to extensive solar power projects, including both photovoltaic (PV) and concentrated solar power (CSP) systems [60,61].

Turkey is rich in geothermal resources, ranking among the top countries globally for geothermal potential. These resources are used for both electricity generation and direct

heating applications, with numerous geothermal plants located mainly in the western part of the country.

Although a smaller part of Turkey's renewable energy landscape, biofuels still contribute to the overall energy strategy. Derived from organic materials, biofuels can be used for heating, electricity generation, and as an alternative to traditional transportation fuels.

These renewable energy sources are integral to Turkey's broader strategy to diversify its energy mix. By investing in and expanding these low-carbon technologies, Turkey aims to enhance its energy security, reduce environmental impact, and support global efforts to combat climate change [61,62].

Turkey has useful and high amount of geothermal and solar energy potential due to its geopolitic location as a mediterreanean country. Thus, Turkey possesses significant potential for both geothermal and solar energy. By implementing coherent energy policies and investing in renewable infrastructure, Turkey can diversify its energy sources, strengthen energy security, and contribute to global sustainability objectives by reducing its carbon footprint.

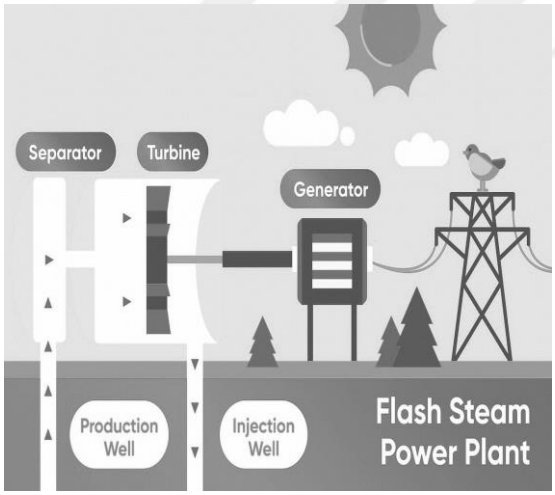


Figure 2.6. Sketch of geothermal and solar resources [69]

Effective utilization of both solar and geothermal energy is essential for Turkey's renewable energy sector. By doing so, Turkey can improve its energy security and actively contribute to global sustainability objectives. Therefore, multigenerational solar and geothermal hybrid systems are significant for Turkey's future position. Turkey's geothermal and solar energy resources can coexist peacefully and support a varied and sustainable energy environment.

Solar energy complements geothermal power generation during the day, while solar panels provide electricity during peak demand. During the day, solar energy can supplement geothermal power generation, particularly when geothermal plants run at a steady baseload. At times of high demand, solar panels can supply energy, while geothermal units can produce consistent amounts of power [62,63].

The Turkish government promotes the combined use of geothermal and solar energy by providing incentives for both types of projects. An energy mix that is more resilient and balanced can be achieved in Turkey by carefully implementing geothermal and solar technologies [63,64].

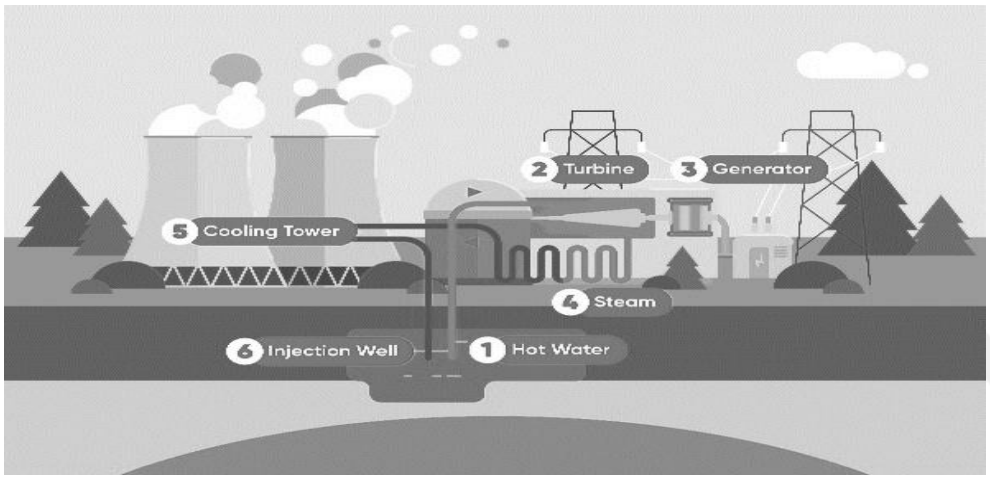


Figure 2.7. Sketch of the multigenerational hybrid system with basic parts [69]

In Figure 2.7, the sketch of the multigenerational system with the basic components geothermal injection well, turbine, generator and cooling tower can be observed.

2.2.1. Turkey's geothermal energy potential

Turkey, known for its distinctive geology and favorable geographic conditions, stands out as a prominent player in the field of geothermal energy. Positioned along significant tectonic fault lines and with a high level of volcanic activity, Turkey boasts one of the world's largest geothermal potentials, primarily concentrated in its western region. Turkey is rich in geothermal resources due to its location on the tectonic boundary between the Eurasian and Arabian plates. Since the 1960s, approximately 460 geothermal fields have been discovered in the country [65,66].

Geothermal energy harnesses the Earth's internal heat by tapping into underground reservoirs of hot water and steam. Turkey's geothermal potential owes much to its location along major fault lines, including the North Anatolian Fault and the East Anatolian Fault.

In Figure 2.8, geothermal resources and applications map of Turkey can be observed according to 2019 MTA data. The red zones are the hottest resources at temperatures between 100℃ and 70℃. The lowest temperatured geothermal resources are lilac colored ones, which are at temperatures between 20 and 49℃. Additionally, the moderate temperatured geothermal resources are yellow colored ones, which are at temperatures between 50 and 69℃. Moreover, the temperature distribution of the geothermal resources differs between these colors from red as high to blue as low, respectively according to the temperature scale in the Figure 2.8 [66,67].

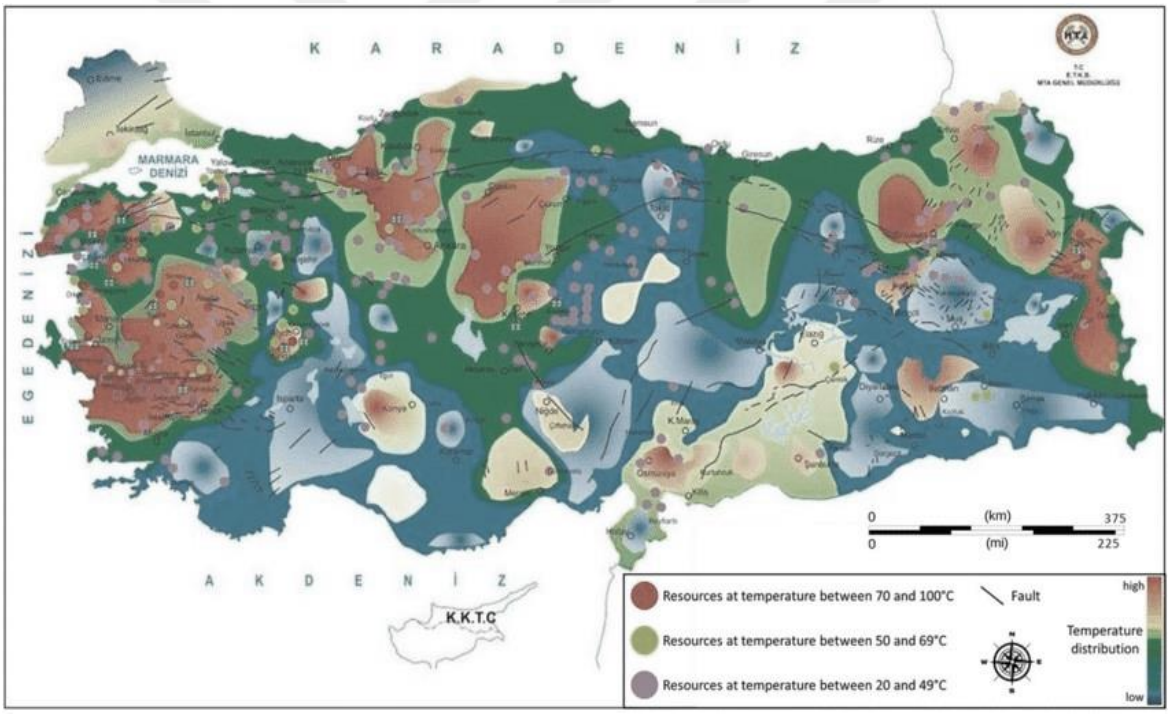


Figure 2.8. Geothermal resources and applications map of Turkey (MTA 2019) [57]

Geological features in Turkey not only increase seismic risks but also create an ideal environment for geothermal activity, particularly in the Menderes Massif and the Gediz Graben regions of Western Anatolia.

Geothermal hot water has been used in Turkish spas since ancient times, including the famous Hierapolis, which is now Pamukkale. Modern geothermal energy development

began in the 1960s with systematic geological and geophysical surveys. After the 1970s global oil crisis, Turkey intensified its search for alternative energy sources [68,69].

Nowadays, Turkey ranks fourth globally in installed geothermal power capacity, with over 1,500 megawatts (MW) primarily used for electricity generation and direct heating in cities like İzmir, Aydın, and Manisa. Ongoing explorations aim to tap into deeper reservoirs for electricity production, with drilling targets reaching depths of up to 4800 meters.

There are many advantages of geothermal energy. Geothermal energy is renewable and provides consistent power, unlike intermittent sources. Geothermal power plants have a small land footprint and emit low greenhouse gases. Geothermal heating supports local economies by enabling year-round crop production in geothermally heated greenhouses.

Although geothermal energy in Turkey has its benefits, it encounters various obstacles. Initial exploration and drilling processes are capital-intensive, especially in poorly documented areas. Environmental concerns include managing geothermal brines with high mineral content. Scaling up technology, particularly adopting enhanced geothermal systems (EGS), is crucial [69,70,71].

The Turkish government recognizes geothermal energy's importance and offers incentives like feed-in tariffs and grants. The goal is to increase geothermal energy's share in the national grid, enhancing energy security [71,72].

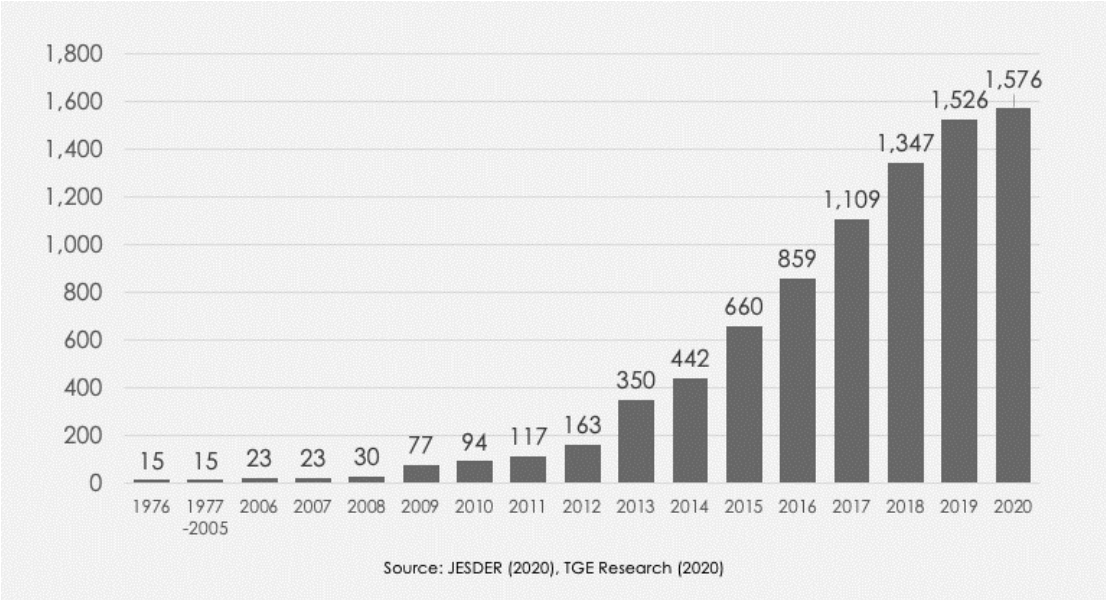


Figure 2.9. Geothermal power generation capacity in Turkey (MW) 1976-2020 (source: ThinkGeoEnergy) [70]

In Figure 2.9, the geothermal power generation capacity in Turkey as MW between the years 1976-2020 can be observed. Since 1976, the geothermal power generation capacity in Turkey has increased more than thousandfold. While the geothermal power generation capacity is 15 MW in 1976, it became 1576 MW in 2020, which is good improvement. Additionally, As of December 2020, Turkey's geothermal electricity production installed capacity stands at 1663 MWe. This capacity includes both binary cycle (approximately 1263 MWe) and flash steam (about 400 MWe) geothermal power plants [71,72,73].

Turkey's geothermal sector has immense growth potential, including district heating systems. Turkey's geothermal energy potential contributes to a sustainable and secure energy future. Continued investment and supportive policies can make geothermal energy a pivotal part of Turkey's energy landscape, combating climate change globally [73,74].

2.2.1.1 Geothermal heat pump

Geothermal heat pumps, also known as ground source heat pumps, these systems efficiently provide both heating and cooling for buildings. They utilize the earth's consistent underground temperature to regulate indoor climate.

Geothermal heat pumps circulate a fluid (usually water or a water-antifreeze mixture) through buried pipes. In winter, the fluid absorbs heat from the ground and transfers it indoors. In summer, the process reverses, cooling the interior by transferring heat back to the ground.

There are different types of systems which are closed-loop systems, open-loop systems, horizontal systems, vertical systems and pond/lake systems. Closed-loop systems are commonly used, these involve continuous loops of buried pipes where the fluid recirculates. In Figure 2.10, three different types of closed loop systems which are horizontal, vertical and pond/lake can be seen, respectively. In terms of pond/lake systems, which can be the most affordable choice if the location has a sizable body of water. To keep it from freezing, a supply line pipe is coiled into circles and run underground, at least eight feet below the surface, from the structure to the water. Only water sources that satisfy minimal standards for volume, depth, and quality should be used with coils [75,76,77].

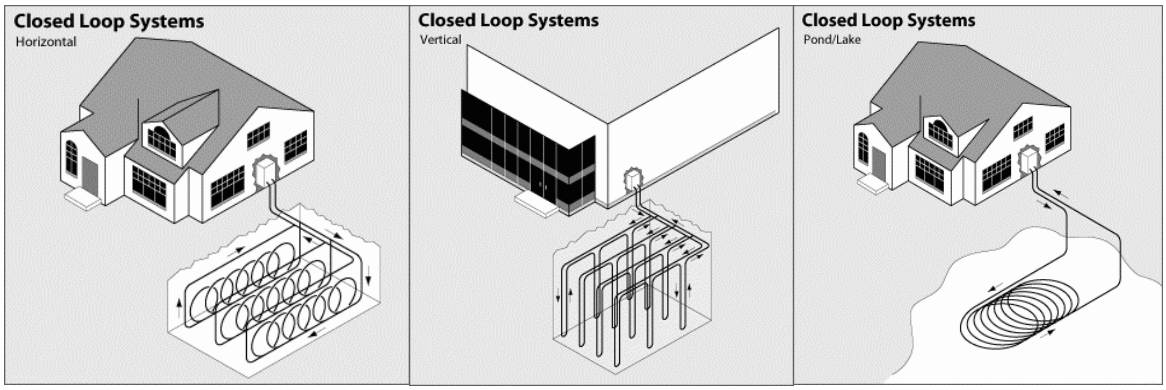


Figure 2.10. Horizontal, vertical and pond/lake closed loop systems [72]

Open-loop systems utilize groundwater from a well as a heat source or sink, returning the water to the ground afterward. Horizontal installation loops require more land area but are cost-effective, while vertical loops are used in limited spaces and involve deep drilling. In Figure 2.11, sketch of open loop systems can be seen.

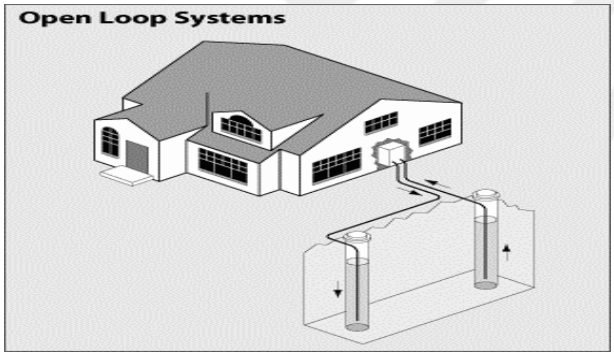


Figure 2.11. Open loop systems [72]

Advantages of geothermal heat pumps are energy efficiency, being cost-effective and environmentally friendly. Geothermal heat pumps outperform traditional systems due to their reliance on stable underground temperatures. Although installation costs are high, long-term savings come from lower operating costs. These systems reduce greenhouse gas emissions by relying on renewable resources [77,78,79].

There are also some disadvantages of geothermal heat pumps, which are high initial investment, and being site-specific since installation feasibility depends on geological and hydrological characteristics. Drilling and pipe laying contribute to the upfront cost.

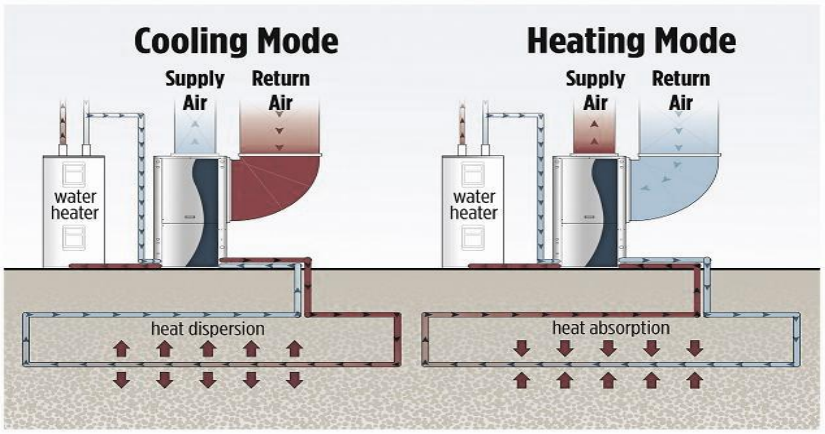


Figure 2.12. Working principle of geothermal heat pump [73]

In terms of working principle of geothermal heat pump as seen in Figure 2.12, a heat exchanger, ducting into the building, and a ground loop system with a water solution are the usual components of a system. The water solution travels via underground pipes during the winter, absorbing heat from the earth. The heated water is brought inside the house, where it is concentrated by a water-to-air heat pump and transferred to air through a traditional ducting system, which is then circulated to heat the space. This process is reversed in the summer, when the house's excess heat is pumped either into the ground or used to heat the hot water used for domestic purposes, keeping the house cold [79,80,81].

As an alternative, the thermal energy needed for a hydronic radiant floor heating system is concentrated using a water-to-water heat pump. In the summer, the process is inverted, with heat from the house being transported via the heat pump into the water solution in the ground pipes, which subsequently release further heat into the earth [81,82].

Overall, geothermal heat pumps align with global efforts to reduce fossil fuel reliance and environmental impact.

2.2.2 Turkey’s solar energy potential

Turkey, a country that is situated at the meeting point of Europe and Asia, has a climate and physical location that make it exceptionally capable of producing solar energy. Blessed with an abundance of sunshine, the country is poised to play a significant role in the global shift towards renewable energy.

Turkey's advantageous geographic and climatic circumstances are the main factors contributing to its solar power potential. With an average of 7.2 hours of sunlight per day

and approximately 2,640 hours of sunshine per year, regions such as Central and Southeastern Anatolia are especially well-suited for solar energy projects. These areas experience long periods of uninterrupted sunshine, making them ideal locations for both large-scale solar farms and smaller, decentralized installations [83,84].



Figure 2.13. Turkey's total solar radiation map [74]

In Figure 2.13, total solar radiation map of Turkey can be checked out. The lowest total solar radiation is from the north side of Turkey, painted with dark blue which means about 1400-1450 kWh/m^2-year according to the scale on the right side of the figure and the highest total solar radiation is from South and South east of Turkey, painted with claret red which means about 1800-2000 kWh/m^2-year. And the moderate total solar radiation is from the center side of Turkey, painted with yellow which means about 1550-1600 kWh/m^2-year. Thus, total solar radiation of Turkey increases from North to South [84,85].

Although Turkey's solar energy adventure started some decades ago, tremendous progress has been accomplished in the previous ten years. From a modest base, the installed capacity for solar power has seen exponential growth. As of recent data, Turkey has installed several gigawatts of solar energy capacity, rapidly becoming a leading country in solar development in the region. This rapid expansion is partly attributable to the global decrease in the costs of photovoltaic (PV) panels and supportive government policies, including feed-in tariffs and subsidies for renewable energy technologies. The growth of solar energy in Turkey is not just limited to utility-scale projects. There has been a noticeable increase in the adoption of solar power in residential, commercial, and industrial sectors. Rooftop solar installations are becoming more common, driven by both economic factors and a growing awareness of environmental issues [85,86,87].

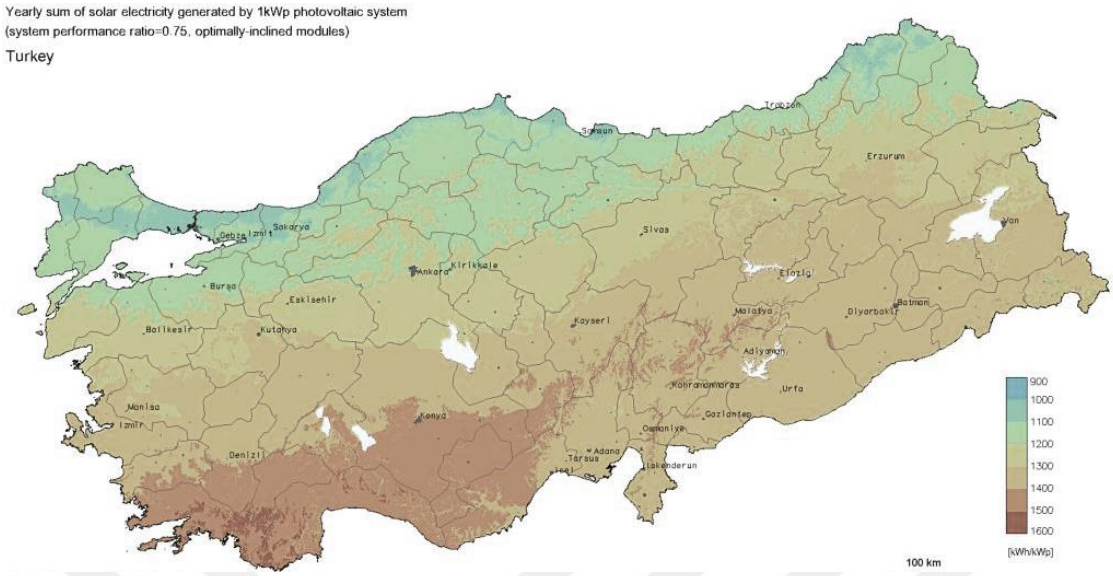


Figure 2.14. Turkey's Solar Energy Map [74]

In Figure 2.14, solar energy map of Turkey can be checked out. According to the scale on the right side of the figure, the highest solar energy is in the South West of Turkey and the lowest solar energy is in the North sides of Turkey. Also, the moderate solar energy is in the center regions of Turkey.

There are numerous advantages to Turkey's solar energy development. Economically, it reduces the country's dependence on imported fossil fuels, which currently account for a significant portion of Turkey's energy consumption. Environmentally, it contributes to reducing carbon emissions and combating climate change. Additionally, solar energy projects often lead to job creation in engineering, manufacturing, and installation roles, which supports local economies [87,88].

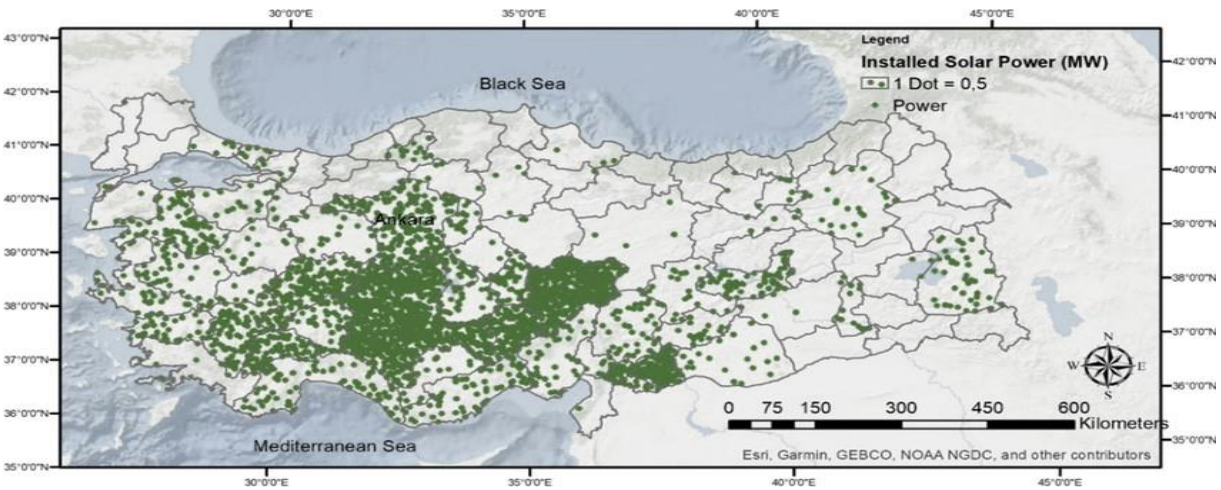


Figure 2.15. Solar power plant distribution map of Turkey [58]

Notwithstanding its promise, Turkey confronts a number of obstacles to the growth of solar energy. One of the primary obstacles is the financial aspect. Although the cost of solar technology has decreased, the initial investment required for large-scale solar installations remains substantial. Financial mechanisms and incentives need to be sustained or adapted to encourage further investment in the sector. Another challenge is the regulatory environment. While there have been improvements, bureaucratic hurdles and delays in licensing can impede the rapid development of new projects. There is also a need for further development of the grid infrastructure to manage the intermittent nature of solar power effectively and integrate it smoothly with other energy sources [88,89].

The Turkish government acknowledges the strategic significance of solar energy within its national energy strategy. The aim is to significantly increase the percentage of renewables in the country's energy mix by 2030, with solar energy expected to contribute a substantial share. Policies such as the Renewable Energy Resource Zone projects are designed to promote large-scale solar investments through competitive auctions, offering attractive prices for solar-generated electricity. Looking forward, the outlook for solar energy in Turkey is highly promising. With continued technological advancements, such as the development of more efficient solar panels and battery storage solutions, the capacity for solar power is set to expand even further. Moreover, as public and governmental attitudes continue to shift towards a more sustainable energy model, solar energy is likely to play a pivotal role in Turkey's energy future [89,90,91].

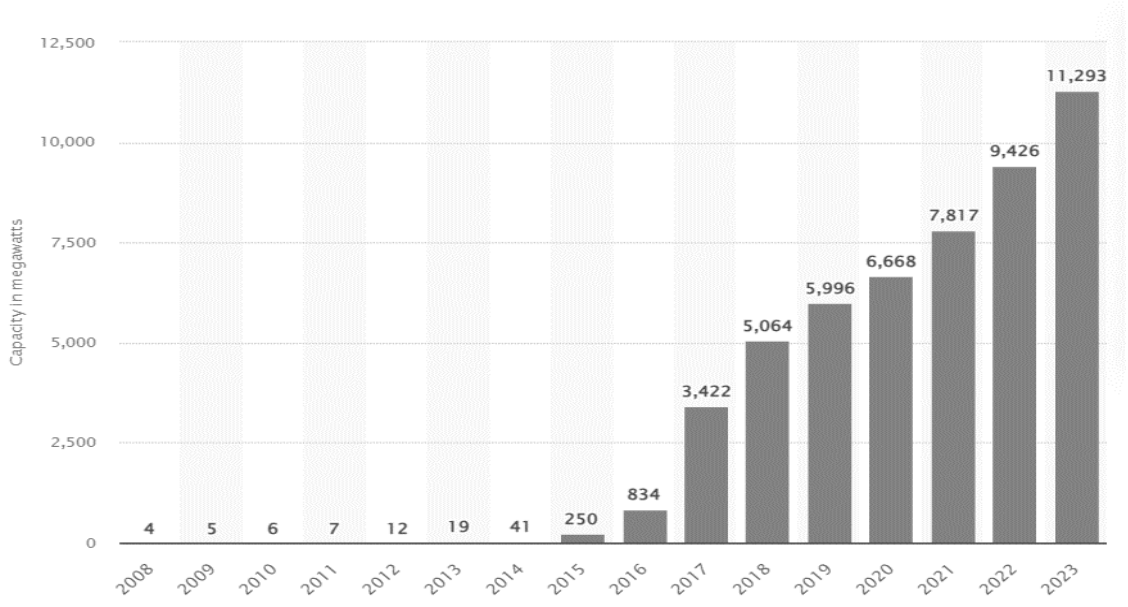


Figure 2.16. Turkish solar energy capacity from 2008 to 2023 [85]

While turkish solar energy capacity is only 4 MW in 2008, it has increased to11293 MW in 2023 as seen in the Figure 2.16. Thus, considerable growth is beneficial for renewable energy utilization.

Turkey’s solar energy potential presents a valuable chance for the nation to transform its energy outlook and establish itself as a regional leader in renewable energy. By capitalizing on its geographic advantages and continuing to foster a supportive environment for solar development, Turkey can not only meet its own energy needs more sustainably but also contribute significantly to global efforts to mitigate climate change. As the sun continues to rise on Turkey’s solar sector, the nation’s commitment to exploring and expanding this clean energy source will be crucial for its energy security and environmental sustainability [91].

2.2.2.1 Solar water heating and energy storage

A solar water heater is a device that uses sunlight that is captured to heat water for home usage. Solar water heaters just concentrate on heating water, as opposed to solar panels that also produce energy. A solar water heating system's components include solar gatherer, tank for storage, heat exchanger and heat transfer fluid. Solar gatherer takes in sunlight and transforms it into thermal energy. Tank for storage holds the heated water till it's needed. Heat exchanger avoids mixing the two fluids by transferring heat from the solar-collected fluid—typically a specialist heat-transfer fluid—to the water supply in your house. Heat transfer fluid works with a heat exchanger to absorb and transfer solar heat to the home's water supply, typically through a heat exchanger [92,93].

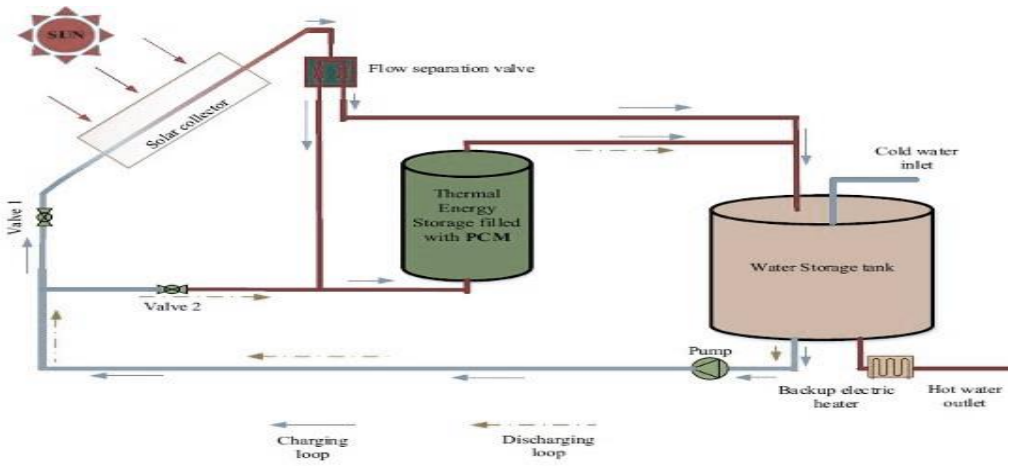


Figure 2.17. Solar heating water system with the termal energy storage, investigated by Mahfuz et al. [55]

Types of solar water heaters are passive systems and active systems as seen in the Figure 2.18. Passive systems rely on natural convection to move heated water. They don't use pumps for circulation. Active systems use pumps to circulate water. They can significantly reduce reliance on conventional energy sources for water heating, making them cost-effective and environmentally friendly.

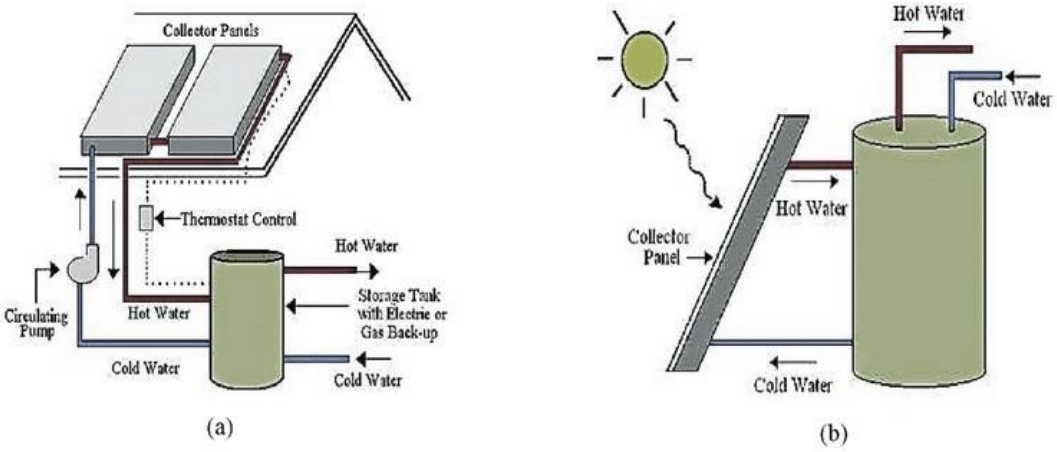


Figure 2.18. (a) Active type solar water heater system; (b) Passive type solar water heater system [78]

Advantages of solar water heaters are energy saving, eco-friendliness and long-term investment. Thus, solar water heaters reduce your reliance on traditional energy sources, resulting in lower energy bills. Additionally, by harnessing sunlight, they contribute to reducing greenhouse gas emissions. And switching to solar water heating is a step toward sustainability and a smaller carbon footprint [93,94].

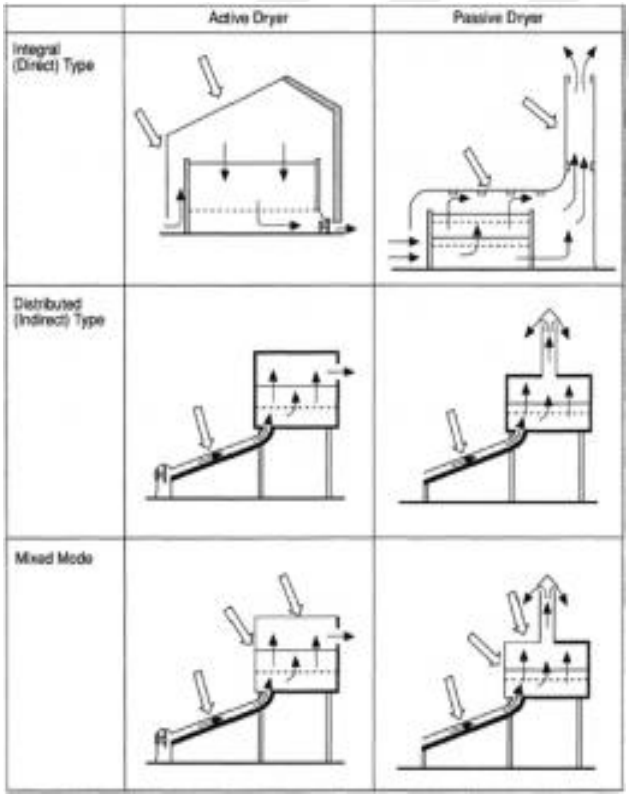
While solar water heaters focus on immediate water heating, energy storage is crucial for overall system efficiency. Residential active solar systems often include short-term heat storage tanks. These tanks store heat for a few hours, extending system operation during cloudy periods or at night [94,95].

Solar water heaters are a sustainable and cost-effective way to heat water using energy of the sun. They are an excellent choice for environmentally conscious homeowners. Combining solar water heating with efficient energy storage can optimize the overall solar system performance.

2.2.2.2 Solar drying

Solar drying is a technique that removes moisture from various materials, including food products and agricultural produce, using the sun's energy. Unlike conventional methods that rely on fossil fuels, solar drying harnesses the natural power of the sun. Solar drying captures solar energy to raise the air temperature, which accelerates moisture evaporation from the material being dried. This can be done through simple open-air methods or more sophisticated solar dryers [96].

Types of solar dryers are direct solar dryers, indirect solar dryers and mixed mode solar dryers as seen in the Figure 2.19. Thus, direct solar dryers expose the product directly to sunlight using trays or racks under a clear cover. The retained heat speeds up the drying process. Indirect solar dryers have a separate solar collector. Air is heated in the collector using solar radiation and then passed into the drying chamber, ensuring materials are not directly exposed to sunlight [96,97].



	Direct Solar Dryer	Indirect Dryer
		
Operating Temperature	Medium temp. usage (45-78°C)	Medium temp. (45-75°C)
Scale of operation	Applicable in small to Industrial Scale	Better in small scale usage
Need of solar collector	No solar collector	Solar collector must
Types of Commodity	Can also be used for products* where direct solar contact is mandatory	Can also be used for products* where direct solar contact is not mandatory
Performance in unfavorable weather	Operatable even in unfavorable weather	Poor performance in unfavorable weather

Figure 2.19. Classification of solar dryers. [79]

Mixed mode solar dryers improve efficiency by capturing solar energy directly and indirectly combining features of both direct and indirect types, which have these advantages:

energy efficiency, cost-effectivity and quality improvement. Accordingly, solar drying uses free and renewable solar energy, reducing reliance on electrical or fossil fuel-based systems. After initial setup, operational costs are minimal as no external energy sources are needed. The gentle drying process helps retain nutritional value and flavor in food products [97,98].

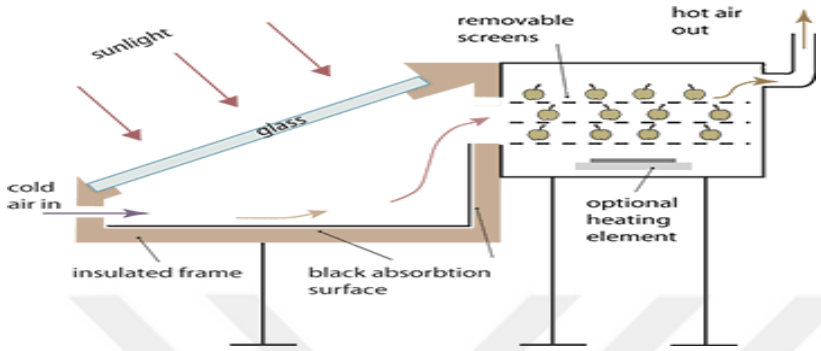


Figure 2.20. Solar drying application. [80]

Applications of solar drying as in the Figure 2.20 are agricultural sector and industrial use. Agricultural sector is commonly used for drying crops like grains, coffee, tea, spices, and fruits, improving storage life and reducing spoilage losses. Industrial use is employed in various industries for drying materials such as lumber, fibers, and other raw materials.

Challenges of solar drying are weather dependency and limited control. As, solar drying efficiency relies heavily on sunlight availability, making it less reliable in cloudy or rainy conditions. Precise regulation of temperature and airflow can be challenging, affecting drying consistency [98,99].

Despite these challenges, solar drying remains a popular choice, especially in regions with abundant sunlight, offering an eco-friendly option aligned with sustainable practices in agriculture and manufacturing.

2.2.2.3 Solar heat pump combination

A solar heat pump combination integrates the efficiency of a heat pump system with the renewable energy of solar power. This approach aims to reduce reliance on conventional energy sources, lower costs, and minimize environmental impact. Components of solar heat pump combination are solar photovoltaic (PV) panels and heat pump. Solar photovoltaic (PV) panels convert sunlight into electrical energy. The generated electricity powers the heat pump and other appliances in the building. Heat pump extracts heat from one

environment (such as outside air, ground, or water) and transfers it indoors. For cooling, the process is reversed [100,101].

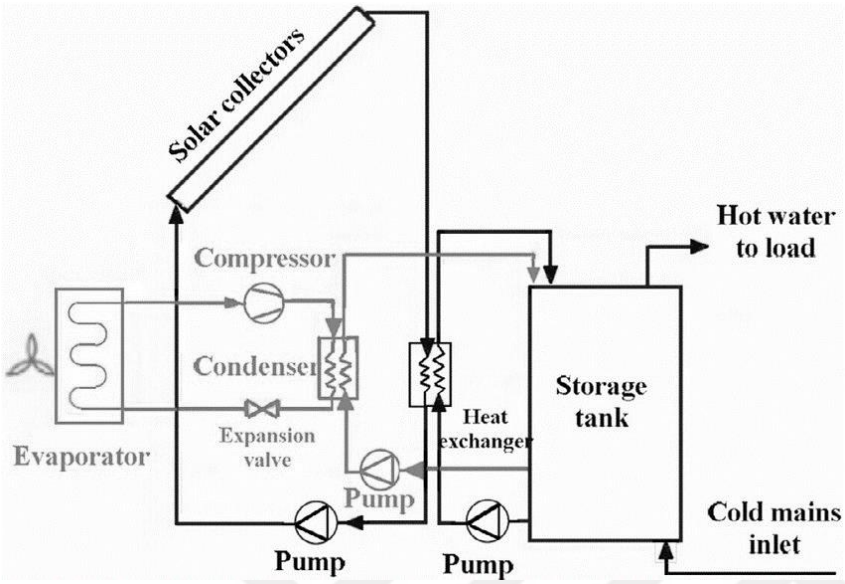


Figure 2.21. Simplified scheme of a solar assisted heat pump in parallel mode (Buker and Riffat, 2016). [81]

Types of solar heat pump systems are PV-powered heat pumps and solar thermal-powered heat pumps. PV-powered heat pumps are standard heat pump systems powered by electricity from solar PV panels. Solar thermal-powered heat pumps are less common, and these systems use solar thermal panels to collect sun-generated heat, assisting the heat pump in heating or cooling [101,102].

Advantages of solar heat pump combination are energy efficiency, reduced environmental impact and cost savings. In terms of energy efficiency, solar heat pump systems operate more efficiently than traditional ones, especially in sunny climates. By relying on renewable energy, they significantly cut greenhouse gas emissions. Although initial installation costs can be high, long-term energy bill reductions make it worthwhile.

Challenges of solar heat pump combination are high initial investment and weather dependency. Installing solar panels and a heat pump system can be costly, but incentives and rebates can help. Moreover, efficiency fluctuates based on sunlight availability. During low-sunlight periods, grid electricity or alternative sources may be needed [102,103].

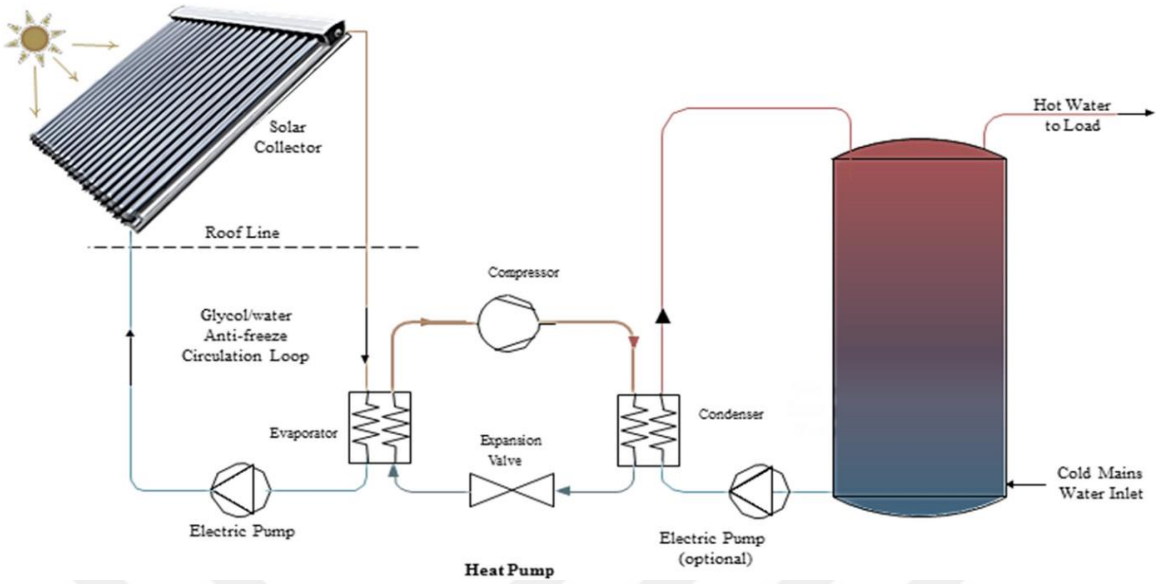


Figure 2.22. Parabolic concentrated solar collector system integrated with heat pump [82]

Applications of solar heat pump combination are versatile for residential, commercial, and industrial settings. Effective in regions with abundant sunlight and moderate climates. And solar heat pump combinations represent an advanced solution for green, efficient climate control in modern buildings.

2.3 Gonen's Geothermal And Solar Energy Potential

2.3.1 Gonen's geothermal energy potential

Balıkesir Gonen, a district in northwestern Turkey, is rapidly emerging as a central hub for geothermal energy due to its unique geological characteristics and abundant geothermal resources as seen in the Figure 2.23. This region, situated in the renowned geothermal province of Western Anatolia, holds a promising future in Turkey's quest for sustainable and renewable energy sources. Balıkesir Gonen's geothermal potential is primarily attributed to its location within one of Turkey's most active geothermal zones. The district lies on the northwestern edge of the Simav Graben, part of the larger Western Anatolian Graben system, which is characterized by significant tectonic activity and widespread volcanic residuals. These geological conditions facilitate the natural heating of underground water reservoirs, creating a rich source of geothermal energy [104,105].

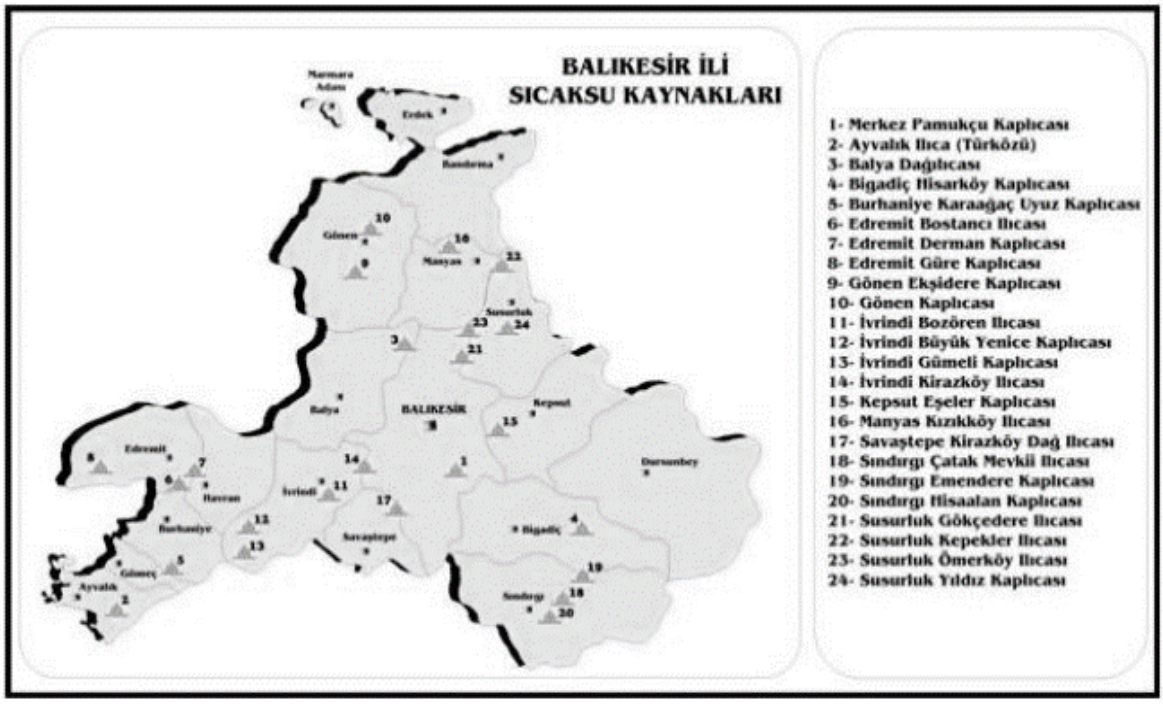


Figure 2.23. Geothermal and hot wellspring resources map of Balıkesir city and Gonen region [84]

Historically, the geothermal resources in Gonen were primarily used for therapeutic purposes, particularly in the region's renowned thermal baths. However, in recent decades, there has been a significant shift towards harnessing this geothermal energy for both electricity generation and direct-use applications. Today, Gonen hosts several geothermal plants that contribute significantly to the local and regional energy supply. These facilities not only generate electricity but also supply heat for agricultural and industrial processes, including greenhouse heating, which has revolutionized local agriculture by enabling year-round production in an environmentally friendly manner [105,1067].

Gonen geothermal field, known as one of the oldest thermal areas, has been utilizing its healing waters for many years. Recent technological advancements have led to the construction of modern facilities. To ensure a sufficient supply of geothermal water, extensive geological, geophysical, and geochemical research and testing have been conducted by the General Directorate of Mineral Research and Exploration (MTA) in Turkey. The first geothermal heating application in Turkey took place in 1964 when Gonen Park Hotel was heated. Since 1987, geothermal heating has been implemented in Balıkesir-Gonen. In the Gonen geothermal area, 17 research and production wells have been drilled, with depths ranging from 133 to 800 meters. The geothermal fluid extracted from these

wells is used for heating residential and industrial areas in thermal facilities. Gonen geothermal heating system's Phase I project began in 1985 and became operational by 1987. Phase II, completed in 1994-1995, provides heating for 1,600 equivalent residential units in Phase I and 1,000 equivalent residential units in Phase II. Currently, it heats 2,600 residential units and hotels (equivalent to 400 residential units) and also meets the hot water demand for industrial facilities, such as tanneries. Table 2.1 details existing and drilling hot water wells in Gonen Kaplıcaları, including construction year, depth, temperature, flow rate, and pressure values [106,107].

Table 2.1. Specific values of Gonen geothermal wells [84]

Well Number	Year Drilled	Depth (m)	Temperature (°C)	Flow Rate (l/s)	Pressure without Pump (bar)
G-1	1976	133		Not used	
G-2	1976	535		Not used	
G-3	1985	308		In use as reinjection	
G-4A	1990	317		Not used	
G-5	1993	332		In use as reinjection	
G-6		385		Not used	
G-7		325	62	20	1.8
G-8		280	62	20	1.8
G-9		560	94	8	
G-10		265	69	20	1.8
G-11	(1999) 2002	816	79	8	
G-12	2002	500		Not used	
G-13	2002	356	71	20	1.4
G-14	2002	350		In use as reinjection	
G-15		188		In use as reinjection	
G-16	2003	316	79	25	1.8
G-17	2004	230	60	20	1.8

Thermal water extracted from production wells undergoes a two-step process. First, it is directed to a balancing tank to stabilize wellhead pressures, and then to a settling tank where unwanted particles are removed. The system distributes an average of 70°C thermal water with a flow rate of 141 l/s to heat exchangers. In the existing setup, heat exchangers are used for residential and hotel heating, as well as for the tannery hot water line. The thermal return water temperature is around 40°C. Hotel heat exchangers handle the hotel's hot thermal water, while the existing system and tannery heat exchangers provide warm thermal water. Additionally, the new system's heat exchangers are used for re-injection. Some wells (G1, G2, G4, G6, and G12) remain unused, while others (G3, G5, G14, and G15) serve the purpose of re-injection. Figure 2.24 shows the layout plan of the Gonen geothermal wells. G9 well is used for the analyses of this thesis [107,108].

The development of geothermal energy in Gönen offers numerous benefits such as energy security, economic development and environmental benefits. It reduces Turkey's dependence on imported fossil fuels, enhancing energy security. The geothermal industry has brought economic growth to Gönen, creating jobs in construction, maintenance, and operation of geothermal plants as well as boosting ancillary sectors such as agriculture. Geothermal energy is a clean and sustainable energy source that significantly lowers greenhouse gas emissions compared to fossil fuels [108,109].

Despite its advantages, the expansion of geothermal energy in Gönen faces several challenges such as environmental concerns, technological barriers, and economic and financial challenges. Issues such as the management of geothermal brines and the risk of induced seismicity need careful monitoring and management. The efficiency of geothermal power plants can be limited by the temperatures of the geothermal fluids. Advances in technology could help exploit lower temperature resources more effectively. The high initial capital required for exploration and development of geothermal resources can be a deterrent, requiring substantial financial inputs and effective risk mitigation strategies [109,110].

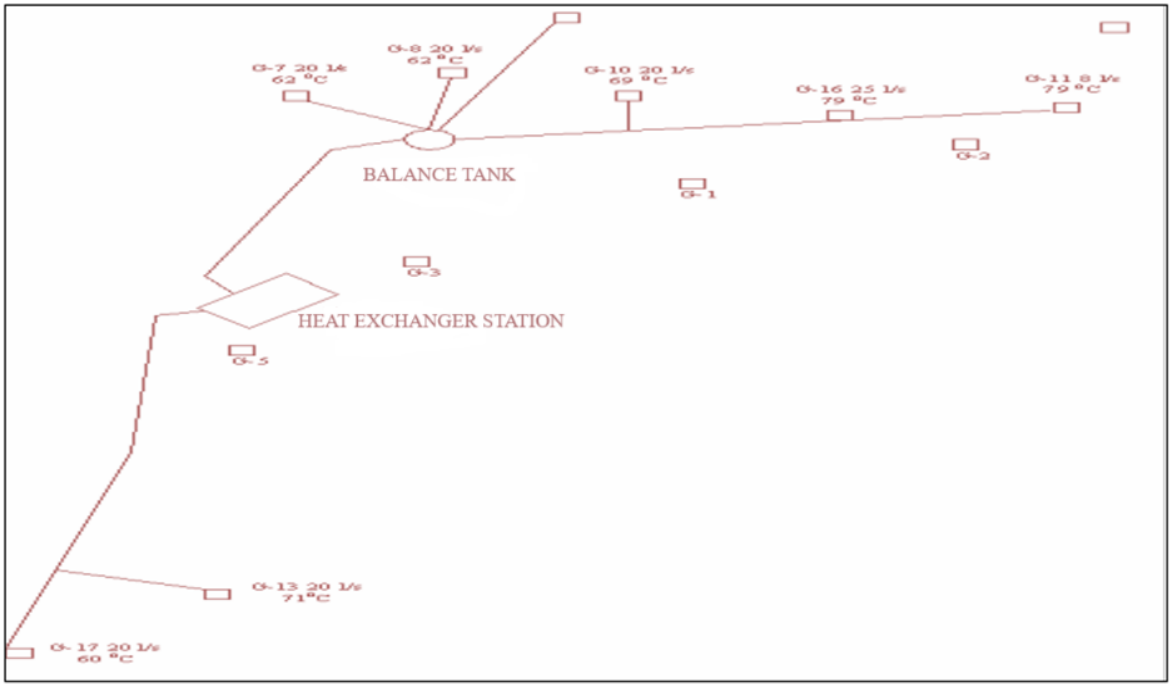


Figure 2.24. Gonen geothermal well layout plan [84]

Recognizing the strategic importance of geothermal energy, both local and national governments have implemented supportive policies to foster the growth of this sector in Gonen. These include subsidies, favorable tariffs, and streamlined regulatory procedures to encourage investment and development. Looking ahead, the potential for geothermal energy in Balıkesir Gonen is vast. With continued investment in research and development, the region could see an increase in the efficiency of existing geothermal operations and the expansion of new projects. Moreover, integrating geothermal energy into the district's heat and power networks could serve as a model for other regions with similar geothermal characteristics [110,111].

2.3.2 Gonen's solar energy potential

Balıkesir Gönen seen in the Figure 2.25, a district in the Marmara region of Turkey, is gaining recognition for its solar energy potential. Gonen benefits from a Mediterranean climate with long, hot summers and mild winters, making it ideal for solar energy production. The region receives abundant sunlight, averaging around 2,700 to 2,900 hours of sunshine annually as observed in the Figure 2.26. Moreover, total solar radiation value

of Gonen according to total solar radiation values of Balıkesir can be observed from the Figure 2.25 [112,113].

Various solar energy projects have been initiated in Gonen, including small-scale rooftop installations and larger solar farms. These projects reduce reliance on fossil fuels and align with Turkey's national energy policies promoting renewables [113].

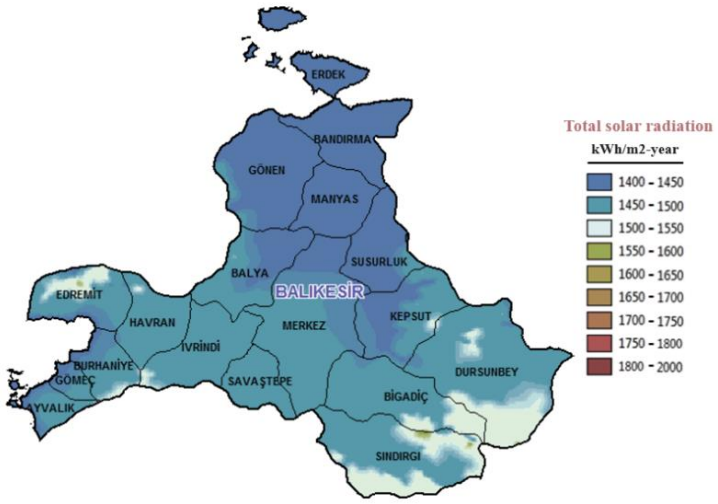


Figure 2.25. Map of Balıkesir city's solar energy potential [85]

Advantages of solar energy in Gonen are energy independence, economic growth and positive environmental impact. Increasing solar capacity reduces dependence on imported energy. The solar sector creates jobs, from installation to technology roles. Solar energy is clean and sustainable, with no greenhouse gas emissions during operation [114].

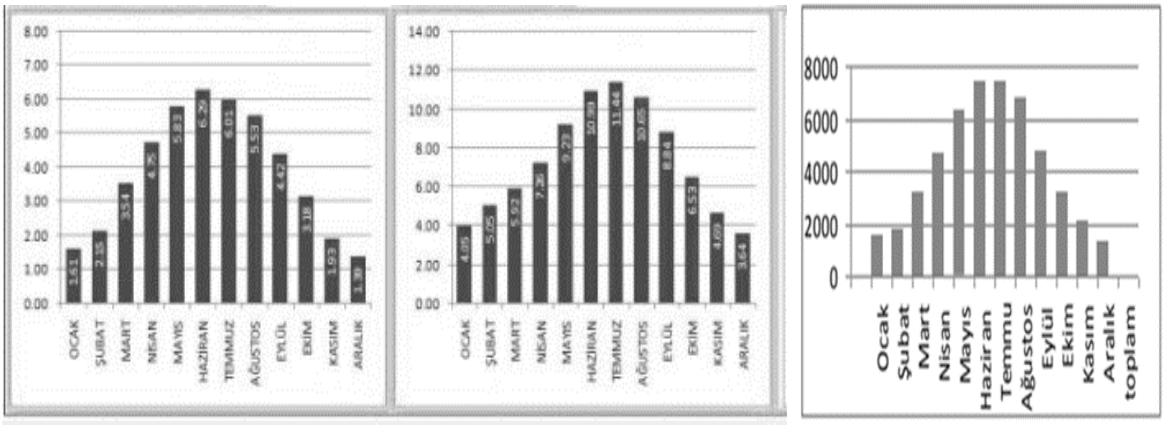


Figure 2.26. Diagrams of Balıkesir global radiation values (kWh/m^2-day), Balıkesir sunshine durations (hour), Balıkesir solar energy values (Wh/m^2) respectively [85]

Challenges to solar energy expansion are initial costs, land use and grid integration. Upfront installation expenses can be high, despite decreasing PV technology costs globally. Large solar farms require significant land, potentially competing with agriculture. Integrating solar energy into the power grid poses technical challenges [114,115].

Continued government support for renewables will stimulate solar growth in Gönen. Advancements in solar technology, efficiency, and energy storage enhance project feasibility. Local policies, such as zoning laws and subsidies, can further promote solar development. Educational programs and public awareness campaigns can boost acceptance and adoption of solar energy among the local population [115,116].

Gönen's solar potential is crucial for Turkey's renewable energy goals. By leveraging its geographic advantages and supportive national policies, Gönen can advance its energy sustainability. The solar sector's growth in this region not only meets local needs but also contributes to global climate change efforts. Gonen exemplifies how localized initiatives align with national strategies for a sustainable energy future.

3 THERMODYNAMIC MODELING OF MULTIGENERATION SYSTEM WITH ORC

Multigenerational hybrid systems are rather beneficial for optimum energy recovery. This study also comprises a multigenerational system consisting solar, geotermal and ORC. Accordingly, ORC system utilization in multigenerational energy systems is rather significant for environment as it recovers low waste heat and produces electrical energy back. ORC system consists of condenser, pump, evaporator and generator parts which supply the cycle for the system. Additionally, organic fluid selection is important for the efficiency, availability and safety of the ORC as being organic fluid utilized system. Mainly, a fine working fluid should reveal not only low toxicity, good material compatibility and fluid stability limits, low flammability, corrosion, and fouling characteristics but also high system performance. Working fluids can generally be classified as dry, wet and isentropic fluids based on their slope of saturated vapour phase in T-s curves [116,117].

Low-temperature plants are not directly so effective for electricity production. Therefore, a more efficient hybrid system is designed by using geothermal water and solar energy together. Solar energy supported geothermal sourced ORC system is designed. This multigenerational system consists of solar collectors, evaporator, turbine, generator,

condenser and pump. This structure of the the multigenerational system with ORC, solar and geothermal can be seen in Figure 7.1. The geothermal water and parabolic solar panels transfers its heat to the ORC fluid in the evaporator (Tgo). The refrigerant enters the heat exchanger at point (2a) and flows into the turbine at point (3). It exits as saturated steam to enter. After work is produced with the saturated steam entering the turbine, the fluid exits the turbine at point (4a). The fluid condensed with cooling water exits from point (1) as a saturated liquid in condenser and the turbine inlet pressure is increased by the pump. Cooling water to condenser (Tai) enters at temperature and exits at (Tao) temperature. In daytime conditions, the refrigerant entering the solar energy system is at point (5) goes into the turbine as superheated steam and reaches the condenser at point (6a) after exiting the turbine. The diagram of the temperature-entropy of the cycle is shown in Figure 7.2.

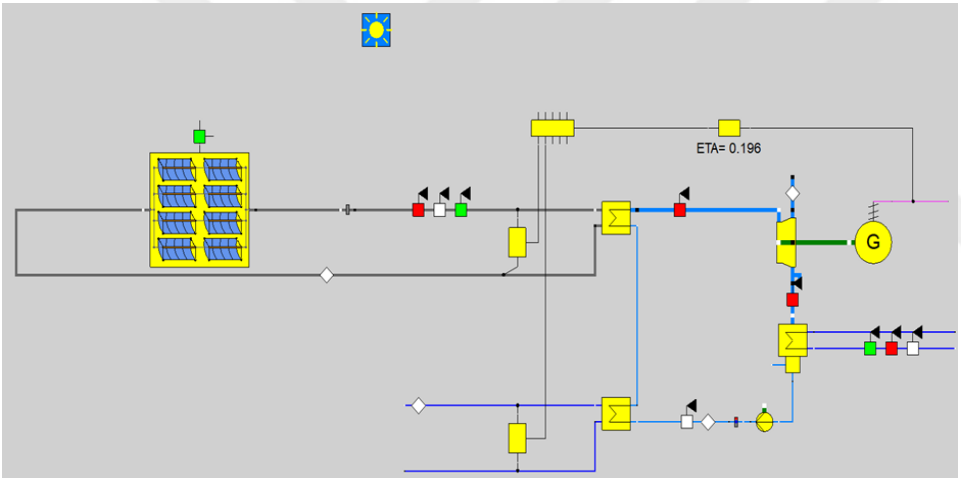


Figure 3.1. Schematic of the multigenerational system with solar, geothermal and ORC

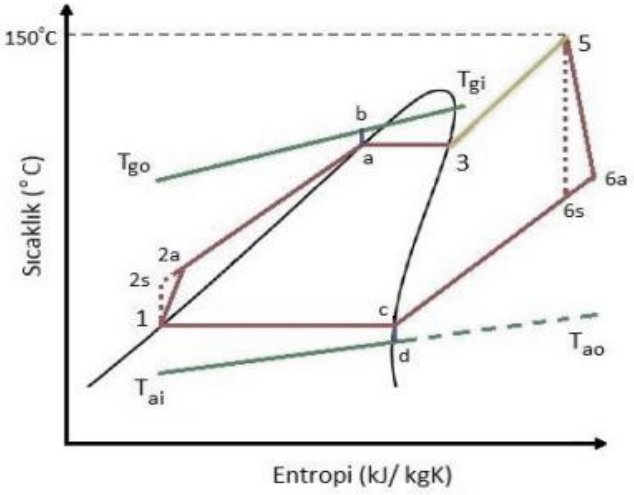


Figure 3.2. Basic t-s diagram of the multigenerational system

In this thesis, studied multigenerational system consists of a hybrid geothermal system located in Gonen district with a solar system at the same region and a ORC system.

Therefore, Gonen the nineth sondage taken values were used for geothermal calculations and also Gonen solar values were used for solar calculations. Solar system utilized in this multigenerational system consists of parabolic trough collectors. In terms of ORC of the multigenerational system, different organic fluids were used to compare the efficiency of the system. ORC besides renewable energy systems solar and geothermal systems utilization is advantageous for energy efficiency and environmental safety as being eco friendly. Ebsilon proffesional programme was used for the simulations of this multigenerational system. In the Figure 3.3, display image of the multigenerational system generated from Ebsilon professional programme can be viewed.

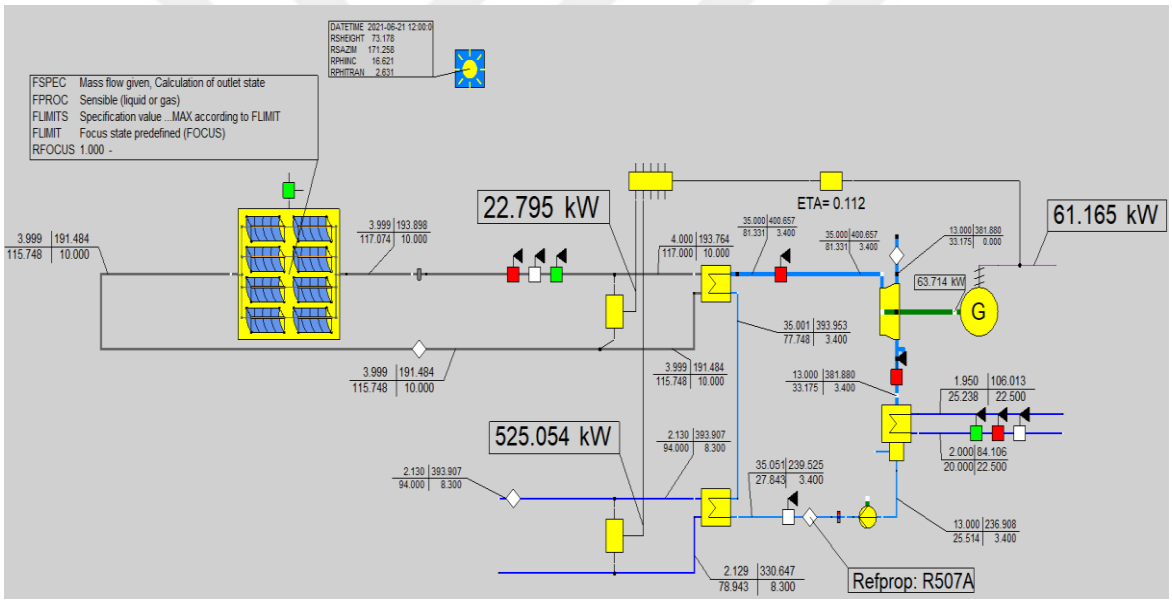


Figure 3.3. Ebsilon proffesional programme display image of the multigenerational system

In order to observe the studied multigenerational system in detail from the Figure 3.3, the solar panels with parabolic trough collectors can be seen on the left upside, the Gonen geothermal system is on the left downside and the ORC system is on the right side with its heat exchangers, pump, condenser, turbine and generator. Additionally, the other colored parts are for temperature, pressure, mass flow and fluid type definitions via Ebsilon Professional programme. For instance, the temperature, pressure and mass flow of solar system were defined with these flagged green, red and white measured value input components for the analyses of simulation. Thus, there are red flagged pressure definition

components before and after the turbine and white flagged mass flow definition component next to pump in the ORC side of this multigenerational system. Temperature, pressure and mass flow of the cooling tower were also defined with these green, red and white flagged components, respectively. Moreover, the fluid definition is made with the diamond shaped white start value components through solar, geothermal and ORC systems. Furthermore, ETA system thermal efficiency calculator is connected to the power summarizer which takes information from difference meters of both solar system and geothermal system.

After designing this multigenerational system with these components, the simulations for the analyses of the system were conducted with the Ebsilon professional programme. Also, seven different organic fluids were applied to the ORC side of the multigenerational system to observe the whole system performances, thermal efficiencies and generator works. Using different organic fluids affects system response of the ORC due to their different specifications.

3.1 Working Fluids Selection Parameters

In order to select an appropriate fluid for the cycle, these critical parameters must be considered: environmental impact (GWP, ODP, biodegradability), second law efficiency, safety of the working fluid (flammability, toxicity), and cost.

A working fluid with low GWP should be chosen to minimize its impact on climate change. High-GWP fluids like hydrofluorocarbons (HFCs) and hydrochlorofluorocarbons (HCFCs) significantly contribute to global warming. Opting for a low-GWP fluid reduces greenhouse gas emissions. In terms of ODP, prioritizing ozone-safe working fluids is essential to avoid harm to the ozone layer [118,119].

Components in the Organic Rankine Cycle (ORC) may wear out over time, leading to fluid leaks. Biodegradability is crucial; if the working fluid contacts the environment directly, it should dissolve easily to prevent harm to ecosystems.

The ORC system aims for heat recovery and power generation using low-to-medium grade heat sources (e.g., solar thermal energy or geothermal energy). Efficient utilization of waste heat is essential. Second Law Efficiency quantifies how effectively waste energy can be harnessed. Balancing 2nd Law efficiency with other factors (thermal efficiency, environmental impact, and cost) is crucial.

When choosing a working fluid, safety is paramount, especially in applications with ignition

sources. Option for non-flammable or low-flammability fluids to significantly reduce fire hazards and ensure the safety of personnel and equipment.

Safeguarding personnel health is crucial, and toxicity plays a significant role in safety considerations. When selecting working fluids, opting for those with low toxicity levels minimizes risks during leaks or exposure. Prioritizing such fluids not only enhances workplace safety but also ensures compliance with health and safety regulations.

When evaluating the feasibility of an ORC system, it's essential to account for both technical and economic factors. In this context, we can divide the investment into two primary components as equipment investment and working fluid investment in terms of cost.

In terms of equipment investment, the costs associated with various ORC system components, including heat exchangers, turbines, pumps, and other hardware. Precise cost estimation for these components is critical for designing an economically efficient system.

In terms of working fluid investment, the choice of working fluid, often referred to as the organic fluid, significantly influences the ORC process. It affects system efficiency, performance, and overall cost. Evaluating the cost of working fluid is essential during investment analysis [120,121].

During cost analysis, this classification is commonly followed to assess the economic viability of ORC systems. However, estimating ORC costs can be challenging due to limited data availability and varying methodologies. Some key points related to ORC investment costs are cost estimation techniques, graphical trends and benchmark case study. Industrial cost estimation practices have a long history. Various techniques exist, but the expected accuracy range for the best research methods typically falls between 10% and 30%. Researchers can enhance estimates by establishing up-to-date correlations specific to the ORC industry. A summary graph of estimated ORC investment costs reveals a trend: as power output increases, costs tend to decrease. Unfortunately, real-world data on actual ORC module costs and projects remain scarce. Analyzing the investment costs of a known heat recovery ORC system provides valuable insights. Different approaches yield varying accuracies (up to +30%). Factorial estimation techniques, such as the module costing technique, tend to yield better results.

In summary, while technical optimization plays a crucial role in ORC development, economic feasibility remains a decisive factor. Improving cost estimation methods and gathering more data from real-world ORC projects will enhance the accuracy of investment

assessments.

Table 3.1. Environmental properties of each fluid [121]

Fluid	**Environmental Effects**			**Safety**	**Regulatory Considerations**
	GWP	**ODP**	**ALT**		
R245fa	950	0	7.6 years	Non-flammable Low toxicity	ASHRAE safety group A1
R1234yf	4	0	11 days	Mildly flammable Low toxicity	ASHRAE safety group A2L
R507A	3985	0	29 to 52 years	Non-flammable Low toxicity	ASHRAE safety group A1
R1233zd	4.5	0.00024	26 days	Non-flammable Low toxicity	ASHRAE safety group A1
R1234ze	7	0	17 days	Mildly flammable Non-toxicity	ASHRAE safety group A2L
R245ca	610	0	6.2 years	Non-flammable Low toxicity	ASHRAE safety group A1
R152A	124	0	1.4 years	Medium flammable Low-toxicity	ASHRAE safety group A2
R134a	1300	0	14 years	Non-flammable Low toxicity	ASHRAE safety group A1

4 ANALYSES OF STUDIED MULTIGENERATION SYSTEM WITH ORC

The analyses of the studied multigenerational system were done with not only Ebsilon professional programme but also EES programme to compare the results. The EES is a highly capable and flexible software tool crafted to address intricate systems of equations, making it particularly advantageous for engineers in various fields. EES provides a range of licensing options to meet different user needs, including student, commercial, and professional licenses. This flexibility ensures that the software is accessible to a wide audience, from students and educators to professional engineers. Some of the prominent features and functionalities of EES are equation solving, thermodynamic and transport properties, optimization and regression, unit conversion and consistency, plotting and visualization, user-friendly interface.

EES is proficient in resolving extensive systems of equations, including thousands of interconnected non-linear algebraic and differential equations. This versatility makes it suitable for a broad spectrum of engineering tasks, from straightforward calculations to complex simulations. A notable feature of EES is its extensive database of thermodynamic and transport properties for numerous substances. This is particularly beneficial for mechanical and chemical engineers who require precise property data for their computations and simulations.

EES comes equipped with robust tools for optimization, uncertainty analysis, and both linear and non-linear regression. These tools are essential for refining models, optimizing processes, and enhancing the accuracy of solutions, ensuring engineers achieve optimal results in their projects. In order to reduce the risk of calculation errors, EES can automatically convert units and verify unit consistency. This feature ensures that all calculations are precise and dependable, saving engineers time and minimizing the likelihood of mistakes.

EES offers sophisticated plotting and visualization capabilities, including high-quality 2D, contour, and 3D plots. These features are crucial for visualizing data and results, enabling engineers to better understand and communicate their findings. Designed with user convenience in mind, EES features an intuitive, menu-driven interface. Along with comprehensive help documentation, this makes the software accessible to both beginners and experienced users [122,123].

EBSILON Professional is a cutting-edge simulation software created by STEAG Energy Services. It is tailored for the planning, design, and optimization of thermodynamic cycle processes, making it an indispensable tool for engineers in the energy sector. Some of the notable features and capabilities of EBSILON Professional are versatile application, accurate simulations, comprehensive libraries, user-friendly interface, error analysis and integration capabilities which supplies optimization, flexibility, support and trust by professionals.

EBSILON Professional is extremely flexible and can be applied to a wide array of projects. These include conventional power plants, nuclear power plants, solar power plants, desalination plants, fuel-cell applications, and various custom processes. This adaptability makes it a valuable resource for engineers handling diverse projects. The software excels in delivering reliable predictions of plant performance and efficiency under various operating conditions. This ability is essential for making well-informed decisions throughout the project lifecycle, from initial feasibility studies to detailed design phases. Engineers can rely on the accuracy of these simulations to guide their planning and optimization efforts.

EBSILON Professional boasts extensive component and material data libraries, encompassing a wide range of working fluids and fuels. These libraries facilitate accurate modeling of different systems, ensuring that all relevant variables are considered in the simulations. The software features an intuitive graphical user interface, designed to be user-friendly for both beginners and experienced users. Additionally, it supports multiple languages, including German, English, French, Spanish, Turkish, and Chinese, enhancing its usability across different regions and user groups [123,124].

EBSILON Professional offers intelligent error analysis and comprehensive online support. These features ensure that users can quickly troubleshoot and resolve any issues, maintaining the efficiency and accuracy of their work. The availability of robust support resources helps users maximize the potential of the software. The software's open architecture and powerful interfaces allow it to be seamlessly integrated into existing software infrastructures. This integration capability ensures that EBSILON Professional can work harmoniously with other tools and systems, enhancing overall workflow efficiency.

EBSILON Professional assists in optimizing plant performance and efficiency, leading to significant cost savings and improved operational reliability. By using the software to fine-tune processes, engineers can achieve better outcomes and enhance the sustainability of their projects. The suitability of the software for a variety of energy systems and processes makes

it a versatile tool for engineers. Whether working on traditional power plants or innovative energy solutions, EBSILON Professional provides the flexibility needed to address different challenges and requirements.

Supported by extensive online resources and documentation, EBSILON Professional ensures that users can access the help they need when they need it. This support network is crucial for maintaining productivity and overcoming any obstacles that may arise during the use of the software. EBSILON Professional is trusted by numerous energy companies, engineering firms, and researchers worldwide. Its reputation as a leading tool in the field of energy system simulation and optimization underscores its reliability and effectiveness in delivering high-quality results [125,126].

Also, seven different organic working fluids, which are R507A, R152A, R245FA, R245CA, R1234yf, R1233zd, R1234ze in the Table 4.1 were used in the analyses to compare the system performance. These working fuids were choosen by considering appropriate fluids for the cycle, since there are four crucial parameters which are effects on environment, 2nd Law efficiency, safety of the working fluid and cost.

The system analyses were based upon the assumptions that all processes are operating at steady state and the thermal, friction losses and the kinetic, potential energy changes are negligible. The heat losses and pressure losses are also negligible. The components such as the turbine in the ORC is isentropic.

Moreover, pressure drops of working fluid in the evaporator and condenser is neglected and the working fluid is in saturated liquid at condenser exit. The isentropic efficiency of expander (turbine) ηt and the pump ηp are 0.80. Atmospheric condition is taken as 1 atm and 293 K.

The outputs such as thermal efficiency, exergy efficiency, turbine work, pump work, heat rejected and heat taken by the cycle were analyzed. After evaluating these parameters with the assumptions, calculations for each organic fluid were made and the results were compared [127].

Table 4.1. Thermo-physical properties of the selected fluids [120]

	R245CA	R507A	R1233zd	R1234yf	R245FA	R152A	R1234ze
Molecular Mass (g/mol)	134.05	98.9	130.5	114.0	134.05	66.05	114.04
Formula	C3F5H3	CF3CHF2 , CF3CH3	C3ClF3H2	C3H2F4	CF3CH2CHF2	C2H4F2	C3F4H2
Critical Temperature (°C)	174.57	70.62	166.6	-29	154.01	113.15	109.52
Critical Pressure (bar)	39.41	37.94	36.237	33.82	36.51	44.96	36.35
Boiling Temperature (°C)	25−26	-52.1	18.1	-30	14.9	-24.7	-16
Tsolarsource (°C)	144	117	193	135	175	131	125
Tsink (°C)	20	20	20	16	20	18	20

Condenser process calculation formula is $Q_{out} = \dot{m}(h_5 - h_1)$ where $\dot{m}$ is mass flow rate of the organic fluid and h_5 is the inlet and h_1 is the outlet enthalpy, respectively. Qout is the amount of heat rejected. Pump Process calculation formula is $W_{in} = \dot{m}(h_{2.a} - h_1)$ where $h_{2.a}$ is the actual outlet enthalpy and $h_1$is the inlet enthalpy. W_{in} is the inlet work to the pump.

Evaporator calculation formulas are $Q_{23} = \dot{m}(h_3 - h_{2,a})$ and $Q_{34} = \dot{m}(h_4 - h_3)$. Here, $Q_{23}$and Q_{34} heat input from geothermal and solar sources, respectively. Turbine process calculation formula is $W_{out} = \dot{m}(h_4 - h_5)$ where Wout is the amount of work received. And the exergy analysis formulas are:

$$x_{heat,34} = \left(1 - \left({}^{T_0}/_{T_{solar}}\right)\right) * Q_{34}$$

$$x_{heat,23} = \left(1 - \left({}^{T_0}/_{T_{geothermal}}\right)\right) * Q_{23}$$

$$x_{expended} = x_{heat,34} + x_{heat,23}$$

$$x_{recovered} = W_{turbine} \quad , \quad n_{sec} = ({}^{x_{recovered}}/_{x_{expended}})$$

4.1 Analysis Of Multigeneration System With R507A Via Ebsilon

In terms of Ebsilon analyses, Figure 3.3 demonstrates Ebsilon sketch of the multigenerational system with R507A organic working fluid for its ORC side. Inspecting this sketch in Figure 3.3, the pressure, temperature, mass flow and entalphy values can be observed. For instance, at left bottom of this sketch, there is Gonen geothermal nineth sondage values 94℃ temperature, 2.13 bar pressure, 8.3 kg/s mass flow of geothermal water were defined through the Ebsilon Professional programme. The heat exchanger connected to the geothermal system, has 27.843℃ input temperature and 77.748℃ output temperature, 35 bar pressure and 3.4 kg/s mass flow and 239.525 kj/kg input entalphy and 393.953 kj/kg output entalphy. At upper left of the sketch, there is parabolic solar panels values were defined to the simulation programme as output temperature 117℃, 4 bar pressure, 10 kg/s mass flow with Therminol VP1 oil fluid. Also, Gonen latitude is 40.1049° and longitude is 27.654°, direct normal irradiance value is 1000 W/m^2, wind speed at Gonen is 5 m/s, and ambient temperature is 20℃ for solar system calculations to run the simulation. The heat exchanger connected to the solar system, has 81.331℃ output temperature, 35 bar pressure and 3.4 kg/s mass flow and 400.657 kj/kg output entalphy. And this heat exchanger is connected to the turbine which has 33.175℃ output temperature, 13 bar output pressure and 3.4 kg/s mass flow, 381.880 kj/kg output entalphy. Then, the condenser connected to this heat exchanger has 33.175℃ output temperature, 13 bar output pressure and 3.4 kg/s mass flow, 236.908 kj/kg output entalphy. Also, the cooling tower, which is connected to the condenser, is defined with 20℃ inlet temperature, 2 bar pressure and 22.5 kg/s mass flow of water. And the pump connected to the condenser has 27.843℃ output temperature, 35 bar output pressure and 3.4 kg/s mass flow, 239.525 kj/kg output entalphy within the organic rankine cycle.

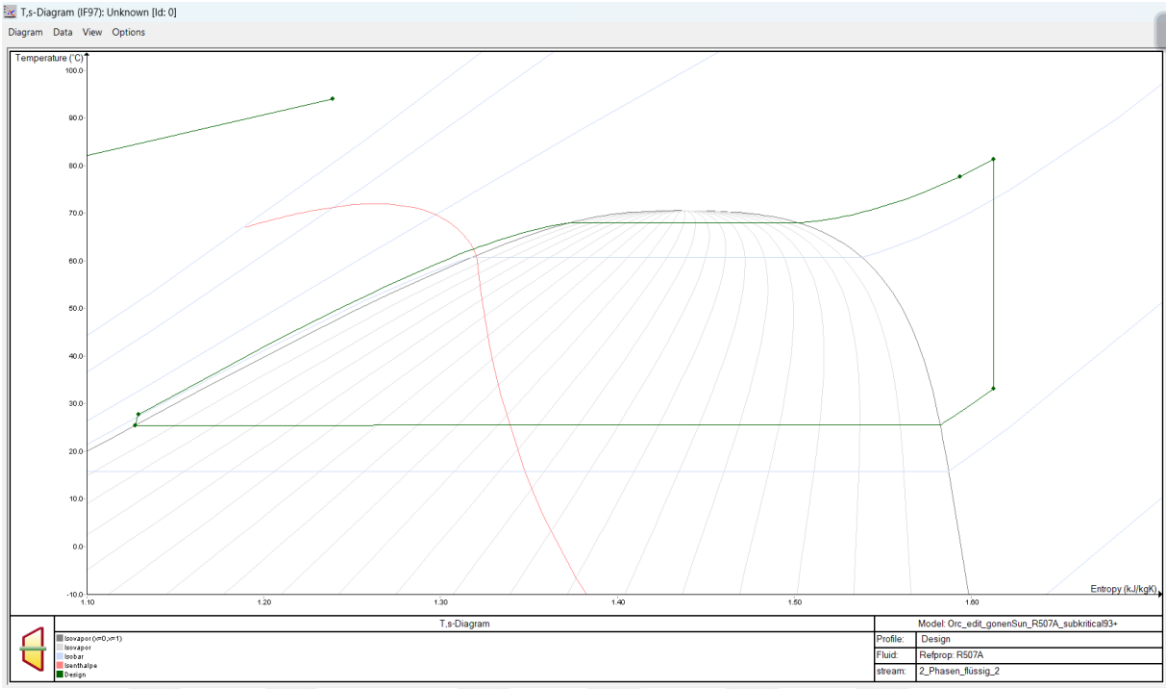


Figure 4. 1. T-s diyagram of the ORC side of the multigeneration system with R507A via Ebsilon Professional programme.

According to these analyzed temperature, pressure values of the components of the multigenerational system, power outputs and ETA thermal efficiency of the system was calculated by Ebsilon Professional programme. Accordingly, the power output of the solar panels for this multigenerational system with R507A is calculated as 22.795 kW, the power output of the geothermal well is calculated as 525.054 kW and the power output of the generator is calculated as 61.165 kW. Thus, ETA thermal efficiency of the multigenerational system was calculated as %11.2 according to the related formula via Ebsilon Professional programme.

4.2 Analysis Of Multigeneration System With R507A Via EES

4.2.1 Energetic thermodynamic analysis of the system with R507A via EES

Besides analyses with the simulation of Ebsilon Professional programme, the system with R507A organic fluid was analyzed thermodynamically with EES programme via the EES codings written in the Appendix A.1.

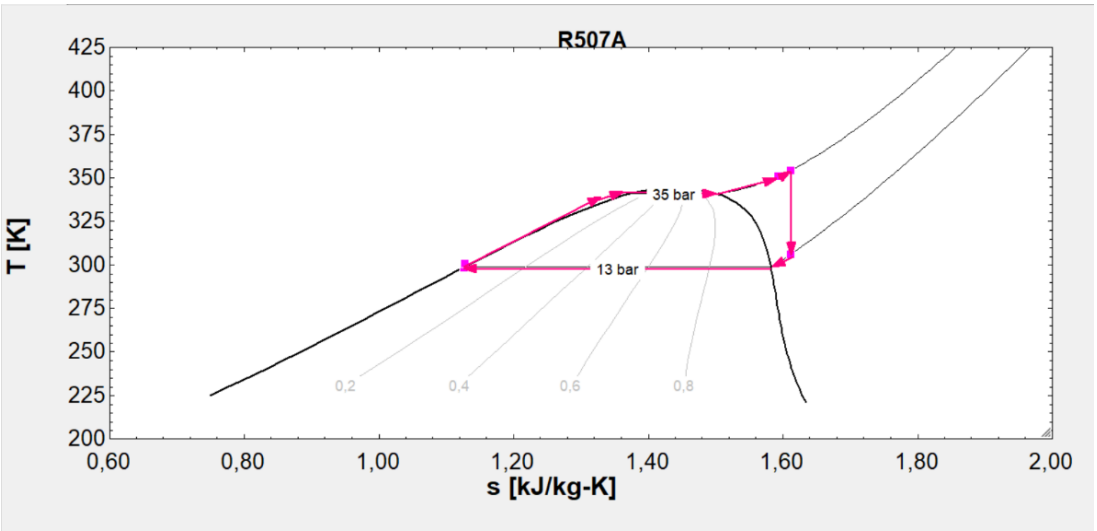


Figure 4.2. T-s diyagram of the ORC side of the multigenerational system with R507A via EES.

The results of energetic analyses of the multigenerational system with R507A, via EES programme is compatible with the results of Ebsilon Professional analyses, which is favorable for crosschecking. Also, t-s diagrams from EES and Ebsilon Professional programmes are also compatible to crosscheck as seen in Figures 4.1 and 4.2.

4.2.2 Exergetic thermodynamic analysis of multigeneration system with R507A via EES

$$\sum \dot{Ex}_{in} - \sum \dot{Ex}_{out} - \dot{Ex}_{dest} = \Delta \dot{E}x_s$$

For steady state $\Delta \dot{Ex}_s = 0$

$$\sum \dot{Ex}_{in} - \sum \dot{Ex}_{out} = \dot{Ex}_{dest}$$

For the isentropic processes (pump and turbine) $s_2 = s_1$, $s_4 = s_5$

$x_{dest} = 0$

Then,

$$x_{dest12} = x_{dest45} = 0$$

Process 2-3 and 3-4 are constant pressure heat addition processes, process 5-1 is constant pressure heat rejection process. These processes are internally reversible.

Due to heat transfer in these processes, the irreversibility occurs between the working fluid and the heat source/sink. $T_0 = 298K$.

For one-inlet, one-exit steady-flow:

$$X_{mass} = \dot{m}\, e_i$$

$$e_i = h_i - h_0 - [T_0(s_i - s_0)]$$

For heat addition processes:

$$X_{dest} = X_{mass} + X_{heat}$$

$$X_{heat_{in}} = Q_{in}(1 - \frac{T_0}{T_H})$$

$$X_{dest} = T_0 \left(s_{out} - s_{in} - (\frac{Q_{in}}{T_H}) \right)$$

For heat rejection processes:

$$X_{dest} = X_{mass} - X_{heat_{out}}$$

$$X_{heat_{out}} = Q_{out}(1 - \frac{T_0}{T_L})$$

$$X_{dest} = T_0 \left(s_{in} - s_{out} + (\frac{Q_{out}}{T_L}) \right)$$

EES codings for exergetic thermodynamic analysis of the system with R507A is in the Appendix A.2. According to these exergy formulations and codings, the values of calculated results can be observed in the Table 4.2 below.

Table 4.2. Results of energy and exergy analyses via EES for R507A fluided hybrid system.

Unit Settings: SI K bar kJ mass deg

h1 = 236,6 [kJ/kg]	$h2_a$ = 239 [kJ/kg]	$h2_s$ = 238,5 [kJ/kg]	h3 = 393,7 [kJ/kg]	h4 = 400,4 [kJ/kg]	h5 = 381,7 [kJ/kg]	h6 = 393,3 [kJ/kg]	h7 = 330,1 [kJ/kg]
$\dot{m}$ = 3,4 [kg/s]	m_{hot} = 8,3 [kg/s]	η_{ij} = 0,5312	$\eta_{ij,eo}$ = 0,6437	η_{pump} = 0,8	η_{th} = 0,1011	P1 = 13 [bar]	P2 = 35 [bar]
P6 = 2,13 [bar]	qin23 = 154,6 [kJ/kg]	qin34 = 6,734 [kJ/kg]	Qin_{23} = 525,7 [kW]	Qin_{34} = 22,89 [kW]	qout51 = 145 [kJ/kg]	Q_{in} = 548,6 [kW]	Q_{out} = 493,2 [kW]
s1 = 1,125 [kJ/(kg*K)]	$s2_a$ = 1,127 [kJ/(kg*K)]	s3 = 1,592 [kJ/(kg*K)]	s4 = 1,611 [kJ/(kg*K)]	s6 = 1,237 [kJ/(kg*K)]	s7 = 1,061 [kJ/(kg*K)]	T1 = 298,5 [K]	T3 = 350,7 [K]
T4 = 354,3 [K]	T6 = 367 [K]	T7 = 351,9 [K]	T_0 = 293 [K]	$T_{h,1}$ = 367 [K]	$T_{h,2}$ = 390 [K]	T_l = 293 [K]	win = 2,425 [kJ/kg]
wout = 18,74 [kJ/kg]	W_{in} = 8,247 [kW]	W_{out} = 63,72 [kW]	x_{dest23} = 12,8 [kJ/kg]	x_{dest34} = 0,5381 [kJ/kg]	x_{dest51} = 2,722 [kJ/kg]	$x_{dest,23}$ = 12,8 [kJ/kg]	$x_{dest,34}$ = 0,5381 [kJ/kg]
x_{exp} = 35,28 [kJ/kg]	$x_{heat,23}$ = 31,18 [kJ/kg]	$x_{heat,34}$ = 1,675 [kJ/kg]	$x_{heat,51}$ = 0 [kJ/kg]	x_{hot} = 97,04 [kW]	$x_{mass,23}$ = -18,37 [kJ/kg]	$x_{mass,34}$ = -1,137 [kJ/kg]	$x_{mass,51}$ = 2,722 [kJ/kg]
$x_{recovered}$ = 18,74 [kJ/kg]							

Click on this line to see the array variables in the Arrays Table window

No unit problems were detected.

Calculation time = 344 ms

Accordingly, the summary of the output parameters can be observed in the Table 4.3.

Table 4.3. Output parameters for R507A fluided hybrid system.

n_th	0,1011
n_exergy	0,5312
W_in[kW]	8,247
W_out[kW]	63,72
Q_in[kW]	548,6
Q_out[kW]	493,2
n_pump	0,8
n_turbine	1

4.3 Analysis Of Multigeneration System With R1234yf Via Ebsilon

In terms of Ebsilon analyses, Figure 4.3 demonstrates Ebsilon sketch of the multigenerational system with R1234yf organic working fluid for its ORC side.

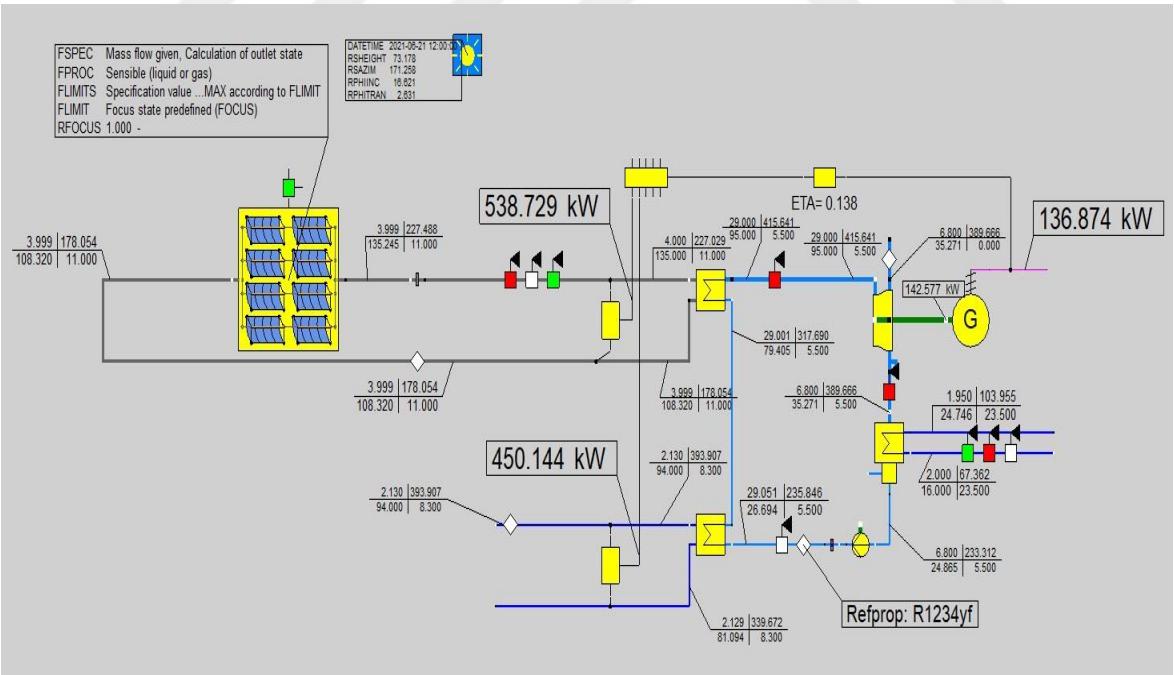


Figure 4.3. Ebsilon display image of the multigenerational system with R1234yf.

Inspecting this sketch in Figure 4.3, the pressure, temperature, mass flow and entalphy values can be observed. For instance, at left bottom of this sketch, there is Gonen geothermal nineth sondage values 94℃ temperature, 2.13 bar pressure, 8.3 kg/s mass flow of geothermal water were defined through the Ebsilon Professional programme. The heat exchanger connected to the geothermal system, has 26.694℃ input temperature and 79.405℃ output temperature, 29 bar pressure and 5.5 kg/s mass flow and 235.846 kj/kg input entalphy and 317.690 kj/kg output entalphy. At upper left of the sketch, there is parabolic solar panels values were defined to the simulation programme as output temperature 135.245℃, 4 bar pressure, 11 kg/s mass flow with Therminol VP1 oil fluid.

As mentioned, Gonen latitude is 40.1049° and longitude is 27.654°, direct normal irradiance value is 1000 W/m^2, wind speed at Gonen is 5 m/s, and ambient temperature is 20℃ for solar system calculations to run the simulation. The heat exchanger connected to the solar system, has 95℃ output temperature, 29 bar pressure and 5.5 kg/s mass flow and 415.641 kj/kg output entalphy. And this heat exchanger is connected to the turbine which has 35.271℃ output temperature, 6.8 bar output pressure and 5.5 kg/s mass flow, 389.666 kj/kg output entalphy. Then, the condenser connected to this heat exchanger has 24.865℃ output temperature, 6.8 bar output pressure and 5.5 kg/s mass flow, 233.312 kj/kg output entalphy. Also, the cooling tower, which is connected to the condenser, is defined with 16℃ inlet temperature, 2 bar pressure and 23.5 kg/s mass flow of water. And the pump connected to the condenser has 26.694℃ output temperature, 29 bar output pressure and 5.5 kg/s mass flow, 235.846 kj/kg output entalphy within the organic rankine cycle. Thus, the source temperature Tsource and the sink temperature Tsink for the solar system as 135℃, 16℃, respectively. Additionally, Tsource for the geothermal system is taken as 94℃ and Tenvironment as 20℃ for all working fluids.

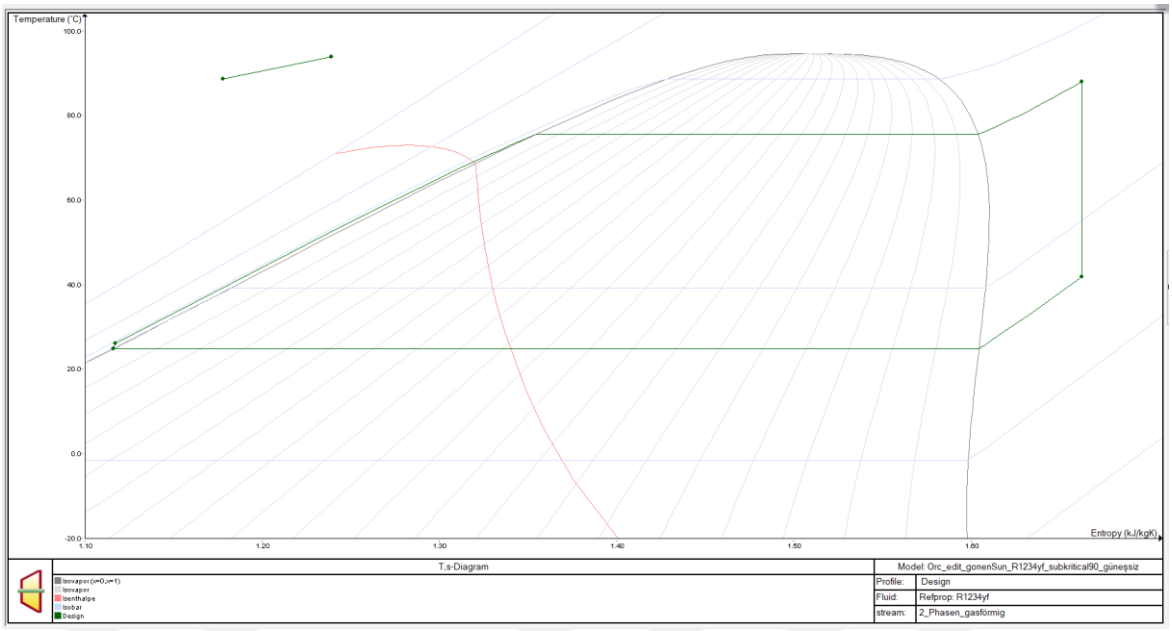


Figure 4.4. T-s diyagram of the ORC side of the multigenerational system with R1234yf via Ebsilon Professional programme.

According to these analyzed temperature, pressure values of the components of the multigeneration system, power outputs and ETA thermal efficiency of the system was calculated by Ebsilon Professional programme. Accordingly, the power output of the solar panels for this multigenerational system with R1234yf is calculated as 538.729 kW, the power output of the geothermal well is calculated as 450.144 kW and the power output of the generator is calculated as 136.874 kW. Thus, ETA thermal efficiency of the multigenerational system was calculated as %13.8 according to the related formula via Ebsilon Professional programme.

4.4 Analysis Of Multigeneration System With R1234yf Via EES

4.4.1 Energetic thermodynamic analysis of the system with R1234yf via EES

Besides analyses with the simulation of Ebsilon Professional programme, the system with R1234yf organic fluid was analyzed thermodynamically with EES programme via the EES codings written in the Appendix A.3.

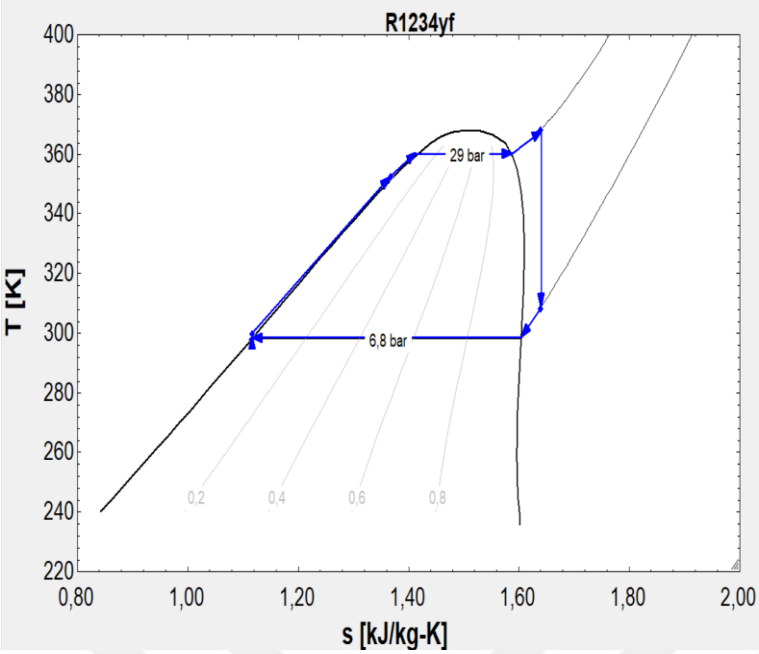


Figure 4.5. T-s diyagram of the ORC side of the multigenerational system with R1234yf via EES.

The results of energetic analyses of the multigenerational system with R1234yf, via EES programme is compatible with the results of Ebsilon Professional analyses, which is favorable for crosschecking. Also, t-s diagrams from EES and Ebsilon Professional programmes are also compatible to crosscheck as seen in Figures 4.4 and 4.5.

4.4.2 Exergetic thermodynamic analysis of multigeneration system with R1234yf via EES

EES codings for exergetic thermodynamic analysis of the system with R1234yf is in the Appendix A.4. According to these codings and exergy formulations, the values of calculated results can be observed in the Table 4.4.

Table 4.4. Results of energy and exergy analyses via EES for R1234yf fluided hybrid system



Unit Settings: SI K bar kJ mass deg

$h1 = 233,1$ [kJ/kg]	$h2_a = 235,6$ [kJ/kg]	$h2_s = 235,1$ [kJ/kg]	$h3 = 317,4$ [kJ/kg]	$h4 = 415,4$ [kJ/kg]
$h5 = 389,4$ [kJ/kg]	$\dot{m} = 5,5$ [kg/s]	$n_{pump} = 0,8$	$n_{th} = 0,1303$	$P1 = 6,8$ [bar]
$P2 = 29$ [bar]	$qin23 = 81,79$ [kJ/kg]	$qin34 = 97,96$ [kJ/kg]	$Qin_{23} = 449,9$ [kW]	$Qin_{34} = 538,8$ [kW]
$qout51 = 156,3$ [kJ/kg]	$Q_{in} = 988,6$ [kW]	$Q_{out} = 859,8$ [kW]	$s1 = 1,115$ [kJ/(kg*K)]	$s2_a = 1,116$ [kJ/(kg*K)]
$s3 = 1,367$ [kJ/(kg*K)]	$s4 = 1,639$ [kJ/(kg*K)]	$T1 = 297,9$ [K]	$T3 = 352,4$ [K]	$T4 = 368$ [K]
$T_0 = 298$ [K]	$T_{h,1} = 367$ [K]	$T_{h,2} = 466$ [K]	$T_l = 293$ [K]	$W_{in} = 13,74$ [kW]
$W_{out} = 142,6$ [kW]	$x_{dest23} = 8,189$ [kJ/kg]	$x_{dest34} = 18,42$ [kJ/kg]	$x_{dest51} = 2,831$ [kJ/kg]	$x_{dest,23} = 8,189$ [kJ/kg]
$x_{dest,34} = 18,42$ [kJ/kg]	$x_{dest,51} = 2,831$ [kJ/kg]	$x_{heat,23} = 15,38$ [kJ/kg]	$x_{heat,34} = 35,32$ [kJ/kg]	$x_{heat,51} = -2,668$ [kJ/kg]
$x_{mass,23} = -7,189$ [kJ/kg]	$x_{mass,34} = -16,9$ [kJ/kg]	$x_{mass,51} = 0,1631$ [kJ/kg]		

Click on this line to see the array variables in the Arrays Table window

No unit problems were detected.

Calculation time = 125 ms

Accordingly, the summary of output parameters can be observed in the Table 4.5.

Table 4.5. Output parameters for R1234yf fluided hybrid system.

n_th	0,1303
n_exergy	0,4903
W_in[kW]	13,74
W_out[kW]	142,6
Q_in[kW]	988,6
Q_out[kW]	859,8
n_pump	0,8
n_turbine	0,998

4.5 Analysis Of Multigeneration System With R245fa Via Ebsilon

In terms of Ebsilon analyses, Figure 4.6 demonstrates Ebsilon sketch of the multigeneration system with R245fa organic working fluid for its ORC side.

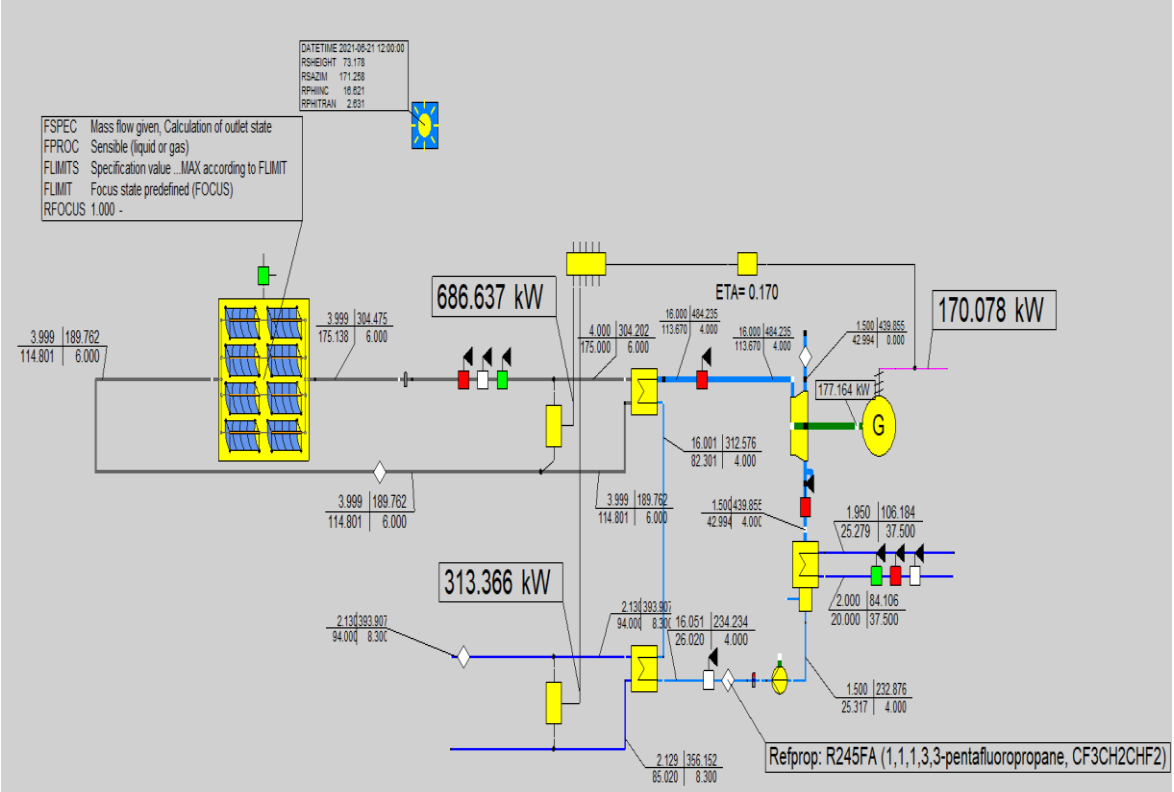


Figure 4.6. Ebsilon display image of the multigenerational system with R245fa.

Inspecting this sketch in Figure 4.6, the pressure, temperature, mass flow and entalphy values can be observed. For instance, at left bottom of this sketch, there is Gonen geothermal nineth sondage values 94°C temperature, 2.13 bar pressure, 8.3 kg/s mass flow of geothermal water were defined through the Ebsilon Professional programme. The heat exchanger connected to the geothermal system, has 26.02°C input temperature and 82.301°C output temperature, 16 bar pressure and 4 kg/s mass flow and 234.234 kj/kg input entalphy and 312.576 kj/kg output entalphy. At upper left of the sketch, there is parabolic solar panels values were defined to the simulation programme as output temperature 175.138°C, 4 bar pressure, 6 kg/s mass flow with Therminol VP1 oil fluid. As mentioned, Gonen latitude is 40.1049° and longitude is 27.654°, direct normal irradiance value is 1000 W/m^2, wind speed at Gonen is 5 m/s, and ambient temperature is 20°C for solar system calculations to run the simulation.

The heat exchanger connected to the solar system, has 113.67℃ output temperature, 16 bar pressure and 4 kg/s mass flow and 484.235 kj/kg output entalphy. And this heat exchanger is connected to the turbine which has 42.994℃ output temperature, 1.5 bar output pressure and 4 kg/s mass flow, 439.855 kj/kg output entalphy. Then, the condenser connected to this heat exchanger has 25.317℃ output temperature, 1.5 bar output pressure and 4 kg/s mass flow, 232.876 kj/kg output entalphy. Also, the cooling tower, which is connected to the condenser, is defined with 20℃ inlet temperature, 2 bar pressure and 37.5 kg/s mass flow of water. And the pump connected to the condenser has 26.02℃ output temperature, 16 bar output pressure and 4 kg/s mass flow, 234.234 kj/kg output entalphy within the organic rankine cycle. Thus, the source temperature Tsource and the sink temperature Tsink for the solar system is as 175℃ and 20℃, respectively. Additionally, Tsource for the geothermal system is taken as 94℃ and Tenvironment as 20℃ for all working fluids.

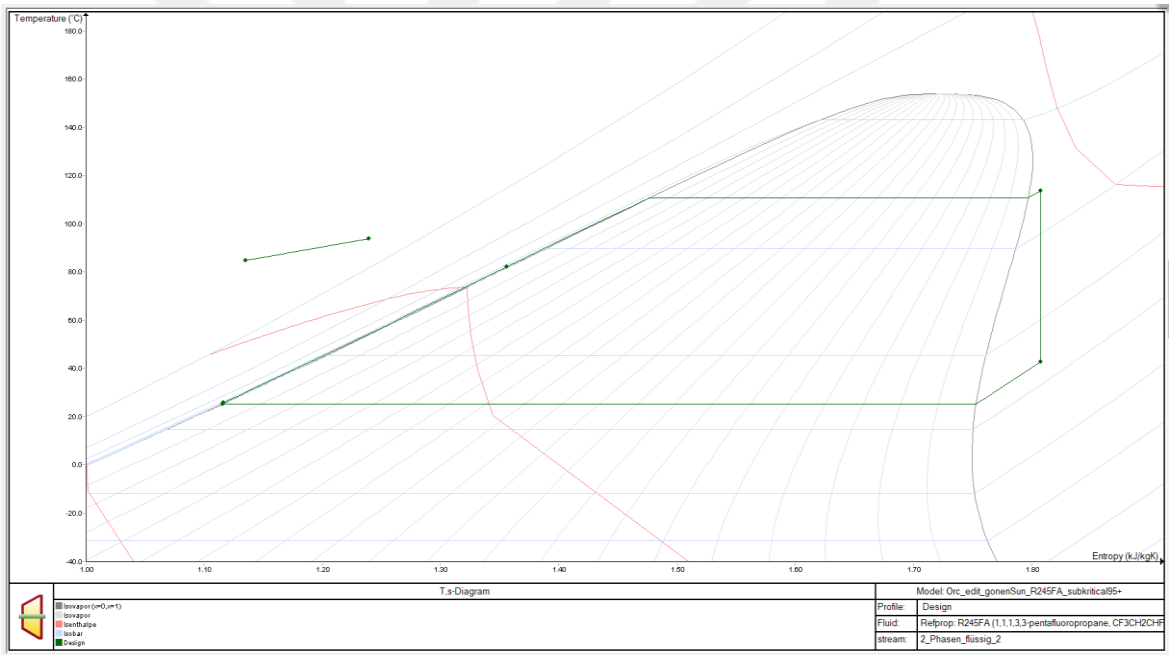


Figure 4.7. T-s diyagram of the ORC side of the multigenerational system with R245fa via Ebsilon Professional programme.

According to these analyzed temperature, pressure values of the components of the multigenerational system, power outputs and ETA thermal efficiency of the system was calculated by Ebsilon Professional programme. Accordingly, the power output of the solar panels for this multigenerational system with R245fa is calculated as 686.637 kW, the power output of the geothermal well is calculated as 313.366 kW and the power output of the

generator is calculated as 170.078 kW. Thus, ETA thermal efficiency of the multigenerational system was calculated as %17 according to the related formula via Ebsilon Professional programme.

4.6 Analysis Of Multigeneration System With R245fa Via EES

4.6.1 Energetic thermodynamic analysis of the system with R245fa via EES

Besides analyses with the simulation of Ebsilon Professional programme, this multigenerational system with R245fa organic fluid was analyzed thermodynamically with EES programme via the EES codings written in the Appendix A.5.

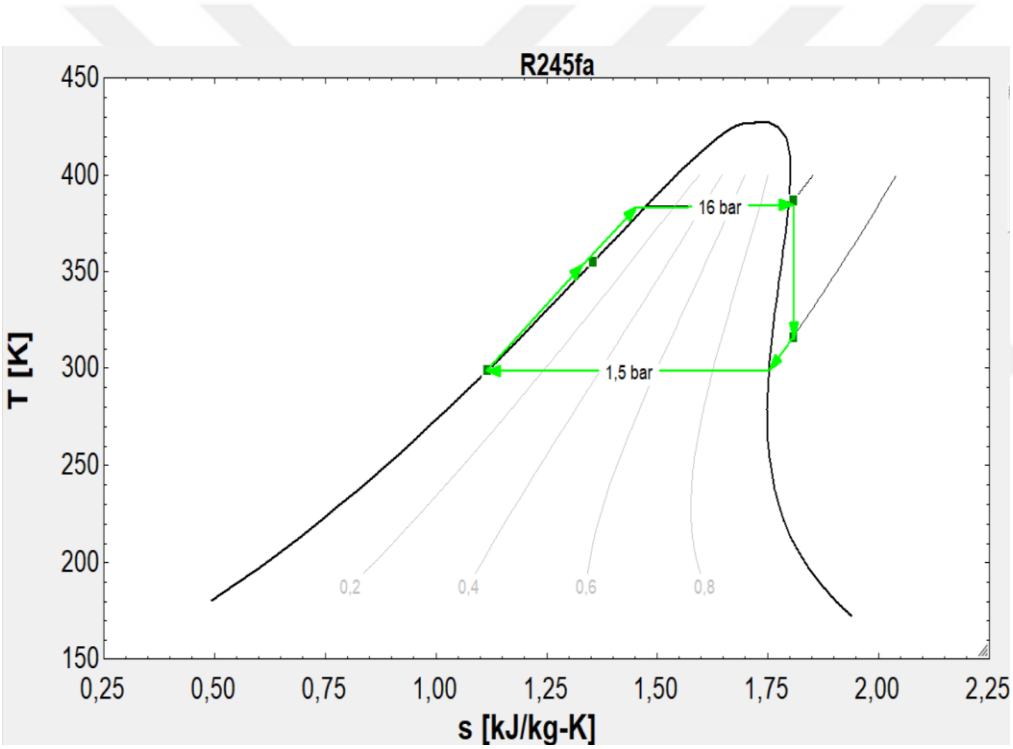


Figure 4.8. T-s diyagram of the ORC side of the multigenerational system with R245fa via EES.

The results of energetic analyses of the multigenerational system with R245fa, via EES programme is compatible with the results of Ebsilon Professional analyses, which is favorable for crosschecking. Also, t-s diagrams from EES and Ebsilon Professional programmes are also compatible to crosscheck as seen in Figures 4.7 and 4.8.

4.6.2 Exergetic thermodynamic analysis of multigeneration system with R245fa via EES

EES codings for exergetic thermodynamic analysis of the system with R1234yf is in the Appendix A.6. According to these codings and exergy formulations, the values of calculated results can be observed in the Table 4.6.

Table 4.6. Results of energy and exergy analyses via EES for R245FA fluided hybrid system.

Unit Settings: SI K bar kJ mass deg

h1 = 232,7 [kJ/kg]	$h2_a$ = 234 [kJ/kg]	$h2_s$ = 233,8 [kJ/kg]	h3 = 312,4 [kJ/kg]	h4 = 484 [kJ/kg]	h5 = 439,7 [kJ/kg]	h6 = 393,3 [kJ/kg]	h7 = 355,6 [kJ/kg]
$\dot{m}$ = 4 [kg/s]	m_{hot} = 8,3 [kg/s]	η_t = 0,5793	η_{pump} = 0,8	η_{sec} = 0,5793	η_{th} = 0,172	P1 = 1,5 [bar]	P2 = 16 [bar]
P6 = 2,13 [bar]	qin23 = 78,32 [kJ/kg]	qin34 = 171,7 [kJ/kg]	Qin_{23} = 313,3 [kW]	Qin_{34} = 686,7 [kW]	qout51 = 207 [kJ/kg]	Q_{in} = 1000 [kW]	Q_{eo} = 313,4 [kW]
Q_{out} = 828 [kW]	s1 = 1,114 [kJ/(kg*K)]	$s2_a$ = 1,115 [kJ/(kg*K)]	s3 = 1,355 [kJ/(kg*K)]	s4 = 1,806 [kJ/(kg*K)]	s6 = 1,237 [kJ/(kg*K)]	s7 = 1,133 [kJ/(kg*K)]	T1 = 298,3 [K]
T3 = 355,3 [K]	T4 = 386,7 [K]	T6 = 367 [K]	T7 = 358 [K]	T_0 = 293 [K]	$T_{h,1}$ = 367 [K]	$T_{h,2}$ = 448 [K]	T_l = 293 [K]
win = 1,353 [kJ/kg]	wout = 44,34 [kJ/kg]	W_{in} = 5,412 [kW]	W_{out} = 177,4 [kW]	x_{dest23} = 7,672 [kJ/kg]	x_{dest34} = 20,01 [kJ/kg]	x_{dest51} = 4,253 [kJ/kg]	$x_{dest,23}$ = 7,672 [kJ/kg]
$x_{dest,34}$ = 20,01 [kJ/kg]	x_{exp} = 76,54 [kJ/kg]	$x_{expended}$ = 306,2 [kW]	x_{heat34} = 237,6 [kW]	$x_{heat,23}$ = 15,79 [kJ/kg]	$x_{heat,34}$ = 59,39 [kJ/kg]	$x_{heat,51}$ = 0 [kJ/kg]	$x_{heat,67}$ = 63,19 [kW]
x_{hot} = 60,08 [kW]	$x_{kazanilan}$ = 177,4 [kW]	$x_{mass,23}$ = -8,121 [kJ/kg]	$x_{mass,34}$ = -39,39 [kJ/kg]	$x_{mass,51}$ = 4,253 [kJ/kg]	$x_{recovered}$ = 44,34 [kJ/kg]		

Click on this line to see the array variables in the Arrays Table window

No unit problems were detected.

Calculation time = 421 ms

Accordingly, the summary of output parameters can be observed in the Table 4.7.

Table 4.7. Output parameters for R245FA fluided hybrid system

n_th	0,172
n_exergy	0,5793
W_out[kW]	177,4
W_in[kW]	5,412
Q_in[kW]	1000
Q_out[kW]	828
n_pump	0,8
n_turbine	0,998

4.7 Analysis Of Multigeneration System With R1233zd Via Ebsilon

In terms of Ebsilon analyses, Figure 4.9 demonstrates Ebsilon sketch of the multigenerational system with R1233zd organic working fluid for its ORC side.

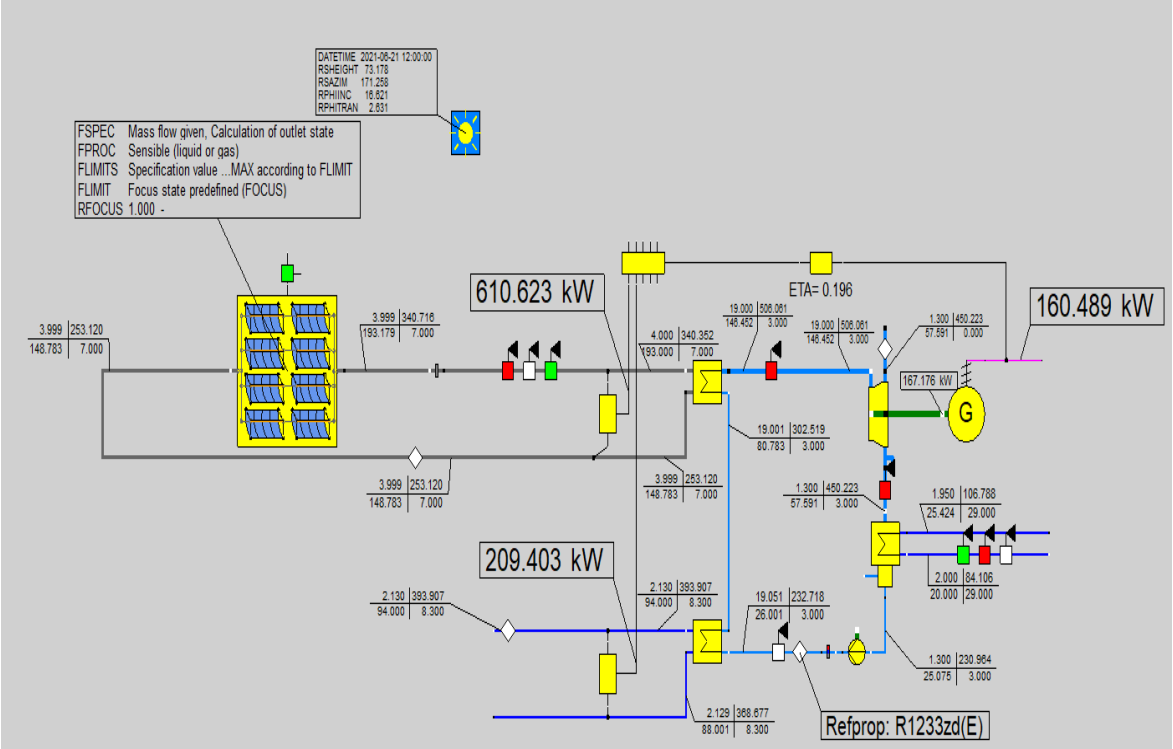


Figure 4.9. Ebsilon display image of the multigenerational system with R1233zd

Inspecting this sketch in Figure 4.9, the pressure, temperature, mass flow and entalphy values can be observed. For instance, at left bottom of this sketch, there is Gonen geothermal nineth sondage values 94°C temperature, 2.13 bar pressure, 8.3 kg/s mass flow of geothermal water were defined through the Ebsilon Professional programme. The heat exchanger connected to the geothermal system, has 26.001°C input temperature and 80.783°C output temperature, 19 bar pressure and 3 kg/s mass flow and 232.718 kj/kg input entalphy and 302.519 kj/kg output entalphy. At upper left of the sketch, there is parabolic solar panels values were defined to the simulation programme as output temperature 193.179°C, 4 bar pressure, 7 kg/s mass flow with Therminol VP1 oil fluid.

As mentioned, Gonen latitude is 40.1049° and longitude is 27.654°, direct normal irradiance value is 1000 W/m^2, wind speed at Gonen is 5 m/s, and ambient temperature is 20°C for solar system calculations to run the simulation. The heat exchanger connected to the solar

system, has 146.452℃ output temperature, 19 bar pressure and 3 kg/s mass flow and 506.061 kj/kg output entalphy. And this heat exchanger is connected to the turbine which has 57.591℃ output temperature, 1.3 bar output pressure and 3 kg/s mass flow, 450.223 kj/kg output entalphy. Then, the condenser connected to this heat exchanger has 25.075℃ output temperature, 1.3 bar output pressure and 3 kg/s mass flow, 230.964 kj/kg output entalphy. Also, the cooling tower, which is connected to the condenser, is defined with 20℃ inlet temperature, 2 bar pressure and 29 kg/s mass flow of water. And the pump connected to the condenser has 26.001℃ output temperature, 19 bar output pressure and 3 kg/s mass flow, 232.718 kj/kg output entalphy within the organic rankine cycle.

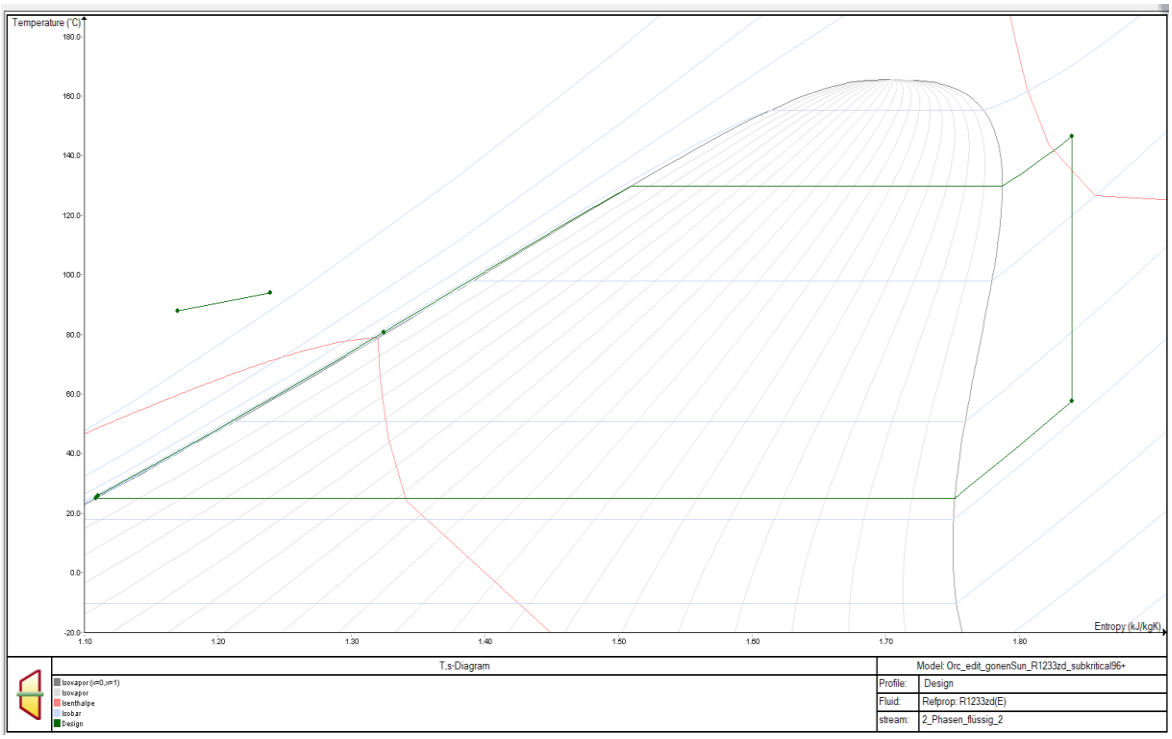


Figure 4.10. T-s diyagram of the ORC side of the multigenerational system with R1233zd via Ebsilon

According to these analyzed temperature, pressure values of the components of the multigenerational system, power outputs and ETA thermal efficiency of the system was calculated by Ebsilon Professional programme. Accordingly, the power output of the solar panels for this multigenerational system with R1233zd is calculated as 610.623 kW, the power output of the geothermal well is calculated as 209.403 kW and the power output of the generator is calculated as 160.489 kW. Thus, ETA thermal efficiency of the multigenerational system was calculated as %19.6 according to the related formula via Ebsilon Professional programme.

4.8 Analysis Of Multigeneration System With R1233zd Via EES

4.8.1 Energetic thermodynamic analysis of the system with R1233zd via EES

Besides analyses with the simulation of Ebsilon Professional programme, this multigenerational system with R1233zd organic fluid was analyzed thermodynamically with EES programme via the EES codings written in the Appendix A.7.

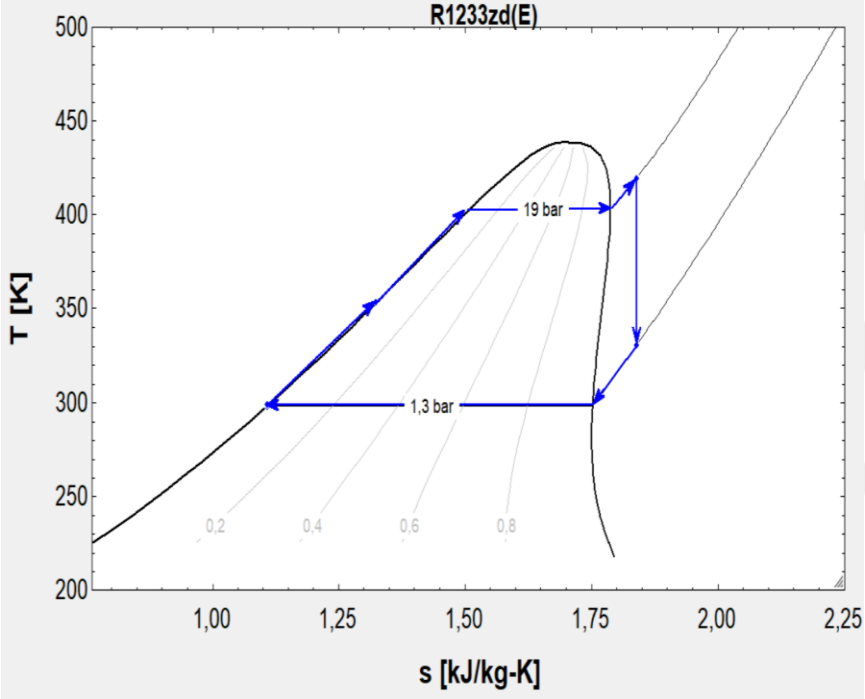


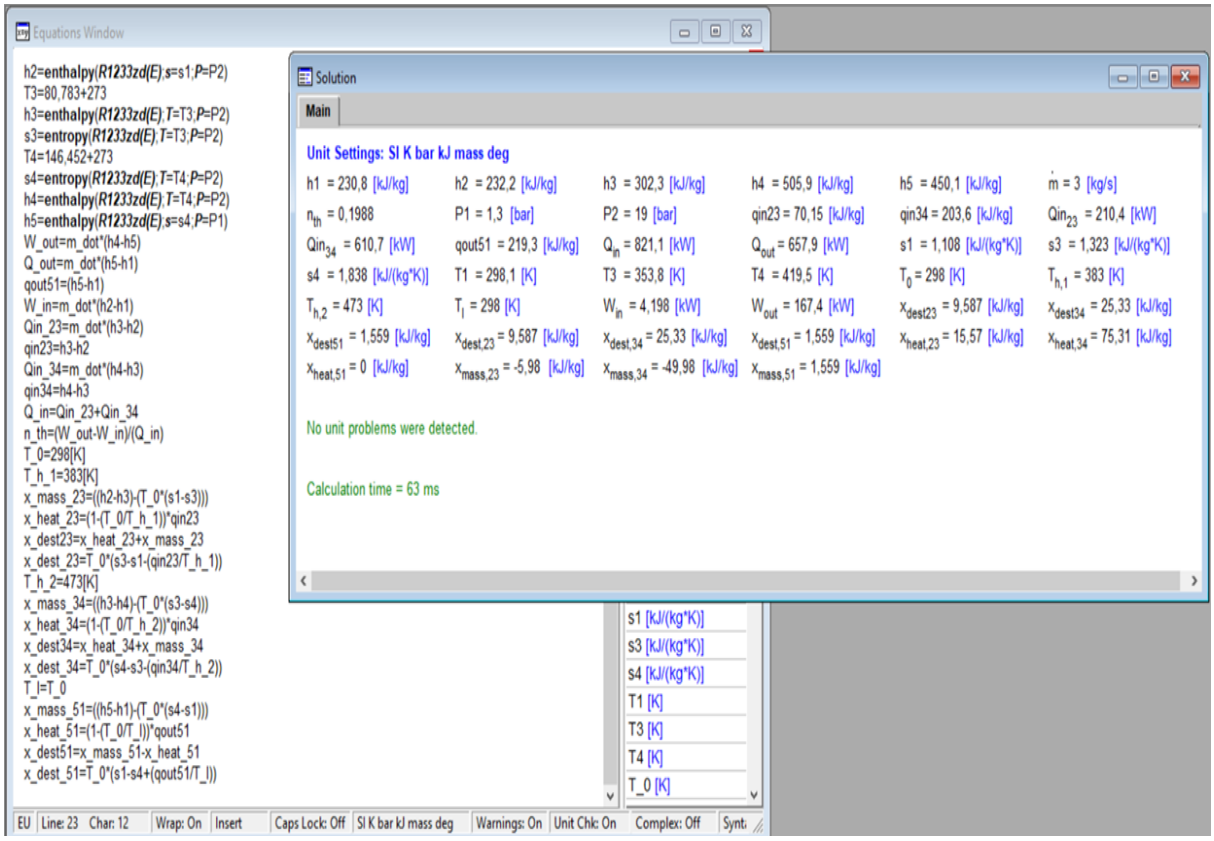
Figure 4.11. T-s diyagram of the ORC side of the multigenerational system with R1233zd via EES

The results of energetic analyses of the multigenerational system with R1233zd, via EES programme is compatible with the results of Ebsilon Professional analyses, which is favorable for crosschecking. Also, t-s diagrams from EES and Ebsilon Professional programmes are also compatible to crosscheck as seen in Figures 4.10 and 4.11.

4.8.2 Exergetic thermodynamic analysis of multigeneration system with R1233zd via EES

EES codings for exergetic thermodynamic analysis of the system with R1233zd is in the Appendix A.8. According to these codings and exergy formulations, the values of calculated results can be observed in the Table 4.8.

Table 4.8. Results of energy and exergy analyses via EES for R1233zd fluided hybrid system.



Accordingly, the summary of output parameters can be observed in the Table 4.9

Table 4.9. Output parameters for R1233zd fluided hybrid system.

n_th	0,1977
n_exergy	0,6105
W_in (kW)	5,248
W_out (kW)	167,4
Q_in (kW)	820,1
Q_out (kW)	657,9
n_pump	0,8
n_turbine	0,998

4.9 Analysis Of Multigeneration System With R1234ze Via Ebsilon

In terms of Ebsilon analyses, Figure 4.12 demonstrates Ebsilon sketch of the multigeneration system with R1234ze organic working fluid for its ORC side.

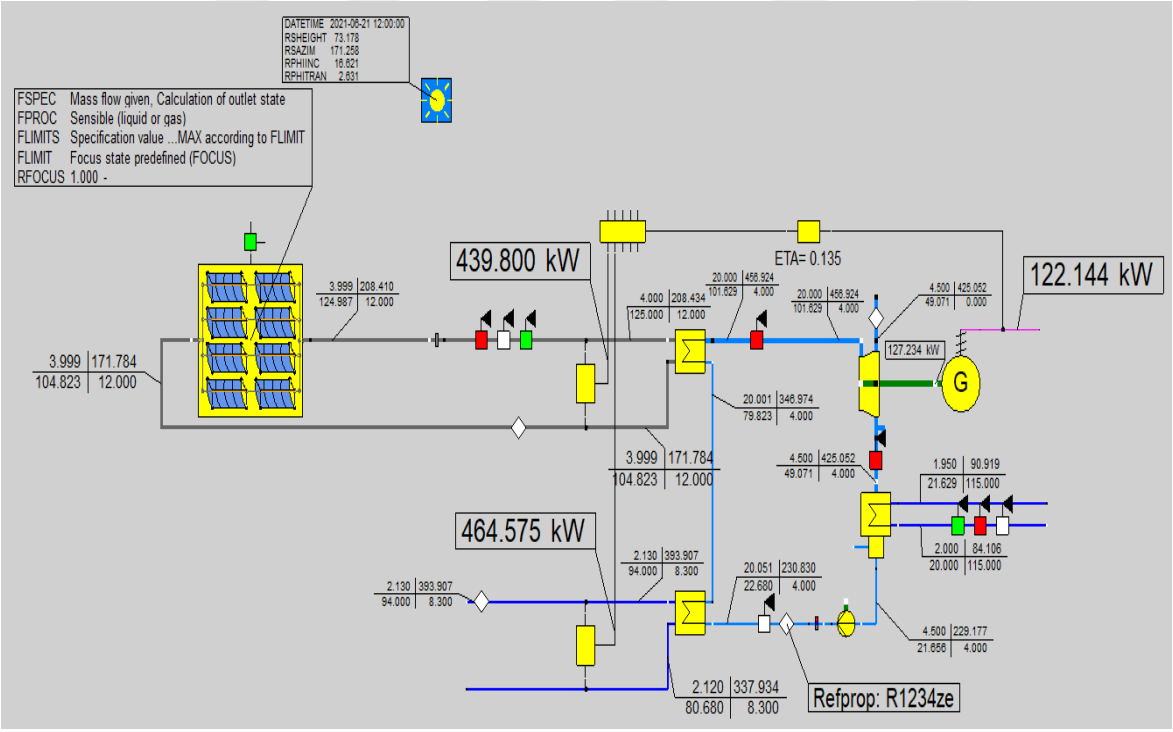


Figure 4.12. Ebsilon display image of the multigenerational system with R1234ze

Inspecting this sketch in Figure 4.12, the pressure, temperature, mass flow and entalphy values can be observed. For instance, at left bottom of this sketch, there is Gonen geothermal

nineth sondage values 94℃ temperature, 2.13 bar pressure, 8.3 kg/s mass flow of geothermal water were defined through the Ebsilon Professional programme. The heat exchanger connected to the geothermal system, has 22.680℃ input temperature and 79.823℃ output temperature, 20 bar pressure and 4 kg/s mass flow and 230.83 kj/kg input entalphy and 346.974 kj/kg output entalphy. At upper left of the sketch, there is parabolic solar panels values were defined to the simulation programme as output temperature 125℃, 4 bar pressure, 12 kg/s mass flow with Therminol VP1 oil fluid.

As mentioned, Gonen latitude is 40.1049° and longitude is 27.654°, direct normal irradiance value is 1000 W/m^2, wind speed at Gonen is 5 m/s, and ambient temperature is 20℃ for solar system calculations to run the simulation. The heat exchanger connected to the solar system, has 101.629℃ output temperature, 20 bar pressure and 4 kg/s mass flow and 456.924 kj/kg output entalphy. And this heat exchanger is connected to the turbine which has 49.071℃ output temperature, 4.5 bar output pressure and 4 kg/s mass flow, 425.052 kj/kg output entalphy. Then, the condenser connected to this heat exchanger has 21.656℃ output temperature, 4.5 bar output pressure and 4 kg/s mass flow, 229.177 kj/kg output entalphy. Also, the cooling tower, which is connected to the condenser, is defined with 20℃ inlet temperature, 2 bar pressure and 115 kg/s mass flow of water. And the pump connected to the condenser has 22.680℃ output temperature, 20 bar output pressure and 4 kg/s mass flow, 230.830 kj/kg output entalphy within the organic rankine cycle.

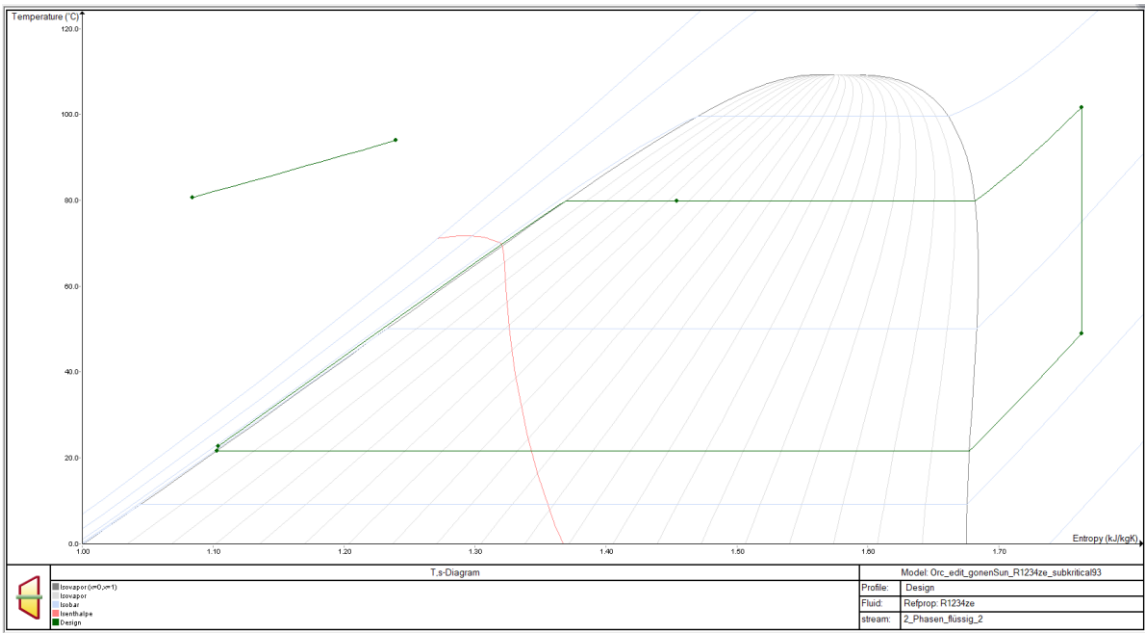


Figure 4.13. T-s diyagram of the ORC side of the multigenerational system with R1234ze via Ebsilon

According to these analyzed temperature, pressure values of the components of the multigenerational system, power outputs and ETA thermal efficiency of the system was calculated by Ebsilon Professional programme. Accordingly, the power output of the solar panels for this multigenerational system with R1234ze is calculated as 439.800 kW, the power output of the geothermal well is calculated as 464.575 kW and the power output of the generator is calculated as 122.144 kW. Thus, ETA thermal efficiency of the multigenerational system was calculated as %13.5 according to the related formula via Ebsilon Professional programme.

4.10 Analysis Of Multigeneration System With R1234ze Via EES

4.10.1 Energetic thermodynamic analysis of the system with R1234ze via EES

Besides analyses with the simulation of Ebsilon Professional programme, this multigenerational system with R1234ze organic fluid was analyzed thermodynamically with EES programme via the EES codings written in the Appendix A.9.

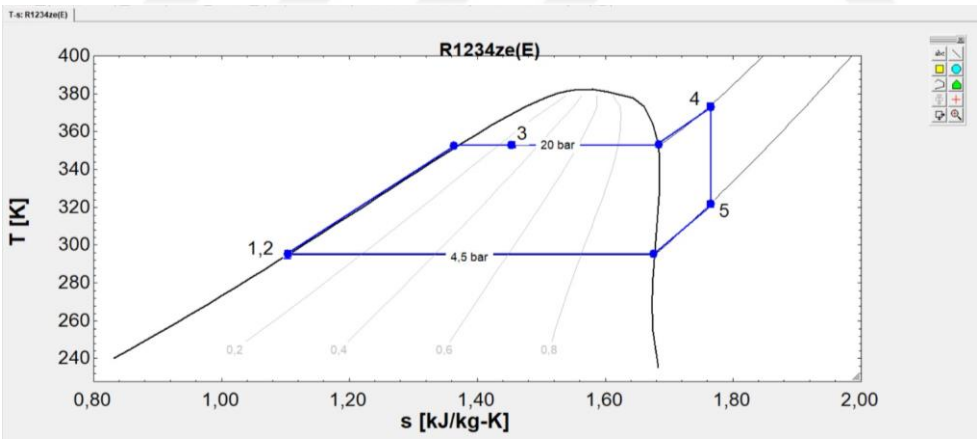


Figure 4.14. T-s diyagram of the ORC side of the multigenerational system with R1234ze via EES.

The results of energetic analyses of the multigenerational system with R1234ze, via EES programme is compatible with the results of Ebsilon Professional analyses, which is favorable for crosschecking. Also, t-s diagrams from EES and Ebsilon Professional programmes are also compatible to crosscheck as seen in Figures 4.13 and 4.14.

4.10.2 Exergetic thermodynamic analysis of multigeneration system with R1234ze via EES

EES codings for exergetic thermodynamic analysis of the system with R1233zd is in the Appendix A.10. According to these codings and exergy formulations, the values of calculated results can be observed in the Table 4.10.

Table 4.10. Results of energy and exergy analyses via EES for R1234ze fluided hybrid system

Unit Settings: SI K bar kJ mass deg								
$h1 = 229,2$ [kJ/kg]	$h2_a = 230,8$ [kJ/kg]	$h3 = 347$ [kJ/kg]	$h4 = 456,9$ [kJ/kg]	$h5 = 425,1$ [kJ/kg]	$\dot{m} = 4$ [kg/s]	$\eta_t = 0,5894$	$\eta_{pump} = 0,8$	$\eta_{th} = 0,1337$
$P1 = 4,5$ [bar]	$P2 = 20$ [bar]	$Qin_{23} = 464,6$	$Qin_{34} = 439,8$	$Q_{in} = 904,4$	$Q_{in,1} = 464,6$ [kW]	$Q_{in,2} = 439,8$ [kW]	$Q_{out} = 783,5$	$s1 = 1,102$ [(kJ)/(kg*K)]
$s2 = 1,103$ [(kJ)/(kg*K)]	$s3 = 1,454$ [(kJ)/(kg*K)]	$s4 = 1,763$ [(kJ)/(kg*K)]	$s5 = 1,763$	$T1 = 294,7$	$T2 = 295,7$	$T3 = 352,8$	$T_0 = 293$ [K]	$T_{h,1} = 367$ [K]
$T_{h,2} = 398$ [K]	$W_{in} = 6,612$	$W_{out} = 127,5$	$x_{exp} = 216,3$	$x_{heat,23} = 93,67$	$x_{heat,34} = 116$	$x_{recovered} = 127,5$		

4.11 Analysis Of Multigeneration System With R152A Via Ebsilon

In terms of Ebsilon analyses, Figure 4.15 demonstrates Ebsilon sketch of the multigeneration system with R152A organic working fluid for its ORC side.

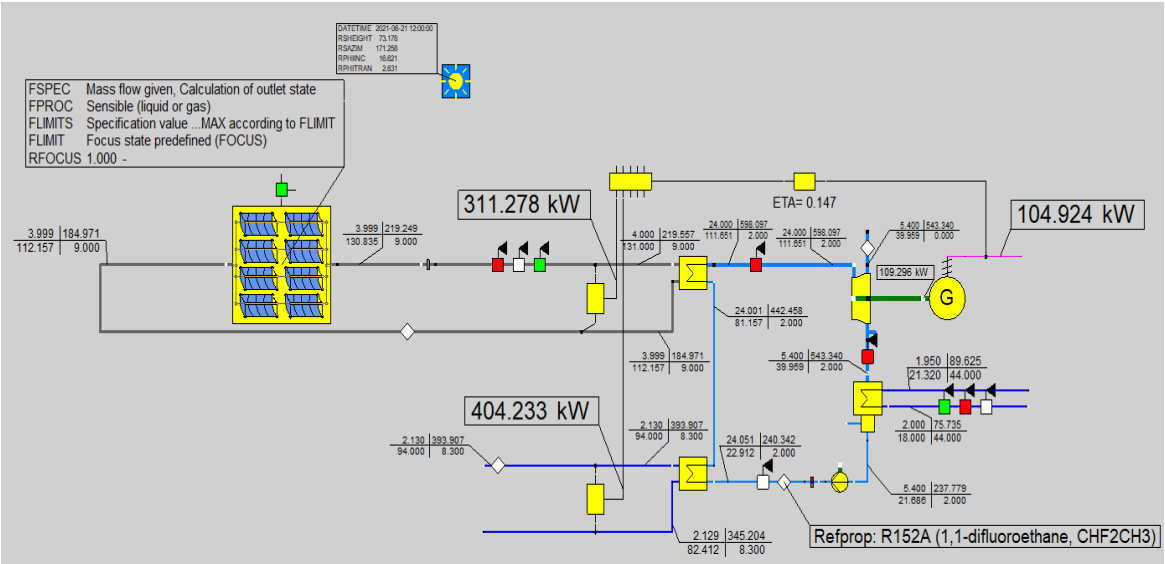


Figure 4.15. Ebsilon display image of the multigenerational system with R152A

Inspecting this sketch in Figure 4.15, the pressure, temperature, mass flow and entalphy values can be observed. For instance, at left bottom of this sketch, there is Gonen geothermal nineth sondage values 94℃ temperature, 2.13 bar pressure, 8.3 kg/s mass flow of geothermal water were defined through the Ebsilon Professional programme. The heat exchanger connected to the geothermal system, has 22.912℃ input temperature and 81.157℃ output temperature, 24 bar pressure and 2 kg/s mass flow and 240.342 kj/kg input entalphy and 442.458 kj/kg output entalphy. At upper left of the sketch, there is parabolic solar panels values were defined to the simulation programme as output temperature 130.835℃, 4 bar pressure, 9 kg/s mass flow with Therminol VP1 oil fluid.

As mentioned, Gonen latitude is 40.1049° and longitude is 27.654°, direct normal irradiance value is 1000 W/m^2, wind speed at Gonen is 5 m/s, and ambient temperature is 20℃ for solar system calculations to run the simulation. The heat exchanger connected to the solar system, has 111.651℃ output temperature, 24 bar pressure and 2 kg/s mass flow and 598.097 kj/kg output entalphy. And this heat exchanger is connected to the turbine which has 39.959℃ output temperature, 5.4 bar output pressure and 2 kg/s mass flow, 543.340 kj/kg output entalphy. Then, the condenser connected to this heat exchanger has 21.686℃ output temperature, 5.4 bar output pressure and 2 kg/s mass flow, 237.779 kj/kg output entalphy. Also, the cooling tower, which is connected to the condenser, is defined with 18℃ inlet temperature, 2 bar pressure and 44 kg/s mass flow of water. And the pump connected to the condenser has 22.912℃ output temperature, 24 bar output pressure and 2 kg/s mass flow, 240.342 kj/kg output entalphy within the organic rankine cycle.

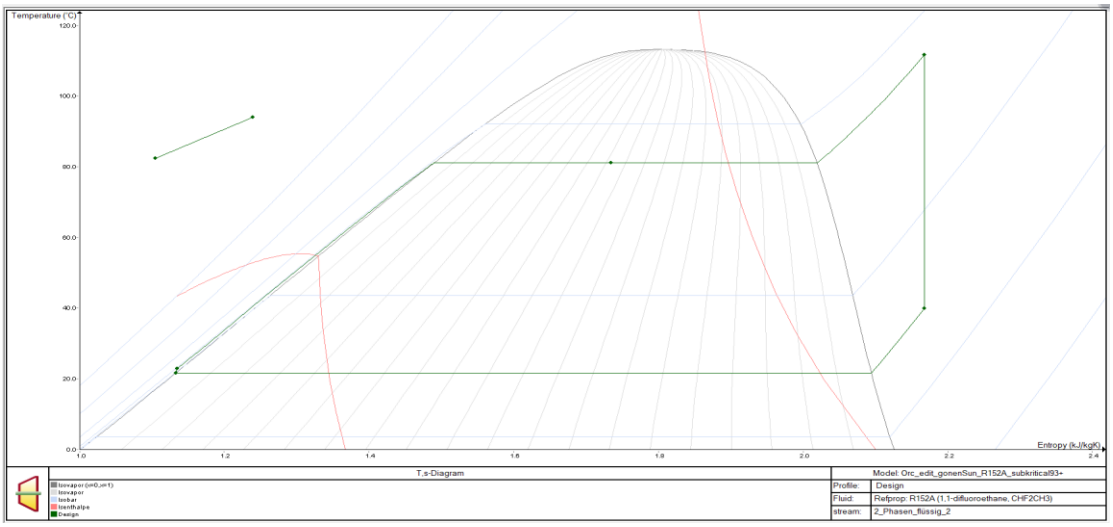


Figure 4.16. T-s diyagram of the ORC side of the multigenerational system with R152A via Ebsilon

According to these analyzed temperature, pressure values of the components of the multigenerational system, power outputs and ETA thermal efficiency of the system was calculated by Ebsilon Professional programme. Accordingly, the power output of the solar panels for this multigenerational system with R152A is calculated as 311.278 kW, the power output of the geothermal well is calculated as 404.233 kW and the power output of the generator is calculated as 104.924 kW. Thus, ETA thermal efficiency of the multigenerational system was calculated as %14.7 according to the related formula via Ebsilon Professional programme.

4.12 Analysis Of Multigeneration System With R152A Via EES

4.12.1 Energetic thermodynamic analysis of the system with R152A via EES

Besides analyses with the simulation of Ebsilon Professional programme, this multigenerational system with R152A organic fluid was analyzed thermodynamically with EES programme via the EES codings written in the Appendix A.11.

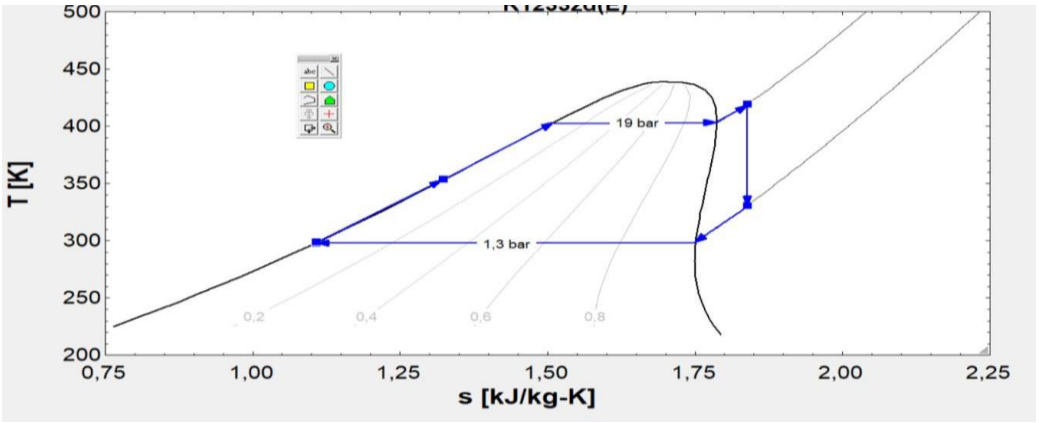


Figure 4.17. T-s diyagram of the ORC side of the multigenerational system with R152A via EES.

The results of energetic analyses of the multigenerational system with R152A, via EES programme is compatible with the results of Ebsilon Professional analyses, which is favorable for crosschecking. Also, t-s diagrams from EES and Ebsilon Professional programmes are also compatible to crosscheck as seen in Figures 4.16 and 4.17.

4.12.2 Exergetic thermodynamic analysis of multigeneration system with R152A via EES

EES codings for exergetic thermodynamic analysis of the system with R152A is in the Appendix A.12. According to these codings and exergy formulations, the values of calculated results can be observed in the Table 4.11.

Table 4.11. Results of energy and exergy analyses via EES for R152A fluided hybrid system

Unit Settings: SI K bar kJ mass deg

$h1 = 237,7$	$h2_a = 240,3$	$h2_s = 239,7$	$h3 = 442,4$	$h4 = 598$	$h5 = 543,4$	$\dot{m} = 2$ [kg/s]	$n_i = 0,6343$	$n_{pump} = 0,8$	$n_{th} = 0,1455$	$P1 = 5,4$ [bar]
$P2 = 24$ [bar]	$Qin_{23} = 404,2$	$Qin_{34} = 311,3$	$Q_{in} = 715,5$	$Q_{in,1} = 404,2$ [kW]	$Q_{in,2} = 311,3$ [kW]	$Q_{out} = 611,4$	$s1 = 1,132$	$s2 = 1,134$	$s3 = 1,733$	$s4 = 2,167$
$s5 = 2,167$	$T1 = 294,7$	$T2 = 295,9$	$T3 = 354,2$	$T_0 = 293$ [K]	$T_{h,1} = 367$ [K]	$T_{h,2} = 404$ [K]	$W_{in} = 5,111$	$W_{out} = 109,2$	$x_{exp} = 172,1$	$x_{heat,23} = 81,51$
$x_{heat,34} = 85,52$	$x_{recovered} = 109,2$									

4.13 Analysis Of Multigeneration System With R245CA Via Ebsilon

In terms of Ebsilon analyses, Figure 4.18 demonstrates Ebsilon sketch of the multigeneration system with R245CA organic working fluid for its ORC side.

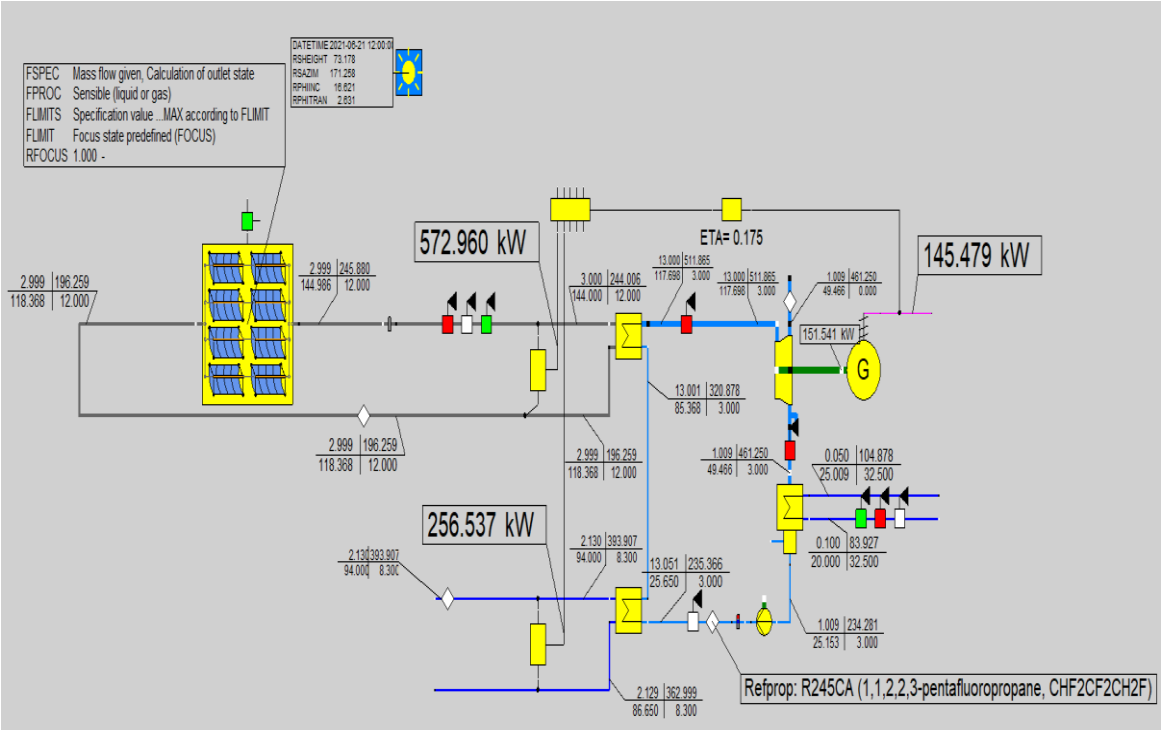


Figure 4.18. Ebsilon display image of the multigenerational system with R245CA

Inspecting this sketch in Figure 4.18, the pressure, temperature, mass flow and entalphy values can be observed. For instance, at left bottom of this sketch, there is Gonen geothermal nineth sondage values 94℃ temperature, 2.13 bar pressure, 8.3 kg/s mass flow of geothermal water were defined through the Ebsilon Professional programme. The heat exchanger connected to the geothermal system, has 25.650℃ input temperature and 85.368℃ output temperature, 13 bar pressure and 3 kg/s mass flow and 235.366 kj/kg input entalphy and 320.878 kj/kg output entalphy. At upper left of the sketch, there is parabolic solar panels values were defined to the simulation programme as output temperature 144℃, 3 bar pressure, 12 kg/s mass flow with Therminol VP1 oil fluid.

As mentioned, Gonen latitude is 40.1049° and longitude is 27.654°, direct normal irradiance value is 1000 W/m^2, wind speed at Gonen is 5 m/s, and ambient temperature is 20℃ for solar system calculations to run the simulation. The heat exchanger connected to the solar system, has 117.698℃ output temperature, 13 bar pressure and 3 kg/s mass flow and 511.865 kj/kg output entalphy. And this heat exchanger is connected to the turbine which has 49.466℃ output temperature, 1.009 bar output pressure and 3 kg/s mass flow, 461.25 kj/kg output entalphy. Then, the condenser connected to this heat exchanger has 25.153℃ output temperature, 1.009 bar output pressure and 3 kg/s mass flow, 234.281 kj/kg output entalphy. Also, the cooling tower, which is connected to the condenser, is defined with 20℃ inlet temperature, 0.1 bar pressure and 32.5 kg/s mass flow of water. And the pump connected to the condenser has 25.65℃ output temperature, 13 bar output pressure and 3 kg/s mass flow, 235.366 kj/kg output entalphy within the organic rankine cycle.

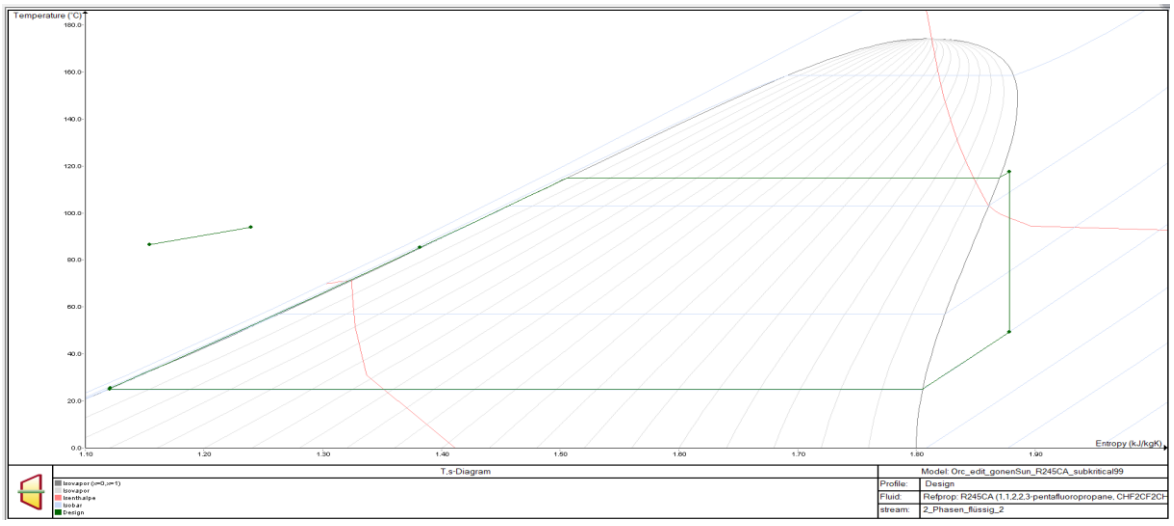


Figure 4.19. T-s diyagram of the ORC side of the multigenerational system with R245CA via Ebsilon

According to these analyzed temperature, pressure values of the components of the multigenerational system, power outputs and ETA thermal efficiency of the system was calculated by Ebsilon Professional programme. Accordingly, the power output of the solar panels for this multigenerational system with R245CA is calculated as 572.960 kW, the power output of the geothermal well is calculated as 256.537 kW and the power output of the generator is calculated as 145.479 kW. Thus, ETA thermal efficiency of the multigenerational system was calculated as %17.5 according to the related formula via Ebsilon Professional programme.

4.14 Analysis Of Multigeneration System With R245CA Via EES

4.14.1 Energetic thermodynamic analysis of the system with R245CA via EES

Besides analyses with the simulation of Ebsilon Professional programme, this multigenerational system with R245CA organic fluid was analyzed thermodynamically with EES programme via the EES codings written in the Appendix A.13.

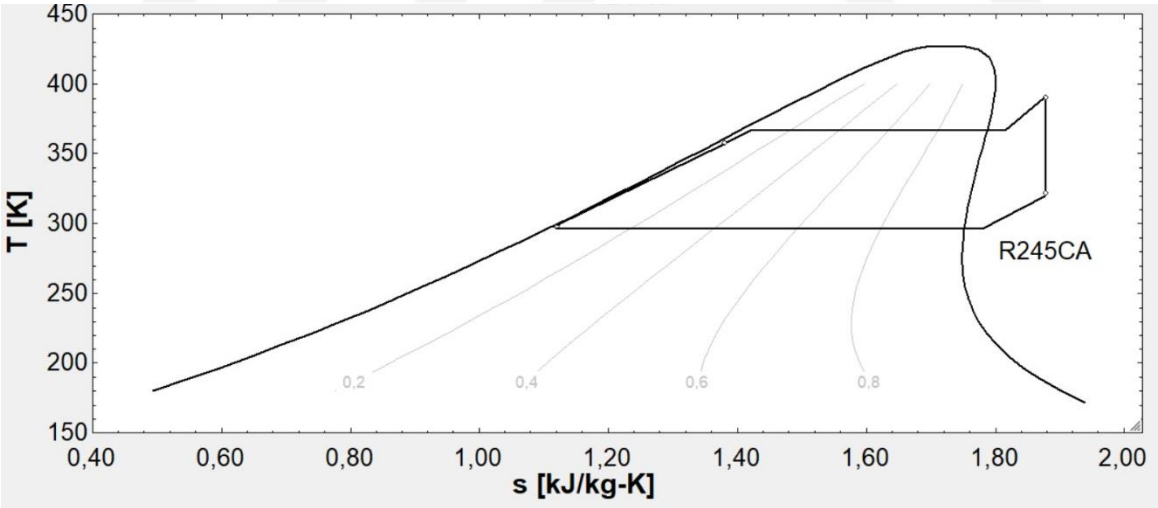


Figure 4.20. T-s diyagram of the ORC side of the multigenerational system with R245CA via EES.

The results of energetic analyses of the multigenerational system with R245CA, via EES programme is compatible with the results of Ebsilon Professional analyses, which is favorable for crosschecking. Also, t-s diagrams from EES and Ebsilon Professional programmes are also compatible to crosscheck as seen in Figures 4.19 and 4.20.

4.14.2 Exergetic thermodynamic analysis of multigeneration system with R245CA via EES

EES codings for exergetic thermodynamic analysis of the system with R245CA is in the Appendix A.14. According to these codings and exergy formulations, the values of calculated results can be observed in the Table 4.12.

Table 4.12. Results of energy and exergy analyses via EES for R245CA fluided hybrid system

Unit Settings: SI K bar kJ mass deg

$h1 = 234,3$ [kJ/kg]	$h2_a = 235,4$ [kJ/kg]	$h3 = 320,9$ [kJ/kg]	$h4 = 511,9$ [kJ/kg]	$h5 = 461,3$ [kJ/kg]	$\dot{m} = 3$ [kg/s]	$\eta_t = 0,6738$	$\eta_{pump} = 0,8$	$\eta_{th} = 0,1791$
$P1 = 1,009$ [bar]	$P2 = 13,05$ [bar]	$Qin_{23} = 256,5$	$Qin_{34} = 573$	$Q_{in} = 829,5$	$Q_{in,1} = 256,5$ [kW]	$Q_{in,2} = 573$ [kW]	$Q_{out} = 680,9$	$s1 = 1,12$
$s2 = 1,121$ [(kJ)/(kg*K)]	$s3 = 1,381$ [(kJ)/(kg*K)]	$s4 = 1,878$ [(kJ)/(kg*K)]	$s5 = 1,878$	$T1 = 298,2$	$T2 = 298,7$	$T3 = 358,4$	$T_0 = 293$ [K]	$T_{h,1} = 367$ [K]
$T_{h,2} = 417$ [K]	$W_{in} = 3,255$	$W_{out} = 151,8$	$x_{exp} = 225,4$	$x_{heat,23} = 51,73$	$x_{heat,34} = 170,4$	$x_{recovered} = 151,8$		

4.15 Second Law Efficiency Analyses Of Multigeneration System

The main purpose of the ORC system is to recover waste heat and produce power by utilizing low-to-medium grade heat sources, such as solar thermal energy and geothermal energy. In order to achieve this objective, efficient utilization of waste heat is essential. The concept of 2nd Law Efficiency quantifies how effectively the waste energy can be harnessed. Optimizing 2nd Law efficiency involves considering additional factors, including thermal efficiency, environmental impact, and cost [128,129].

Second law efficiency analyses were calculated via EES. For these calculations, there were R245fa, R1234yf, R507A, R1233zd in the library of the used programme version. Therefore, the results of these working fluided hybrid systems can be observed below, respectively. In Figure 4.21, diagrams of second law efficiency versus geothermal source mass flow rate of the multigeneration systems with R245fa, R1234yf, R1233zd, R245CA, R507A, R1234ze and R152A are seen, respectively.

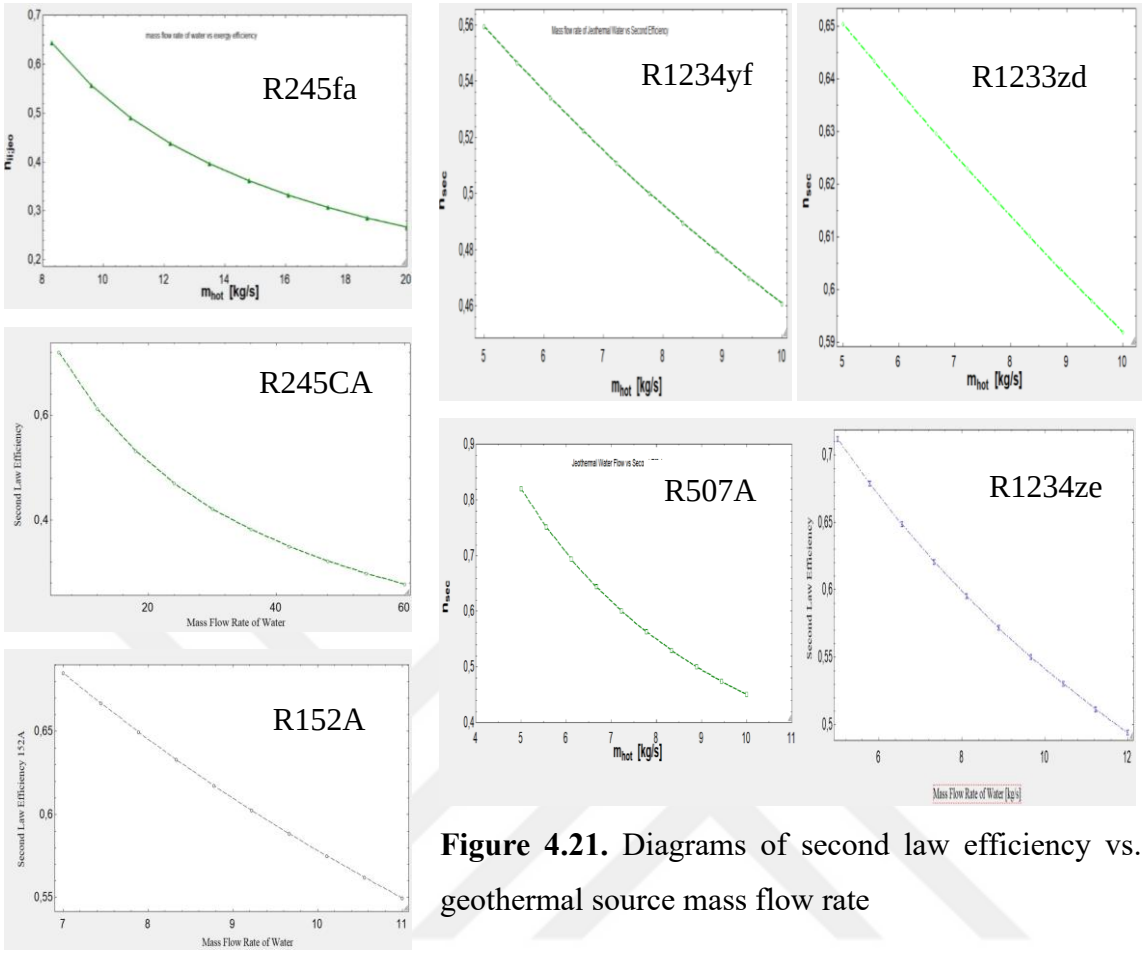


Figure 4.21. Diagrams of second law efficiency vs. geothermal source mass flow rate

The mass flow rate of the geothermal source fluid (water) directly impacts the system's heat input. As flow rate increases, more heat enters the system, leading to greater irreversibility. Irreversibility represents unavoidable losses or inefficiencies during energy conversion. Exergy efficiency measures how well a system converts available energy into useful work. High heat input rates can raise irreversibility, reducing exergy efficiency. Excessive heat input can result in energy conversion inefficiencies. Increasing heat input can sometimes be beneficial. When input raises the evaporator's outlet temperature (the turbine's inlet), it affects enthalpy. Higher temperature input means a larger enthalpy difference for turbine work output. If heat input significantly boosts outlet temperature, turbine work output may increase. This contributes to improved 2nd law efficiency (exergy efficiency). Balancing these factors optimizes geothermal energy systems.

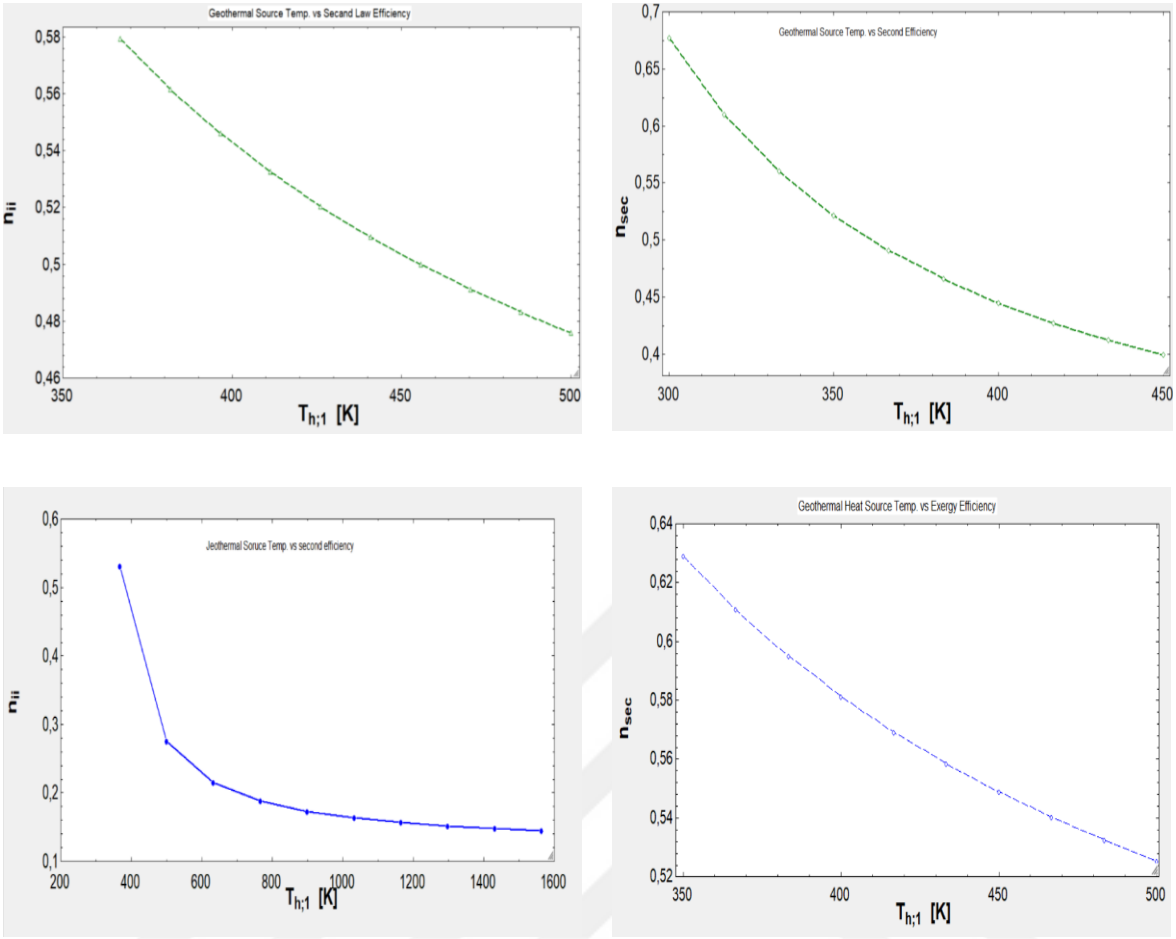


Figure 4.22. Diagrams of second law efficiency vs. geothermal source temperature

In Figure 4.22, diagrams of second law efficiency versus geothermal source temperature of the multigeneration systems with R245fa, R1234yf, R507A, R1233zd can be observed, respectively. Although geothermal source temperature is constant at 94°C, these diagrams are only to see what would happen if geothermal source temperature changed, supposingly. When the geothermal source temperature rises, the overall exergy efficiency of the ORC tends to decrease. This relationship is crucial for optimizing energy conversion systems. The working fluid in the ORC cycle exchanges heat with the geothermal water. As the source temperature increases, the temperature difference between the working fluid and water also grows. The evaporator, a critical component, absorbs heat from the geothermal water. Higher source temperatures lead to increased heat absorption, contributing to the system's energy input. Unfortunately, greater heat absorption results in higher irreversible losses within the system. Irreversibility refers to unavoidable inefficiencies during energy conversion. While higher geothermal source temperatures enhance heat absorption, they

also exacerbate irreversibility, ultimately impacting the ORC's exergy efficiency. Balancing these factors is essential for efficient energy utilization.

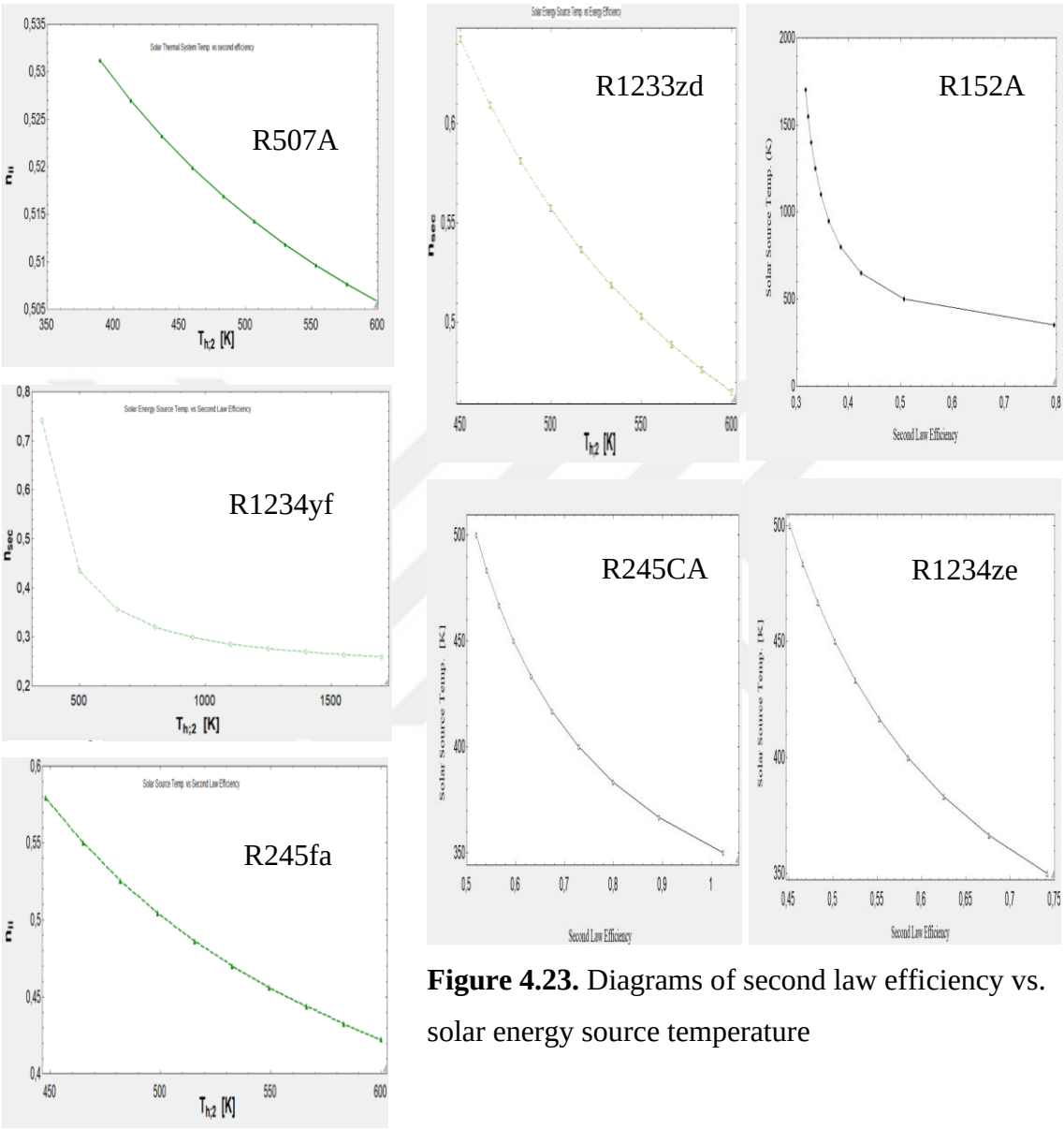


Figure 4.23. Diagrams of second law efficiency vs. solar energy source temperature

In Figure 4.23, diagrams of second law versus solar energy source temperature of the multigeneration systems with R507A, R1233zd, R152A, R1234yf, R245CA, R1234ze, R245fa can be observed, respectively. The Carnot efficiency, a fundamental concept in thermodynamics, depends solely on the temperature difference between the heat source and the heat sink. It represents the maximum possible efficiency achievable by any heat engine. Irreversibilities occur during heat transfer due to factors like friction and turbulence. These lead to energy losses, reducing overall system efficiency. Irreversibilities cause a loss of

available, usable energy. When energy dissipates or is lost, it becomes less useful for performing work. Exergy efficiency (also known as second law efficiency) considers useful work produced and energy conversion quality. Higher irreversibilities decrease exergy efficiency. Understanding the interplay between Carnot efficiency, irreversibilities, and exergy efficiency is crucial for optimizing energy systems. Balancing these factors ensures efficient energy utilization.

4.16 Cost Analyses Of Multigeneration System

Exploring the investment cost aspects of the multigeneration system that integrates ORC, solar, and geothermal technologies, there are two key areas equipment investment and working fluid investment during cost analysis. Equipment investment covers critical components within the multigeneration system. These components include the ORC system (with its evaporator, expander/turbine, generator, condenser, and pump), solar collectors, and geothermal heat exchangers. Accurate cost estimation for these components is vital during preliminary design. Working fluid investment involves selecting and procuring the fluids used in the system. In the context of ORC, the choice of organic working fluid significantly impacts both system performance and cost. Factors such as working fluid properties, availability, and cost influence the overall investment [129,130].

Engineers often employ cost equations to estimate equipment costs during the initial design phase. These equations draw from established practices used in chemical process analysis, synthesis, and design. However, it's important to recognize that the accuracy of these estimates can vary, typically falling within a range of 10% to 30%. Balancing cost considerations with system performance ensures efficient resource utilization during design and implementation [130,131].

4.16.1 Equipment investment

Equipment investment covers critical components within the multigeneration system. These components include the turbine (expander), condenser, pump, and evaporator. Each component plays a crucial role in the overall system performance. For turbines and pumps, the investment calculation is typically based on their capacity (size). Larger turbines and pumps generally incur higher costs due to their increased capacity. Properly sizing these

components ensures efficient energy conversion. Heat exchangers (such as the evaporator and condenser) are essential for transferring heat between the working fluid and external sources (e.g., geothermal water or solar collectors). The heat transfer surface area directly impacts the cost of these exchangers. Larger surface areas result in higher investment costs. Thus, understanding the cost implications of each component and optimizing their sizing ensures effective equipment investment. Balancing capacity, surface area, and cost considerations contributes to an efficient system design [130,131].

The purchased cost of heat exchanger can be estimated by the following equation:

$$\log(C_{p,}) = K_1 + K_2 \log(A) + K_3[\log(A)]^2$$

Where A is the total heat transfer surface area for the heat exchangers. K_1, K_2, and K_3 are the correction factors that are given in the table of correction factors for purchased cost of heat exchanger.

The purchased cost of pump and expander can be estimated by the following equation:

$$\log(C_p) = K_1 + K_2 \log(W) + K_3[\log(W)]^2$$

C_p represents the basic purchased cost.

Table 4.13. Correction factors for purchased cost of heat exchanger[131]

Correction Factors	Value	Correction Factors	Value
K_1	3.2138	B_1	1.8
K_2	0.2688	B_2	1.5
K_3	0.0796	F_M	1.25
C_1	-0.0650	$CEPCI_{1996}$	382
C_2	0.0503	$CEPCI_{2016}$	606
C_3	0.0147		

Table 4.14. Correction factors for purchased cost of pump and expander[131]

Correction Factors	Value for Pump	Value for Expander
K_1	3.4771	2.2476
K_2	0.135	1.4965
K_3	0.1438	−0.1618
C_1	−0.245832	0
C_2	0.259016	0
C_3	−0.01363	0
B_1	1.89	0
B_2	1.35	0
F_M	1.4	0
$CEPCI_{1996}$	382	382
$CEPCI_{2016}$	606	606

The correction factors for purchased cost of heat exchanger, pump and expander in Figures 4.24 and 4.25 are to be used in the purchased cost calculation equations above.

When material and pressure corrections are involved, Bare Module Cost of equipment is

estimated by:

$$C_{BM} = C_P(B_1 + B_2 F_M F_P)$$

Where F_M and F_P are the material correction and pressure correction, respectively.

4.16.2 Working fluid investment

The investment cost of the working fluid is calculated simply the multiplication of total mass of the working fluid and its price per kg.

$$C_{BM} = p_w M_w$$

Where p_w is the price of the working fluid in unit of $/kg.

4.16.3 Total cost of ORC system

At the beginning of the cost analysis, which type of components are going to be used for the study have been determined. The type of components that is decided to be used is kaplan turbine, centrifugal pump, plate heat-exchanger and water cooled condenser.

After decision of type, we have tried to evaluate the prices by getting contact with the manufacturer companies.

Total investment cost can be calculated as:

$$M_{t,c} = M_c + M_t + M_p + M_{hx}$$

The installation cost is taken as the %10 of the total cost.

$$M_{i,c} = 0.10(M_{t,c})$$

According to that, the initial investment cost can be evaluated as:

$$M_{inv} = M_{i,c} + M_{t,c}$$

The operating cost of the system consists of the cost of the refrigerant circulating in the system, the electricity cost of the pump and the cost of maintenance and repair.

The maintenance and repair cost of the power plant is included in the calculations as 15% of the initial investment cost [132,133,134].

$$M_{r,c} = (0.15)M_{inv}$$

4.16.4 Net Earnings (NE) of ORC

NE is the multiplication of unit grid price and annual net power output. Net power output

refers the net electricity produced by the ORC. NE is formulized as:

$$NE = pe(W_t - W_p)t_{op}$$

Where pe is the unit grid price whose value is 0.127$/kWh, for Turkey. t_{op} is the annual period of operation for the system which is around 8000 h.

4.16.5 Payback Period (PP) of the ORC

PP is the time required for accumulated benefit to become equal to the initial investment cost. PP is calculated by:

$$PP = \frac{ln\left(\frac{NE - COM}{NE - COM - iC_{tot}}\right)}{ln(1+i)}$$

Where COM (cost of maintenance) is taken as 1.5% of the total cost, COM=1.5%C_{tot}. Also, i represents the annual interest rate that is taken 10%, in 2024 for Turkey [134,135,136].

4.16.6 Return on Investment (ROI)

ROI is the ratio of NE to C_{tot}, and can be formulized as:

$$ROI = \frac{NE}{C_{tot}}$$

4.16.7 Levelized Energy Cost (LEC)

Levelized cost of energy (LCOE) is a method used to calculate the unit energy cost of electric generating plants. This method is calculated by taking the initial investment cost, operation and maintenance cost, and fuel/fluid expenses used. In this way, the minimum price at which the energy produced should be sold to avoid loss can also be calculated. LCOE can actually be evaluated as the unit energy price resulting from dividing all expenditures by the electrical energy produced.

$$LEC = \frac{\frac{i(1+i)^{Ts}}{i(1+i)^{Ts}-1}C_{tot} + COM}{(W_t - W_p)t_0}$$

During the calculations, the system service life T_S is taken as 20 years.

4.16.8 Present value of total profit in system service life

NPV is the difference between the sum of discounted expenses according to a certain discount rate and the sum of the discounted net revenues and the present value of scrap.

$$C_{pv} = \sum_{t=0}^{20} \frac{NE - COM}{(1+i)^t} - C_{tot}$$

Cost analysis for the R245fa has been done and used the Bare Module ratio to other fluids to evaluate others' cost analysis. Cost analysis of R245fa has been done by extracting real data from related manufacturer companies and accorded the methods in our country economical manner.

The mass of the fluid, which is used in the cycle, is determined by the multiplication of volume of the heat exchanger and the density of the fluid. Cost analyses of other working fluid cycles have been evaluated by using Bare Module ratio.

The service life is taken as 20 years and operation duration is around 8000 h. During the service life (20 yrs), the price of the electricity is taken as 0.127$/kWh [136,137,138].

4.16.9 R245fa cost analysis

The related EES codings for the cost analyses of the system with R245fa is in the Appendix A.15. Accordingly, the results are as below:

- Kaplan Turbine ($\dot{W}_{out}$=177.164 kW) :80,500.00$
- Centrifugal Pump ($\dot{W}_{in}$=5.432 kW): 17,500.00$
- Heat Exchangers (700.00$+750.00$+3,000.00$):4,450.00$
- Solar Collector (686.637 kW capacity): 225.610,875$
- Geothermal Source (313.366 kW) = 766.78$
- Installation Cost (10% of Equipment Cost) = (0.10x452,450.00$) = 45,245.00$
- Scrap Cost= Installation Cost = 45,245.00$
- Working Fluid Cost (For R245fa) = (25$/kg)(100kg) = 2,500.00$
- Total Cost=Installation Cost+ Equipment Cost = 500,195.00$
- NE (Net Earnings) = (0.127$/kWh)(Wout-Win) t_{op} =192,216.22$
- Present Value of Total Profit in System: (i:0.10, service life:20yrs)=1,328,160.87$
- Payback Period (PP) = 3.3134 years

4.16.10 R1234yf cost analysis

The related EES codings for the cost analyses of the system with R1234yf is in the Appendix A.16. Accordingly, the results are as below:

- Kaplan Turbine ($\dot{W}_{out}$=142.577 kW): 58,906.476$
- Centrifugal Pump ($\dot{W}_{in}$=16.74 kW): 24,053.77$
- Heat Exchangers (700.00$+1,000.00$+2,350.00$): 4,050.00$
- Solar Collector (538.729 kW capacity): 176,564.925$
- Geothermal Source (450.144 kW) = 976.86$
- Installation Cost (10% of Equipment Cost) = (0.10x407,009.4762$) = 40,700.947$
- Scrap Cost= Installation Cost = 40,700.947$
- Working Fluid Cost (For R1234yf) = (85$/kg)(100kg)=8,500.00$
- Total Cost=Installation Cost+ Equipment Cost=455,710.4232$
- NE (Net Earnings) = (0.127$/kWh)($\dot{W}_{out}$-$\dot{W}_{in}$) t_{op} = 141,395.501$
- Present Value of Total Profit in System: (i:0.10, service life:20yrs)=889,459.92$
- Payback Period (PP) = 4.338 years

4.16.11 R507A cost analysis

The related EES codings for the cost analyses of the system with R507A is in the Appendix A.17. Accordingly, the results are as below:

- Kaplan Turbine ($\dot{W}_{out}$=63.714 kW) :26,743.206$
- Centrifugal Pump ($\dot{W}_{in}$=8.247 kW): 4,845.06$
- Heat Exchangers (350.00$+1,200.00$+200.00$):1,750.00$
- Solar Collector (22.795 kW capacity): 7,234.2$
- Geothermal Source (525.054 kW) = 1,208.59$
- Installation Cost (10% of Equipment Cost) = (0.10x73,338.266$) = 7,333.8266$
- Scrap Cost= Installation Cost = 7,333.8266$
- Working Fluid Cost (For R507A) = (45$/kg)(100kg)=4,500.00$
- Total Cost=Installation Cost+ Equipment Cost=85,172.0926$
- NE (Net Earnings) = (0.127$/kWh)($\dot{W}_{out}$-$\dot{W}_{in}$) t_{op} = 60,862.8298$
- Present Value of Total Profit in System: (i:0.10, service life:20yrs)=493,850.32$

4.16.12 R1233zd cost analysis

The related EES codings for the cost analyses of the system with R1233zd is in the Appendix A.18. Accordingly, the results are as below:

- Kaplan Turbine ($\dot{W}_{out}$=167.176 kW) :79,520.00$
- Centrifugal Pump ($\dot{W}_{in}$=5.248 kW): 23,850.00$
- Heat Exchangers (700.00$+1,000.00$+2,350.00$):3,750.00$
- Solar Collector (610.623 kW capacity): 201,087.9$
- Geothermal Source (209.403 kW) = 492.76$
- Installation Cost (10% of Equipment Cost) = (0.10x407,120.00$) = 40,712.00$
- Scrap Cost= Installation Cost = 40,712.00$
- Working Fluid Cost (For R1233zd) = (30$/kg)(100kg)=3,000.00$
- Total Cost=Installation Cost+ Equipment Cost=450,832.00$
- NE (Net Earnings) = (0.127$/kWh)($\dot{W}_{out}$-$\dot{W}_{in}$) t_{op} = 177,680.3558$
- Present Value of Total Profit in System: (i:0.10, service life:20yrs)=1,232,206.12$
- Payback Period (PP) = 3.213 years

4.16.13 R152A cost analysis

The related EES codings for the cost analyses of the system with R152A is in the Appendix A.19. Accordingly, the results are as below:

- Turbine Cost (109.2 kW) = 18,538.00$
- Pump Cost (5.11 kW) = 7,049.00$
- Solar Collector (311.3 kW) = 158,668.00$
- Geothermal Source (404,4 kW) = 903,3.00$
- Condenser (611.6 kW) = 517.00$
- Initial Investment Cost = 187,036.00$
- Installation Cost = 18,704.00$
- Total Cost = Installation Cost + Equipment Cost = 205,739.00$
- Net Earnings = (0.127$/kWh)($\dot{W}_{out}$-$\dot{W}_{in}$) t_{op} =114,229.292$
- Present Value of Total Profit in System: (i:0.10, service life:20yrs)=846,570.92$
- Payback Period (PP) = 2.15 years

4.16.14 R245CA cost analysis

The related EES codings for the cost analyses of the system with R245CA is in the Appendix A.20. Accordingly, the results are as below:

- Turbine Cost (151.541 kW) = 73,929.00$
- Pump Cost (3.255 kW) = 18,692.00$
- Solar Collector (572.960 kW) = 292,055.00$
- Geothermal Source (256.537 kW) = 573,1.00$
- Condenser (680.907 kW) = 575,6.00$
- Initial Investment Cost = 388,329.00$
- Installation Cost = 38,833.00$
- Total Cost = Installation Cost + Equipment Cost = 427,161.00$
- Net Earnings = (0.127$/kWh)($\dot{W}_{out}$-$\dot{W}_{in}$) t_{op} =162,711.027$
- Present Value of Total Profit in System: (i:0.10, service life:20yrs)=1,123,815.00$
- Payback Period (PP) = 3.35 years

4.16.15 R1234ze cost analysis

The related EES codings for the cost analyses of the system with R1234ze is in the Appendix A.21. Accordingly, the results are as below:

- Turbine Cost (127.234 kW) = 55,166.00$
- Pump Cost (6.612 kW) = 7,601.00$
- Solar Collector (439.800 kW) = 1,922.00$
- Geothermal Source (464.575 kW) = 1,038.00$
- Condenser (783.5 kW) = 662,4.00$
- Initial Investment Cost = 290,568.00$
- Installation Cost = 29,057.00$
- Total Cost = Installation Cost + Equipment Cost = 319,624.00$
- Net Earnings = (0.127$/kWh)($\dot{W}_{out}$-$\dot{W}_{in}$) t_{op} = 132,355.97$
- Present Value of Total Profit in System: (i:0.10, service life:20yrs) = 942,123.52$
- Payback Period (PP) = 3.03 years

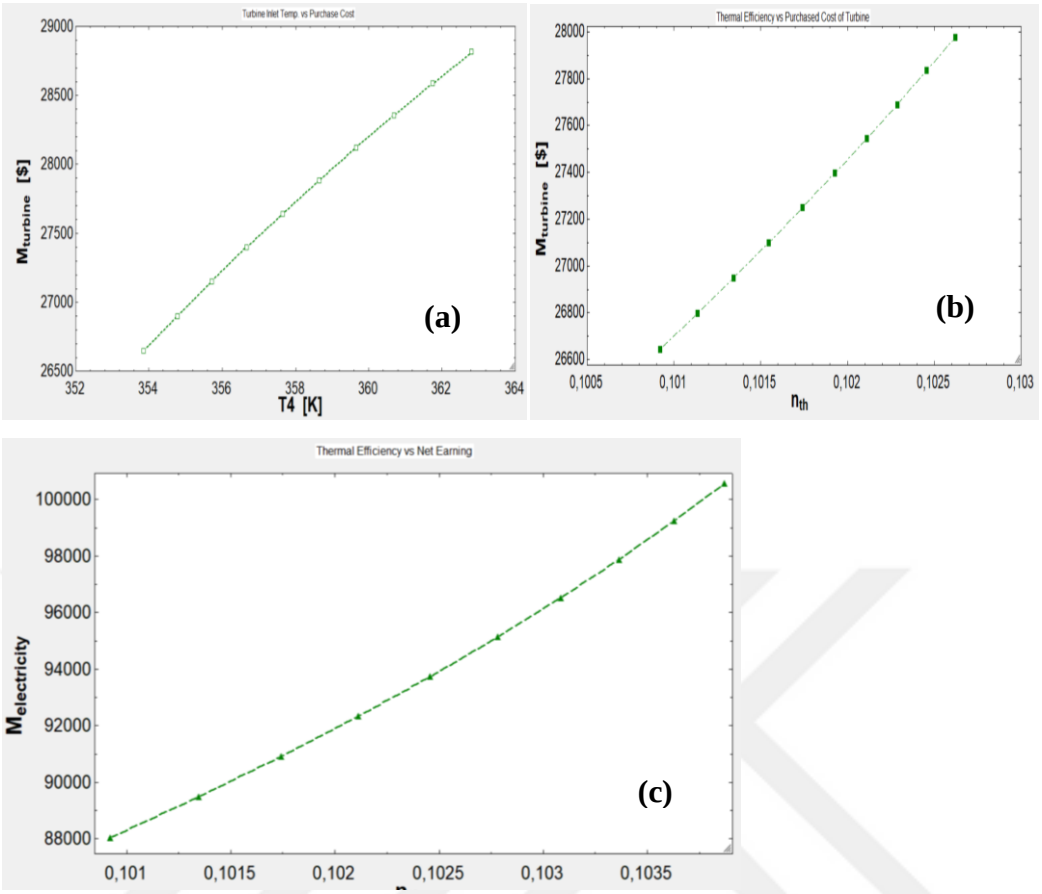


Figure 4.24. (a) Inlet temperature vs Purchased Cost of Turbine. **(b)** Thermal efficiency vs Purchased Cost of Turbine. **(c)** Thermal efficiency vs Net Earning.

According to the cost calculations via the equations written above, the diagrams seen in the Figure 4.24 were drawn. Accordingly, inspecting the Figure 4.24 (a), the inlet temperature increases with the increasing purchased cost of the turbine. Additionally, the thermal efficiency increases with the increasing purchased cost of turbine as observing the Figure 4.24 (b). Moreover, thermal efficiency also increases with the increasing net earning as seen in the Figure 4.24 (c). Furthermore, Figure 4.25 demonstrates that solar energy input rising causes total cost rising, too, which is not cost effective. Thus, solar energy input should not be so high for a cost effective design. Therefore, it is studied to utilize more geothermal energy input than solar energy input with this multigeneration system design.

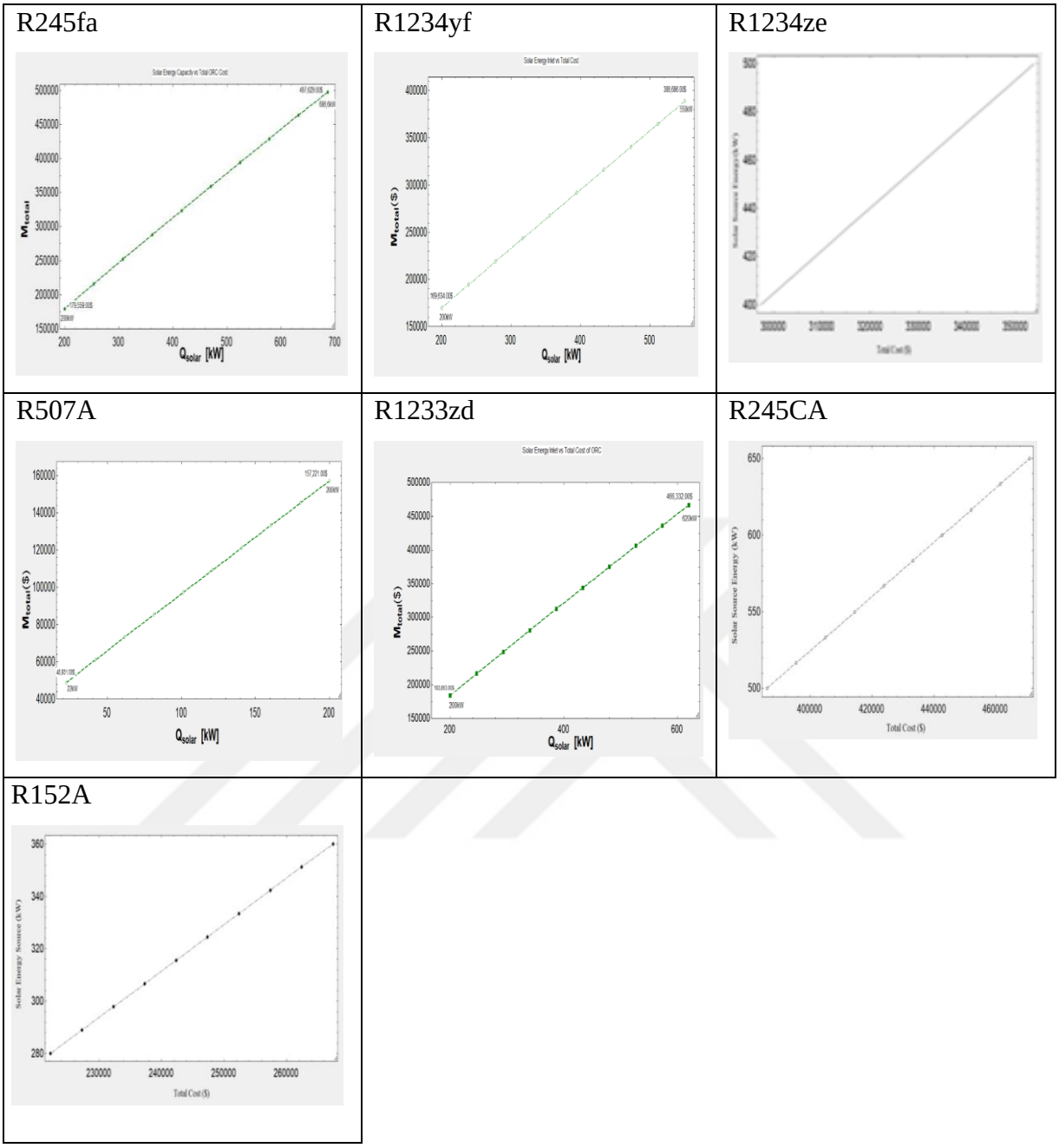


Figure 4.25. Solar Energy Input vs. Total Cost

The systems, which are mentioned, have different solar energy input. In order to compare the fluids with each other, the range of the values where the solar energy inputs are the same, is also examined.

4.16.16 Cost analyses with respect to engineering economy

In terms of engineering economy, the formulas used for this study are:

$P=A[\frac{(1+i)^n-1}{i(1+i)^n}]$ for engineering cost of current value and $P=F[\frac{1}{(1+i)^n}]$ for future equivalent or salvage cost where A is the annual earning or net earning of the system, i is the interest rate, n is the number of years as service life as 20 years, F is the future value, P is the present value and P(i) is total cost of installation cost plus equipment cost.

The first formula calculates the present value of an annual cash flow, where each payment, denoted as 'A', occurs at the end of each period. This is particularly useful for evaluating investments or financial products that involve regular, equal payments. The present value in this scenario is derived using the partial-sum formula for geometric series, which effectively discounts each end-of-period payment back to its value at the present time. Similar to the first formula, 'i' denotes the interest rate per period, and 'n' signifies the number of periods over which these payments are made. This approach helps in understanding the total value of a series of future payments in today's terms, facilitating better financial decision-making.

The second formula establishes a relationship between the present value (P) and future value (F) of a cash flow over a specified period. In this context, 'i' represents the interest rate per period, while 'n' stands for the number of periods. Unless stated otherwise, this formula assumes the interest is compounded, which is why the term $(1 + i)^n$ is included in the equation. This factor accounts for the effect of compound interest, where interest is calculated on the initial principal and also on the accumulated interest from previous periods.

Here, the inputs and outputs according to the current value of the entire system are calculated and a comparison with the initial investment cost is executed. Thus, in this analysis, the inputs and outputs based on the present value of the entire system are meticulously evaluated. This comprehensive approach allowed assessing accurately the current performance and efficiency of the system. Furthermore, a detailed comparison between these current values and the initial investment cost is conducted, providing a clear picture of the system's economic viability and return on investment. This comparison helps to understand whether the system is delivering the expected financial benefits or if adjustments are needed to improve its performance [139,140,141].

In terms of this study for R245fa fluided multigeneration system; A=192,216.22$

P(i)=500,195.00$, i=0.10 , n=20

$P=A[\frac{(1+i)^n-1}{i(1+i)^n}]$ → $P=192{,}216.22[\frac{(1+0.10)^{20}-1}{0.10(1+0.10)^{20}}]$ → P=1,636,445.04$

P-P(i)= 1,636,445.04-500,195.00 → P-P(i)= 1,136,250.04$

Table 4.15. Calculation of future values of R245fa fluided system for ten years (half of service life)

P=	1,636,445.04$	P=	1,636,445.04$
$F_1=P*(1+i)^1$=1,636,445.04 * (1+0,10)^1 =	1,800,089.544	P(1+0,10)^1+F1=	3,600,179.088
$F_2=P*(1+i)^2$=1,636,445.04 * (1+0,10)^2 =	1,980,09.4984	F_1(1+0,10)^1+F2=	3,960,196.9968
$F_3=P*(1+i)^3$=1,636,445.04 * (1+0,10)^3 =	2,178,108.34824	F_2(1+0,10)^1+F3=	4,356,207.896
$F_4=P*(1+i)^4$=1,636,445.04 * (1+0,10)^4 =	2,395,919.18	F_3(1+0,10)^1+F4=	4,791,838.366
$F_5=P*(1+i)^5$=1,636,445.04 * (1+0,10)^5 =	2,635,511.1	F_4(1+0,10)^1+F5=	5,271,022.199
$F_6=P*(1+i)^6$=1,636,445.04 * (1+0,10)^6 =	2,899,062.2115	F_5(1+0,10)^1+F6=	5,798,124.4215
$F_7=P*(1+i)^7$=1,636,445.04 * (1+0,10)^7 =	3,188,968.43	F_6(1+0,10)^1+F7=	6,377,936.865
$F_8=P*(1+i)^8$=1,636,445.04 * (1+0,10)^8 =	3,507,865.2759	F_7(1+0,10)^1+F8=	7,015,730.5489
$F_9=P*(1+i)^9$=1,636,445.04 * (1+0,10)^9 =	3,858,651.8	F_8(1+0,10)^1+F9=	7,717,303.6

$P=F[\frac{1}{(1+i)^n}]$

$1{,}636{,}445.04=F[\frac{1}{(1+0{,}10)^{20}}]$

F=11,009,183.92$

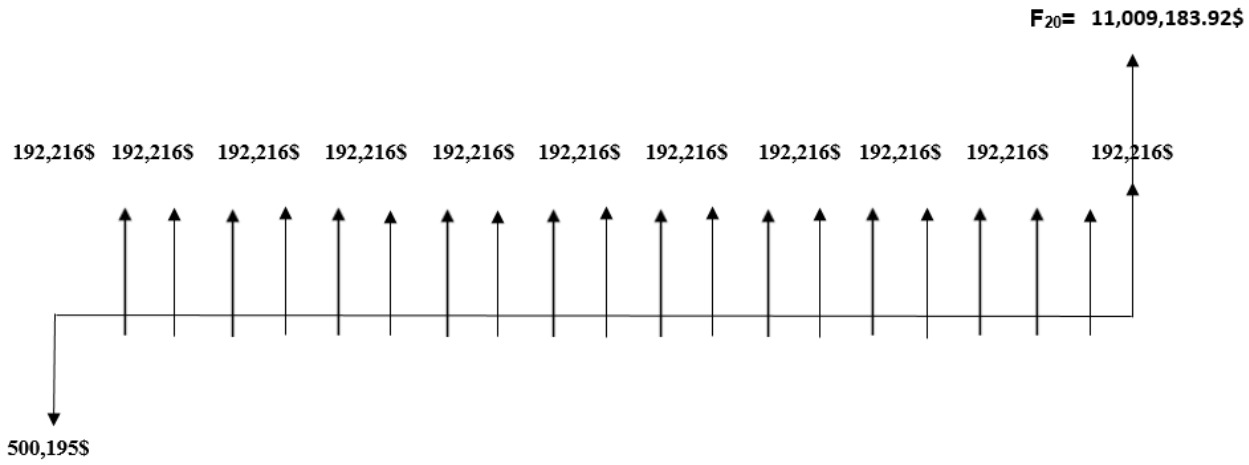


Figure 4.26. Cost flow diagram of R245fa fluided system for service life of 20 years

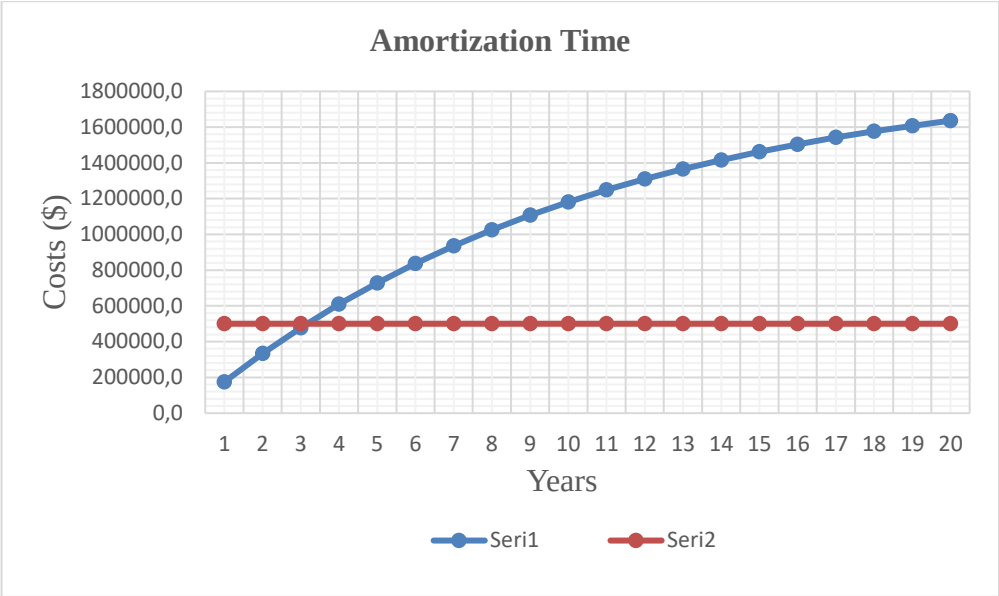


Figure 4.27. Diagram of present value of cumulative investment cost (Seri2) vs. present value of net earnings (Seri1) for R245fa fluided system

The coindicency point of Seri1 and Seri2 plots refers the amortization and payback period which is 3.3 years for R245fa fluided system as seen in the Figure 4.27.

In terms of R1234yf fluided multigeneration system; A=141,395.501$

P(i)= 455,710.4232$

i=0.10

n=20

$P=A[\frac{(1+i)^n-1}{i(1+i)^n}]$

$P=141{,}395.501[\frac{(1+0.10)^{20}-1}{0.10(1+0.10)^{20}}]$

P=1,203,779.607$

P-P(i)= 1,203,779.607-455,710.4232

P-P(i)= 748,069.18$

Table 4.16. Calculation of future values of R1234yf fluided system for ten years (half of service life)

P=	1,203,779.607$	P=	1,203,779.607$
$P_1=P*(1+i)^1=$ 1,203,779.607 * (1+0,10)^1 =	1.324.157,5677	$P(1+0,10)^1+P1=$	2.648.315,1354
$P_2=P*(1+i)^2$=1,203,779.607 * (1+0,10)^2 =	1.456.573,32	$P_1(1+0,10)^1+P2=$	2.913.146,6489
$P_3=P*(1+i)^3$=1,203,779.607 * (1+0,10)^3 =	1.602.230,6569	$P_2(1+0,10)^1+P3=$	3.204.461,3089
$P_4=P*(1+i)^4$=1,203,779.607 * (1+0,10)^4 =	1.762.453,7226	$P_3(1+0,10)^1+P4=$	3.524.907,445
$P_5=P*(1+i)^5$=1,203,779.607 * (1+0,10)^5 =	1.938.699,09	$P_4(1+0,10)^1+P5=$	3.877.398,1897
$P_6=P*(1+i)^6$=1,203,779.607 * (1+0,10)^6 =	2.132.569,004	$P_5(1+0,10)^1+P6=$	4.265.138,003
$P_7=P*(1+i)^7$=1,203,779.607 * (1+0,10)^7 =	2.345.825,90	$P_6(1+0,10)^1+P7=$	4.691.651,809
$P_8=P*(1+i)^8$=1,203,779.607 * (1+0,10)^8 =	2.580.408,495	$P_7(1+0,10)^1+P8=$	5.160.816,985
$P_9=P*(1+i)^9$=1,203,779.607 * (1+0,10)^9 =	2.838.449,34	$P_8(1+0,10)^1+P9=$	5.676.898,689

$P=F[\frac{1}{(1+i)^n}]$

$1,203,779.607=F[\frac{1}{(1+0,10)^{20}}]$

F=8,098,427.245$

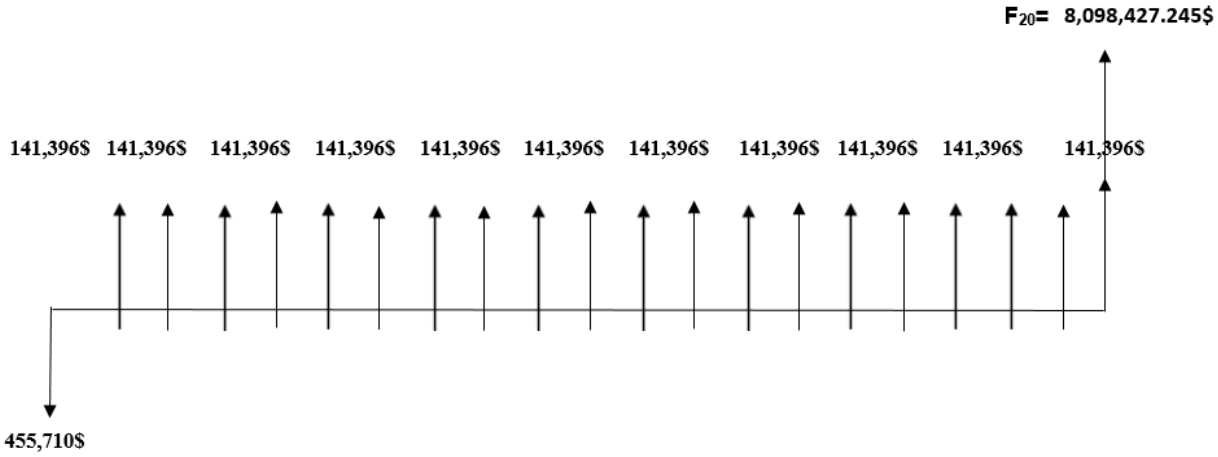


Figure 4.28. Cost flow diagram of R1234yf fluided system for service life of 20 years

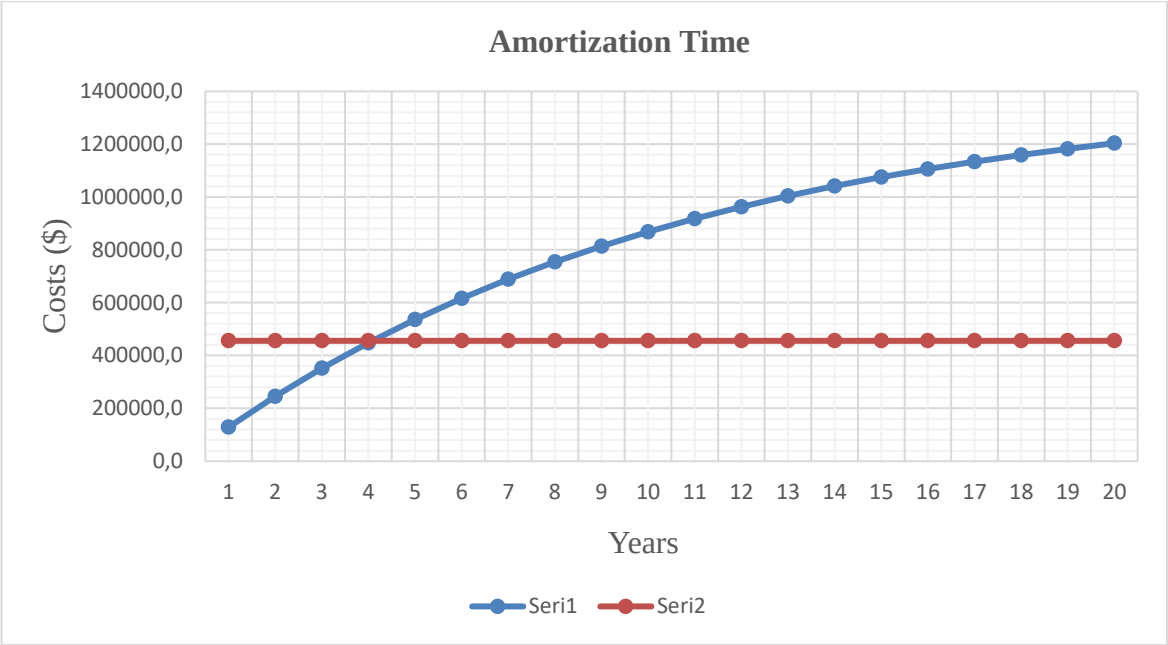


Figure 4.29. Diagram of present value of cumulative investment cost (Seri2) vs. present value of net earnings (Seri1) for R1234yf fluided system

The coindicency point of Seri1 and Seri2 plots refers the amortization and payback period which is 4.3 years for R1234yf fluided system as seen in the Figure 4.29.

In terms of R507A fluided multigeneration system; A=60,862.8298$

P(i)= 85,172.0926$

i=0.10

n=20

$P=A[\frac{(1+i)^n-1}{i(1+i)^n}]$

$P=60{,}862.8298[\frac{(1+0.10)^{20}-1}{0.10(1+0.10)^{20}}]$

P=518,159.58$

P-P(i)= 518,159.58-85,172.0926

P-P(i)= 432,987.487$

Table 4.17. Calculation of future values of R507A fluided system for ten years (half of service life)

P=	518159,58$	P=	518159,58$
$P_1=P*(1+i)^1=518159,58*(1+0,10)^1=$	569.975,538	$P(1+0,10)^1+P_1=$	1.139.951,076
$P_2=P*(1+i)^2=518159,58*(1+0,10)^2=$	626.973,09	$P_1(1+0,10)^1+P_2=$	1.253.946,1836
$P_3=P*(1+i)^3=518159,58*(1+0,10)^3=$	689.670,4	$P_2(1+0,10)^1+P_3=$	1.379.340,8
$P_4=P*(1+i)^4=518159,58*(1+0,10)^4=$	758.637,441	$P_3(1+0,10)^1+P_4=$	1.517.274,881
$P_5=P*(1+i)^5=518159,58*(1+0,10)^5=$	834.501,185	$P_4(1+0,10)^1+P_5=$	1.669.002,37
$P_6=P*(1+i)^6=518159,58*(1+0,10)^6=$	917.951,3	$P_5(1+0,10)^1+P_6=$	1.835.902,607
$P_7=P*(1+i)^7=518159,58*(1+0,10)^7=$	1.009.746,434	$P_6(1+0,10)^1+P_7=$	2.019.492,864
$P_8=P*(1+i)^8=518159,58*(1+0,10)^8=$	1.110.721,077	$P_7(1+0,10)^1+P_8=$	2.221.442,15
$P_9=P*(1+i)^9=518159,58*(1+0,10)^9=$	1.221.793,185	$P_8(1+0,10)^1+P_9=$	2.443.586,3699

$P=F[\frac{1}{(1+i)^n}]$

$518,159.58=F[\frac{1}{(1+0,10)^{20}}]$

F=3,485,918.548$

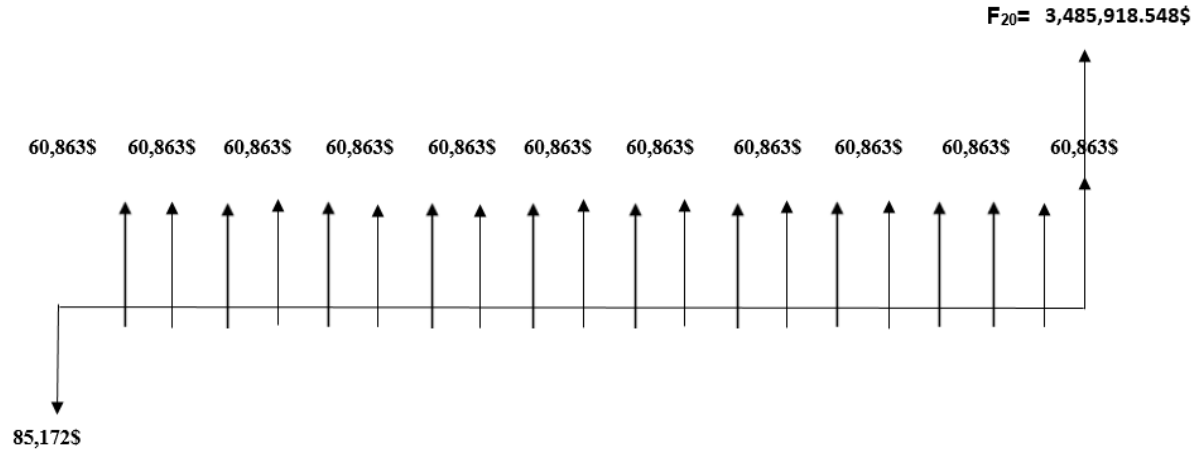


Figure 4.30. Cost flow diagram of R507A fluided system for service life of 20 years

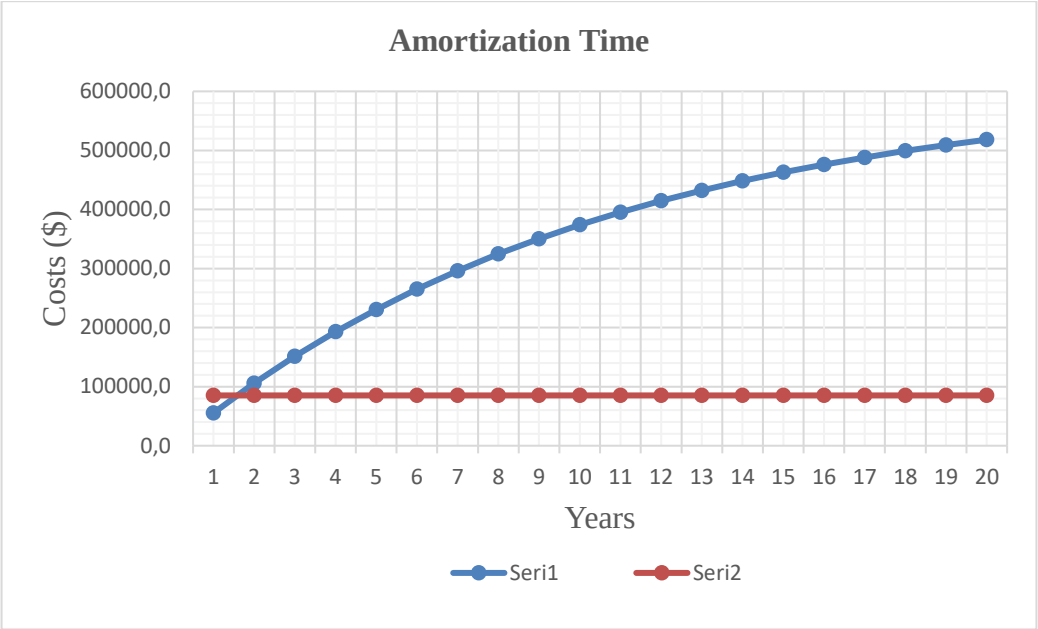


Figure 4.31. Diagram of present value of cumulative investment cost (Seri2) vs. present value of net earnings (Seri1) for R507A fluided system

The coindicency point of Seri1 and Seri2 plots refers the amortization and payback period for R507A fluided system as seen in the Figure 4.31.

In terms of R1233zd fluided multigeneration system; A=177,680.3558$

P(i)= 450,832.00$

i=0.10

n=20

$P=A[\frac{(1+i)^n-1}{i(1+i)^n}]$

$P=177,680.3558[\frac{(1+0.10)^{20}-1}{0.10(1+0.10)^{20}}]$

P=1,512,693.031$

P-P(i)= 1,512,693.031-450,832.00

P-P(i)= 1,061,861.031$

Table 4.18. Calculation of future cost values of R1233zd fluided system for ten years (half of service life)

$P_1=P*(1+i)^1=1,512,693.031*(1+0,10)^1=$	1.663.962,3341	$P(1+0,10)^1+P1=$	3.327.924,6682
$P_2=P*(1+i)^2=1,512,693.031*(1+0,10)^2=$	1.830.358,5675	$P_1(1+0,10)^1+P2=$	3.660.717,135
$P_3=P*(1+i)^3=1,512,693.031*(1+0,10)^3=$	2.013.394,424	$P_2(1+0,10)^1+P3=$	4.026.788,8
$P_4=P*(1+i)^4=1,512,693.031*(1+0,10)^4=$	2.214.733,87	$P_3(1+0,10)^1+P4=$	4.429.467,733
$P_5=P*(1+i)^5=1,512,693.031*(1+0,10)^5=$	2.436.207,25	$P_4(1+0,10)^1+P5=$	4.872.414,51
$P_6=P*(1+i)^6=1,512,693.031*(1+0,10)^6=$	2.679.827,98	$P_5(1+0,10)^1+P6=$	5.359.655,95
$P_7=P*(1+i)^7=1,512,693.031*(1+0,10)^7=$	2.947.810,78	$P_6(1+0,10)^1+P7=$	5.895.621,55
$P_8=P*(1+i)^8=1,512,693.031*(1+0,10)^8=$	3.242.591,854	$P_7(1+0,10)^1+P8=$	6.485.183,71
$P_9=P*(1+i)^9=1,512,693.031*(1+0,10)^9=$	3.566.851,04	$P_8(1+0,10)^1+P9=$	7.133.702,079

$P=F[\frac{1}{(1+i)^n}]$

$1,512,693.031=F[\frac{1}{(1+0,10)^{20}}]$

$F=10,179,630.087\$$

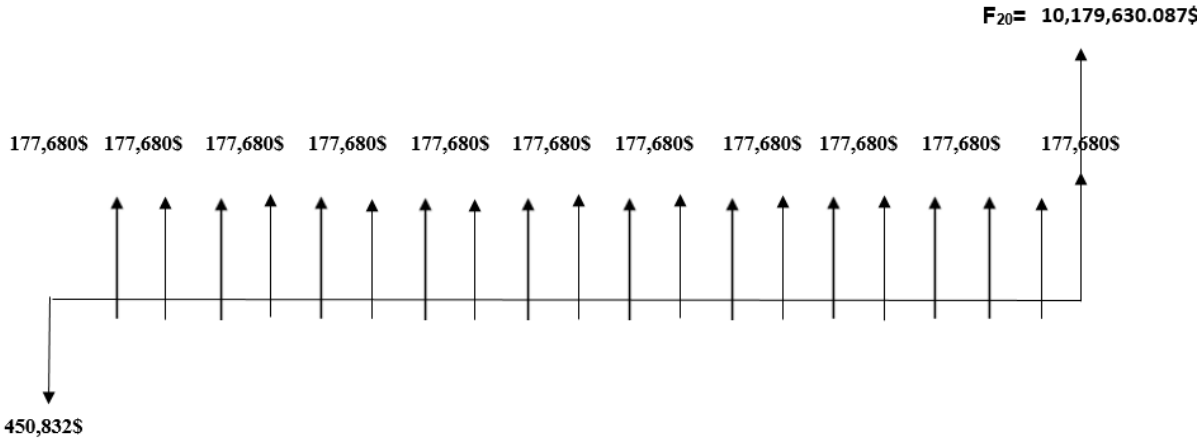


Figure 4.32. Cost flow diagram of R1233zd fluided system for service life of 20 years

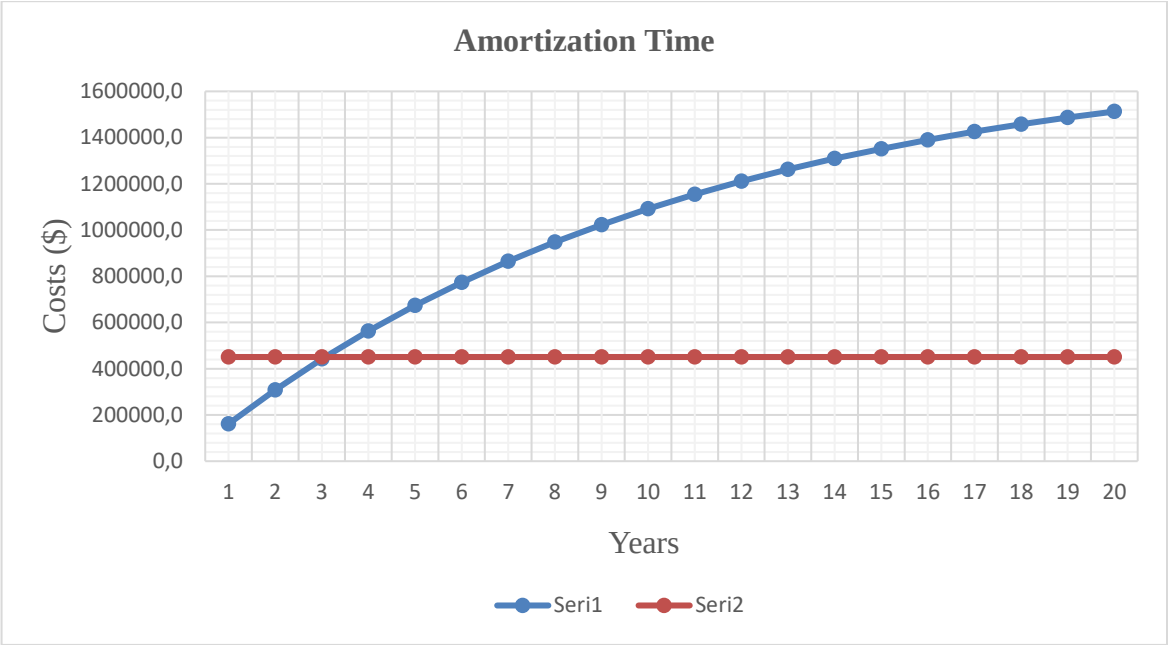


Figure 4.33. Diagram of present value of cumulative investment cost (Seri2) vs. present value of net earnings (Seri1) for R1233zd fluided system

The coindicency point of Seri1 and Seri2 plots refers the amortization and payback period which is 3.2 years for R1233zd fluided system as seen in the Figure 4.33.

In terms of R152A fluided multigeneration system; A=114,229.292$

P(i)= 205,739.00$

i=0.10

n=20

$P=A[\frac{(1+i)^n-1}{i(1+i)^n}]$

$P=114{,}229.292[\frac{(1+0.10)^{20}-1}{0.10(1+0.10)^{20}}]$

P=972,498.356$

P-P(i)= 972,498.356-205,739.00

P-P(i)= 766,759.356$

Table 4.19. Calculation of future cost values of R152A fluided system for ten years (half of service life)

P=	972,498.356$	P=	972,498.356$
$F_1=P*(1+i)^1=972,498.356*(1+0,10)^1=$	1,069,748.19	$P(1+0,10)^1+F1=$	2,139,496.38
$F_2=P*(1+i)^2=972,498.356*(1+0,10)^2=$	1,176,723.01	$F_1(1+0,10)^1+F2=$	2,353,446.02
$F_3=P*(1+i)^3=972,498.356*(1+0,10)^3=$	1,294,395.31	$F_2(1+0,10)^1+F3=$	2,588,790.62
$F_4=P*(1+i)^4=972,498.356*(1+0,10)^4=$	1,423,834.843	$F_3(1+0,10)^1+F4=$	2,847,669.684
$F_5=P*(1+i)^5=972,498.356*(1+0,10)^5=$	1,566,218.327	$F_4(1+0,10)^1+F5=$	3,132,436.65
$F_6=P*(1+i)^6=972,498.356*(1+0,10)^6=$	1,722,840.16	$F_5(1+0,10)^1+F6=$	3,445,680.32
$F_7=P*(1+i)^7=972,498.356*(1+0,10)^7=$	1,895,124.176	$F_6(1+0,10)^1+F7=$	3,790,248.352
$F_8=P*(1+i)^8=972,498.356*(1+0,10)^8=$	2,084,636.59	$F_7(1+0,10)^1+F8=$	4,169,273.187
$F_9=P*(1+i)^9=972,498.356*(1+0,10)^9=$	2,293,100.253	$F_8(1+0,10)^1+F9=$	4,586,200.502

$P=F[\frac{1}{(1+i)^n}]$

$972,498.356=F[\frac{1}{(1+0,10)^{20}}]$

F=6,542,482.64$

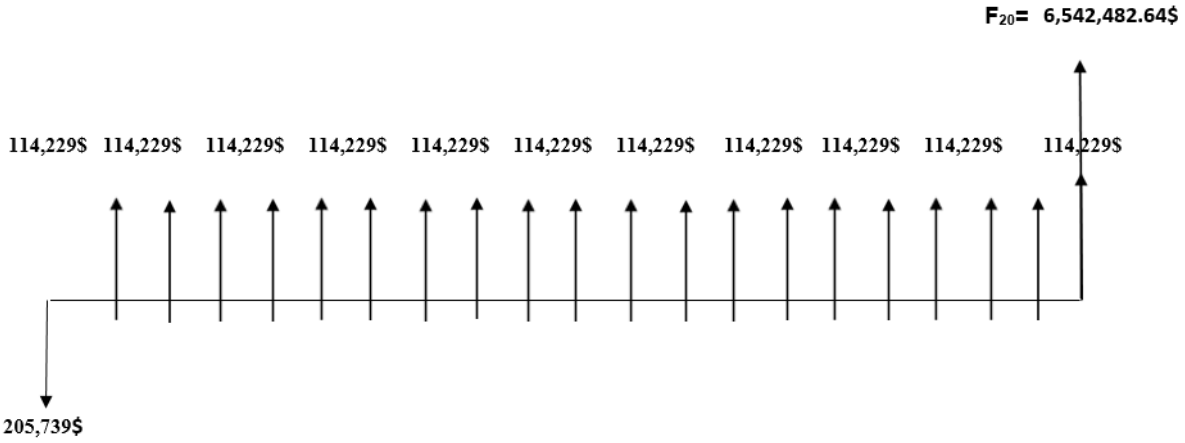


Figure 4.34. Cost flow diagram of R152A fluided system for service life of 20 years

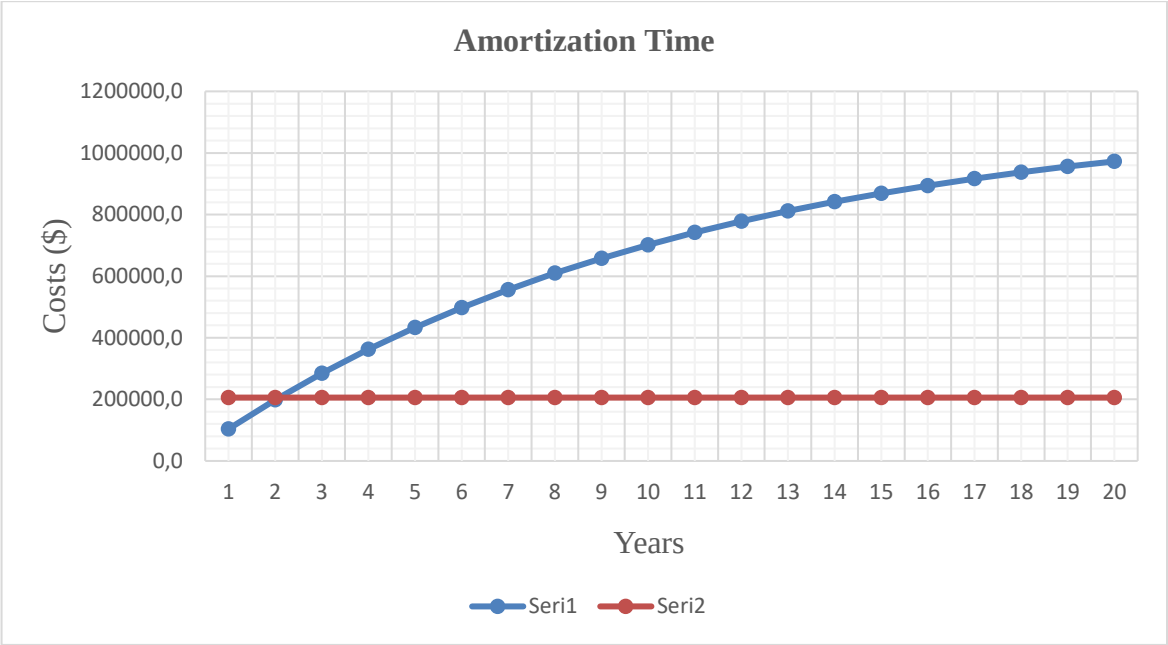


Figure 4.35. Diagram of present value of cumulative investment cost (Seri2) vs. present value of net earnings (Seri1) for R152A fluided system

The coindicency point of Seri1 and Seri2 plots refers the amortization and payback period for R125A fluided system as seen in the Figure 4.35.

In terms of R245CA fluided multigeneration system; A=162,711.027$

P(i)= 427,161.00$

i=0.10

n=20

$P=A[\frac{(1+i)^n-1}{i(1+i)^n}]$

$P=162{,}711.027[\frac{(1+0.10)^{20}-1}{0.10(1+0.10)^{20}}]$

P=1,385,250.696$

P-P(i)= 1,385,250.696-427,161.00

P-P(i)= 958,089.696$

Table 4.20. Calculation of future cost values of R245CA fluided system for ten years (half of service life)

P=	1,385,250.696$	P=	1,385,250.696$
$F_1=P*(1+i)^1=1,385,250.696*(1+0,10)^1=$	1,523,775.77	$P(1+0,10)^1+F1=$	3,047,551.5312
$F_2=P*(1+i)^2=1,385,250.696*(1+0,10)^2=$	1,676,153.342	$F_1(1+0,10)^1+F2=$	3,352,306.689
$F_3=P*(1+i)^3=1,385,250.696*(1+0,10)^3=$	1,843,768.676	$F_2(1+0,10)^1+F3=$	3,687,537.35
$F_4=P*(1+i)^4=1,385,250.696*(1+0,10)^4=$	2,028,145.544	$F_3(1+0,10)^1+F4=$	4,056,291.09
$F_5=P*(1+i)^5=1,385,250.696*(1+0,10)^5=$	2,230,960.098	$F_4(1+0,10)^1+F5=$	4,461,920.197
$F_6=P*(1+i)^6=1,385,250.696*(1+0,10)^6=$	2,454,056.108	$F_5(1+0,10)^1+F6=$	4,908,112.216
$F_7=P*(1+i)^7=1,385,250.696*(1+0,10)^7=$	2,699,461.719	$F_6(1+0,10)^1+F7=$	5,398,923.44
$F_8=P*(1+i)^8=1,385,250.696*(1+0,10)^8=$	2,969,407.891	$F_7(1+0,10)^1+F8=$	5,938,815.78
$F_9=P*(1+i)^9=1,385,250.696*(1+0,10)^9=$	3,266,348.68	$F_8(1+0,10)^1+F9=$	6,532,697.36

$P=F[\frac{1}{(1+i)^n}]$

$1,385,250.696=F[\frac{1}{(1+0,10)^{20}}]$

F=9,319,273.987$

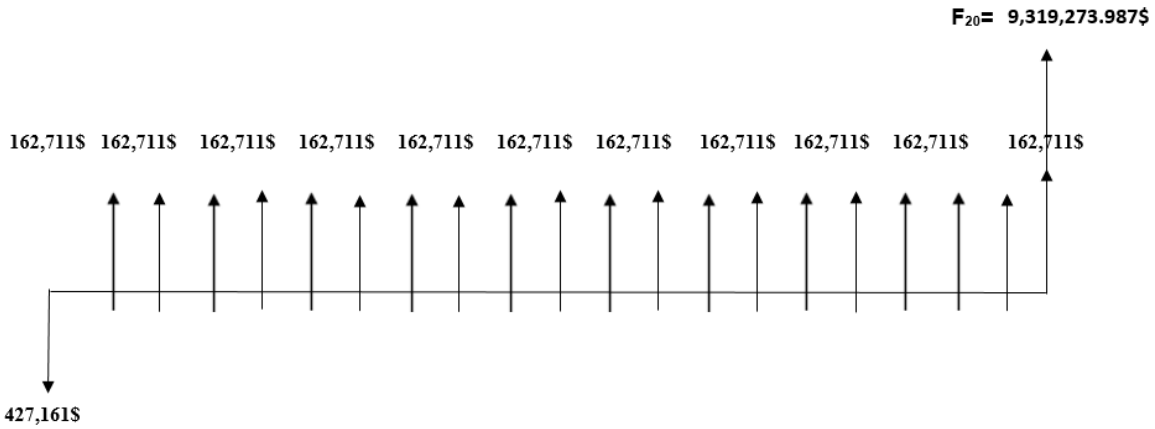


Figure 4.36. Cost flow diagram of R245CA fluided system for service life of 20 years

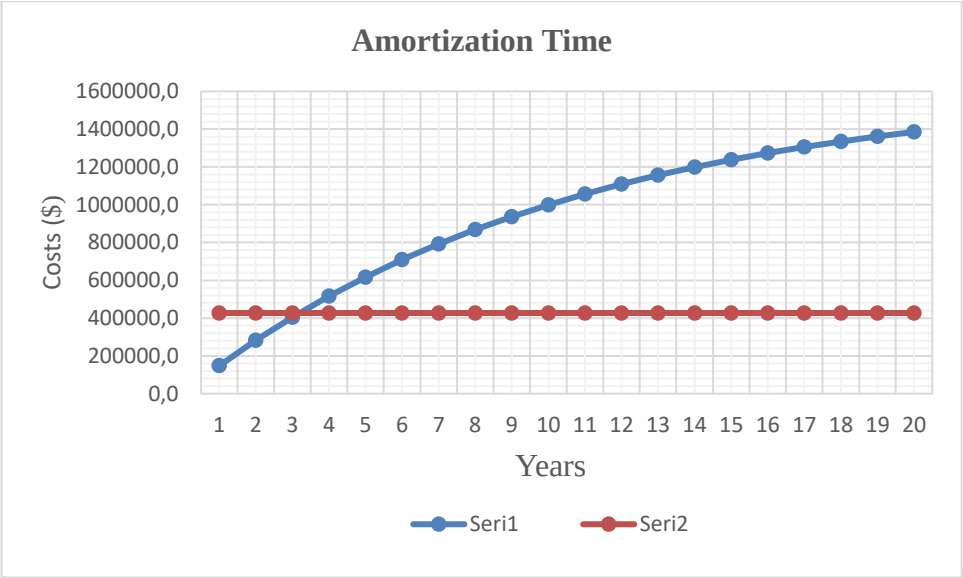


Figure 4.37. Diagram of present value of cumulative investment cost (Seri2) vs. present value of net earnings (Seri1) for R245CA fluided system

The coindicency point of Seri1 and Seri2 plots refers the amortization and payback period which is 3.35 years for R245CA fluided system as seen in the Figure 4.37.

In terms of R1234ze fluided multigeneration system; A=132,355.97$

P(i)= 319,624.00$, i=0.10 , n=20

$P=A[\frac{(1+i)^n-1}{i(1+i)^n}] \rightarrow P=132{,}355.97[\frac{(1+0.10)^{20}-1}{0.10(1+0.10)^{20}}] \rightarrow P=1{,}126{,}820.984\$$

P-P(i)= 1,126,820.984-319,624.00 → P-P(i)= 807,196.984$

Table 4.21. Calculation of future cost values of R1234ze fluided system for ten years (half of service life)

P=	1,126,820.984$	P=	1,126,820.984$
$P_1=P*(1+i)^1=1{,}126{,}820.984*(1+0{,}10)^1=$	1,239,503.08	$P(1+0{,}10)^1+P_1=$	2,479,006.16
$P_2=P*(1+i)^2=1{,}126{,}820.984*(1+0{,}10)^2=$	1,363,453.39	$P_1(1+0{,}10)^1+P_2=$	2,726,906.78
$P_3=P*(1+i)^3=1{,}126{,}820.984*(1+0{,}10)^3=$	1,499,798.73	$P_2(1+0{,}10)^1+P_3=$	2,999,597.46
$P_4=P*(1+i)^4=1{,}126{,}820.984*(1+0{,}10)^4=$	1,649,778.603	$P_3(1+0{,}10)^1+P_4=$	3,299,557.21
$P_5=P*(1+i)^5=1{,}126{,}820.984*(1+0{,}10)^5=$	1,814,756.463	$P_4(1+0{,}10)^1+P_5=$	3,629,512.93
$P_6=P*(1+i)^6=1{,}126{,}820.984*(1+0{,}10)^6=$	1,996,232.109	$P_5(1+0{,}10)^1+P_6=$	3,992,464.22
$P_7=P*(1+i)^7=1{,}126{,}820.984*(1+0{,}10)^7=$	2,195,855.32	$P_6(1+0{,}10)^1+P_7=$	4,391,710.64
$P_8=P*(1+i)^8=1{,}126{,}820.984*(1+0{,}10)^8=$	2,415,440.85	$P_7(1+0{,}10)^1+P_8=$	4,830,881.70
$P_9=P*(1+i)^9=1{,}126{,}820.984*(1+0{,}10)^9=$	2,656,984.937	$P_8(1+0{,}10)^1+P_9=$	5,313,969.872

$P=F[\frac{1}{(1+i)^n}]$

$1{,}126{,}820.984=F[\frac{1}{(1+0{,}10)^{20}}]$

F=7,580,688.11$

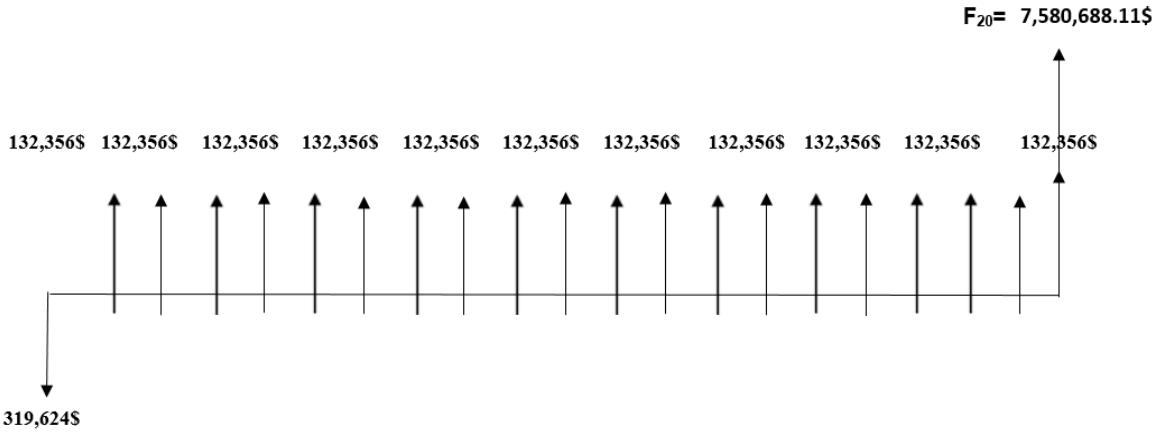


Figure 4.38. Cost flow diagram of R1234ze fluided system for service life of 20 years

Cost flow diagram in Figure 4.38 demonstrate the total cost 319,624$ as outgoing, net earnings for each 20 year as 132,356$ and future value 7,580,688.11$ as income.

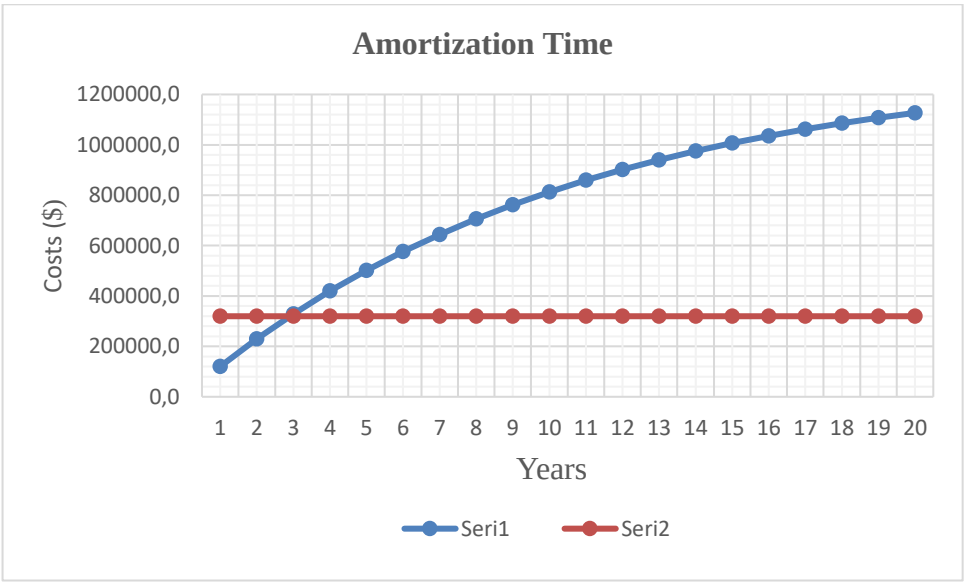


Figure 4.39. Diagram of present value of cumulative investment cost (Seri2) vs. present value of net earnings (Seri1) for R1234ze fluided system

The coindicency point of Seri1 and Seri2 plots refers the amortization and payback period which is 3.03 years for R1234ze fluided system as seen in the Figure 4.39.

Thus, checking out this calculations with respect to engineering economy, it can be concluded that these results are compatible with the previous calculations of the cost analyses. Additionally, results of this calculations of engineering economy demonstrate that all systems are profitable to be performed. Furthermore, the highest current profit values P-P(i) and future values F are calculated for the system with R245fa and R1233zd.

5 RESULTS AND DISCUSSION

In this thesis, a groundbreaking multigenerational hybrid system that combines solar energy harvested from parabolic solar collectors with geothermal energy sourced from a well is delved into. The primary objective of this system is to achieve maximum efficiency while minimizing investment costs. Accordingly, in the multigenerational hybrid system, the evaporator efficiently uses the heat comes from both parabolic solar collectors and geothermal well. Thus, the evaporator plays a pivotal role in this multigenerational hybrid system since the heat transfer process within the evaporator ensures optimal energy utilization. Then, the resulting superheated steam, reaching temperatures up to a maximum of 146.5 ℃, is directed into the turbine for power generation. Thus, the key components of this study are turbine, evaporator, solar collectors and geothermal well.

One of the most important parameters for designing this multigenerational system is to determine the solar collector area that the hybrid system needs. Accordingly, the minimum collector area supplying the maximum collector capacity is significant to find the minimum collector area capable of supplying the maximum collector capacity. The working fluid goes into the solar collector area after the heat transfer at the evaporator between the geothermal source and the organic fluid. Accordingly, the minimum solar collector area is calculated as 32,152 m^2 with Ebsilon programme for R507A fluided system with solar output pressure 4 bar, 117℃ and 1000 W/m^2 direct normal irradiance. Moreover, the maksimum solar collector area is calculated as 501,36 m^2 with Ebsilon for R245fa fluided system with solar output pressure 4 bar, 175℃.

Coming to saturated liquid phase of the fluid returning from the turbine is also one of the most important parameters in order to add it to the hybrid system again at the state of maximum working capacity. It was observed that the net work amount produced from the multigeneration system is consistent with the solar radiation values. When designing this multigenerational hybrid system, it was also tried to decrease the solar panel investment cost and to emphasize geothermal system work.

According to the results from Ebsilon programme, it was calculated that the exact work produced by this multigeneration system varied between 486.7 kW and 852 kW with the different organic fluids utilized in the ORC. Thus, for the R507A used system, the generator work is 61.165 kW, the solar panels work is 22.795 kW and the geothermal work is 525.054 kW. For the R1234yf used system, the generator work is 136.874 kW, the solar panels work

is 538.729 kW and the geothermal work is 450.144 kW. For the R245fa used system, the generator work is 170.078 kW, the solar panels work is 686.637 kW and the geothermal work is 313.366 kW. For the R1233zd used system, the generator work is 160.489 kW, the solar panels work is 610.623 kW and the geothermal work is 209.403 kW. For the R1234ze used system, the generator work is 122.144 kW, the solar panels work is 439.800 kW and the geothermal work is 464.575 kW. For the R152A used system, the generator work is 104.924 kW, the solar panels work is 311.278 kW and the geothermal work is 404.233 kW. For the R245CA used system, the generator work is 145.479 kW, the solar panels work is 572.96 kW and the geothermal work is 256.537 kW.

One of the most important parameters of a system is also the thermal efficiency after work. The efficiency of this multigenerational hybrid system designed with different organic fluids is varying between 11.2 and 19.6. Accordingly, the efficiency (ETA) of this hybrid system with R507A is 11.2. The efficiency of this hybrid system with R1234yf is 13.8. The efficiency of this hybrid system with R245FA is 17. The efficiency of this hybrid system with R1233zd is 19.6. The efficiency of this hybrid system with R1234ze is 13.5. The efficiency of this hybrid system with R152A is 14.7. The efficiency of this hybrid system with the R245CA is 17.5. These all output results for each fluids can also be observed from the Table 5.1 below.

Table 5.1. Total output parameters for each fluided system

	R245FA	**R1234yf**	**R507A**	**R1233zd**	**R1234ze**	**R245CA**	**R152A**
n_th	0,172	0,138	0,112	0,196	0,135	0,175	0,147
n_exergy	0,5793	0,4903	0,5312	0,6105	0,5678	0,5513	0,5965
W_in (kW)	5,412	13,74	8,247	5,248	6,437	5,374	5,012
W_out (kW)	177,4	142,6	61,165	167,4	122,144	145,479	104,924
Q_in (kW)	1000	988,6	547,849	820,1	904,375	829,497	715,511
Q_out (kW)	828	859,8	493,2	657,9	736,5	687,8	605,1
n_pump	0,8	0,8	0,8	0,8	0,8	0,8	0,8
n_turbine	0,998	0,998	0,998	0,998	0,998	0,998	0,998

Furthermore, in terms of validation of the analyses, the simulation results from Ebsilon is consistent with the results obtained from EES which is fine to check the accuracy of the

results. The simulation results obtained from Ebsilon align with those from EES, ensuring the accuracy of our findings.

Table 5.2. Outputs of each cycle

	R245fa	**R1234yf**	**R507A**	**R1233zd**	**R1234ze**	**R152A**	**R245CA**
n_{th}	0,172	0,1303	0,1011	0,1977	0,1332	0,1455	0,175
n_{exergy}	0,5793	0,4903	0,5312	0,6105	0,5742	0,6231	0,5513
W_{out}	177,4	142,6	63,72	167,4	127	109,2	145,479
Total Cost	500,195.00$	455,710.4232$	85,172.0926$	450,832.00$	319,624$	205,739.00$	427,161.00$
Present Value	1,328,160.87$	889,459.92$	493,850.32$	1,232,206.12$	942,123.52$	846,570.92$	1,123,815.00$

Up to now, the ORCs with respect to their organic fluids, capacities of the components and solar system energy input were analyzed. In our study, there are two main important goals; the first one is that we need to select an organic working fluid for such cycles instead of R134a fluid, whose reactions have responsible in depletion of ozone layer. In this manner we have analyzed the ORCs and examined which organic fluids satisfy mostly and in an affordable way. The other concern is the reduction of solar heat source energy. The point here is eliminating use of fossil fuels. As a result, this innovative multigenerational hybrid system represents a sustainable approach to energy integration, emphasizing both solar and geothermal sources.

6 CONCLUSIONS AND RECOMMENDATIONS

An energy efficient and nature friendly innovative multigenerational hybrid system consisting renewable solar and geothermal with ORC in the Gonen district was designed with this groundbreaking study. There is no such a design in Gonen before, which is originality of this study as the uniqueness of our approach lies in the fact that no such system has been previously implemented in this specific region. Multigenerational renewable energy systems offer several advantages in terms of energy efficiency. Optimization for this studied multigenerational system was worked on to make it more energy efficient. Unlike traditional single-generation energy systems, the multigenerational design optimizes energy utilization across different generations. This holistic approach ensures efficient energy transfer and utilization, benefiting both current and future users.

Renewable energy integration is one of the significance of this thesis since the hybrid system seamlessly integrates two abundant and sustainable energy sources: solar and geothermal. By harnessing the power of the sun and the Earth's natural heat, it is aimed to create a harmonious balance between energy production and environmental preservation. By combining solar and geothermal energy, the overall system performance is maximized while minimizing waste. This approach aligns with global efforts to reduce carbon emissions and combat climate change.

It is worked diligently to optimize the multigeneration system. Through rigorous analysis and modeling, various parameters are fine-tuned to achieve higher energy efficiency. This involved considering factors such as component sizing, operating conditions, and fluid selection.

In order to improve the system design and make a decision for selecting the most suitable working fluid to utilize, the following optimization steps are carried out. One of them is equal heat energy supplement via solar energy system. In order to make a proper comparison, it is tried to make solar energy inlet equivalent for each working fluid cycle. The concern was the solar collector cost, which forms the majority of the total cost of the multigeneration system, besides the improvement of the exergy efficiency. When it is tried to supply the same amount of heat energy (amount of 200-300-400 kW) to each cycle, R245fa could not exceed its saturation temperature at related working pressure (16 bar), which means that the fluid could not become superheated vapor. As result of that, the work

and power of electricity obtained from the turbine have been decreased dramatically as well as thermal and exergy efficiencies.

Also, the multigeneration system is tried to be optimized with no solar only with geothermal heat input and ORC. Accordingly, working fluids could not exceed its saturation temperature at related working pressure, which means that fluids could not become superheated vapor. Work and power of electricity obtained from turbine have been decreased dramatically as well as thermal and exergy efficiencies.

The other optimization step is the manipulations with the energy sources (geothermal); it is proceeded in the same path with the same aim and tried to manipulate the physical properties of the geothermal energy source. In order to meet the energy requirement, which has been occurred when the supplement of heat energy from the solar system is reduced, the change in the exergy efficiency and total cost with the increasing the mass flow rate of the water that is utilized in the geothermal source are analyzed. The change in the related parameters are also observed with the change of the geothermal source temperature which is taken as 94℃ during this study. Though these restorations have exhibited more beneficial results in theory, the characteristic properties of the geothermal system (Gonen geothermal-G9 well) can not be changed.

Reduction of the working pressure is another improvement method applied. In this way, the boiling temperature of the working fluids would be reduced with the reduction of the pressure. This means, the requirement of the heat energy would be decreased as well. However, R245fa (the fluid that requires the most amount of heat to evaporate) leaves the geothermal system at 350℃. The saturation temperature of R245fa at 16 bar is 384℃, where solar energy that is provided to the ORC was 686,684kW. As we reduced the working pressure from 16 to 8 bar, provided heat energy from the solar energy system has decreased to almost 420kW besides the decrease of boiling temperature to 334.6℃. Although reduction of the working pressure has leaded to less heat energy requirement that also means less absorption of heat from the solar system, thermal efficiency has decreased to almost 9%.

Increasing the mass flow rate of the organic fluid lastly, and it is observed that the results as other parameters (solar and geothermal heat energy inlets, working pressure) are kept the same. Each mass flow rate is adjusted to obtain the same amount of 1000kW heat inlet (R245fa is taken as the reference fluid due to the highest heat absorption) for each cycle. As a result of that, it is observed that all turbine work and produced electricity have been

increased. As well as the turbine work, exergy efficiencies also have increased to superior levels. The results are given in the following Table 6.1 as:

Table 6.1. The outputs evaluated for the same heat energy input for each working fluid

	Q_{in} Before(kW)	Q_{in} After (kW)	W_{out} Before (kW)	W_{out} After (kW)	$\dot{m}$ Before (kg/s)	$\dot{m}$ After (kg/s)	2nd Law Efficiency
R245fa	1000	1000	177.2	177.2	4	4	0.5793
R1234yf	988.4	1000	142.2	143.8	5.5	5.565	0.5286
R507A	547.3	1000	63.12	115.4	3.4	6.215	0.4841
R1233zde	819.7	1000	167	203.8	3.0	3.66	0.796

Additionally, it is important to underline that the thermal efficiency does not change as the mass flow rate of the organic fluid changes due to the fact that the working temperature and so the enthalpy of each step (turbine inlet-solar outlet, solar inlet-geothermal outlet, etc) stays constant. The energy (kJ/kg) that is extracted from energy sources does not change. Also the energy achieved from turbine does not change. So, in this improvement, thermal efficiency does not change and so is not added to the Table 6.1. It is also read from the Table 6.1 that R507 can be thought as the most affordable working fluid, again. R245fa has the highest second law of efficiency. R1234yf has the less second of efficiency.

The heart of our system is the ORC, which converts thermal energy into mechanical work. We explored seven different organic fluids—R507A, R1234yf, R245FA, R1233zd, R1234ze, R152A, and R245CA—to determine the most suitable fluid for our specific application. In order to evaluate system performance comprehensively, both energetic and exergetic result values are calculated. These analyses allowed us to assess energy losses, irreversibilities, and overall efficiency. We cross-validated our findings using Ebsilon Professional and EES programs to ensure robust results. And, not only the energetic but also the exergetic result values and efficiencies were calculated, analyzed and compared with Ebsilon and EES programmes. The results of analyses of the multigenerational system via Ebsilon Professional programme is compatible with the results of analyses via EES programme, which is favorable for crosschecking. Accordingly, the maximum generator

work for electrical power production is gained as 170.078 kW with R245FA organic fluided hybrid system and the minimum generator work for electiricty production is 61.165 kW with R507A organic fluided hybrid system. Moreover, the maximum thermal efficiency of the designed hybrid system is 19.6% with R1233zd organic fluid and the minimum thermal efficiency of the designed hybrid system is 11.2% with R507A organic fluid. Thus, among the organic fluids tested, the R245FA-based hybrid system achieved the highest generator work for electrical power production, reaching an impressive 170.078 kW. Conversely, the R507A-based system had the lowest generator work at 61.165 kW. Additionally, the thermal efficiency varied, with R1233zd yielding the highest (19.6%) and R507A the lowest (11.2%).

Furthermore, the multigeneration system was also optimized to decrease solar panel investment cost with the help of Gonen geothermal well and ORC. In terms of cost-effective solar integration, cost-saving measures by optimizing solar panel investment is also explored. Leveraging the Gonen geothermal well allowed us to reduce the overall system cost while maintaining performance. In order to prevent such cases, other heat sources (solar and geothermal heat sources) are utilized. The point in our study is the reduction of solar heat energy source, which is costly to use.

As it is obviously seen in the Figure 4.25 that the majority of the total cost is the solar heat energy source. In our study; the type of solar collectors is “parabolic trough collectors” and there are 2 solar collectors for R245fa, R1234yf, and R1233zd(E). On the other hand, there is only 1 single solar collector is used for R507A. As it is also confirmed from the Table 5.2, total cost is smallest for ORC whose working fluid is R507A.

We read from the Table 5.2 that R507 can be thought as the most affordable working fluid, again. However, due to its high GWP value, R507A is not preferable. R245fa has the highest second law of efficiency. R1234yf has the less second of efficiency.

Moreover, analyzing this novel multigeneration system, these t-s and p-v diagrams below in Figure 6.1 are obtained, which demonstrate the best organic working fluid to select among these seven organic fluids which are the originality of this doctorate thesis.

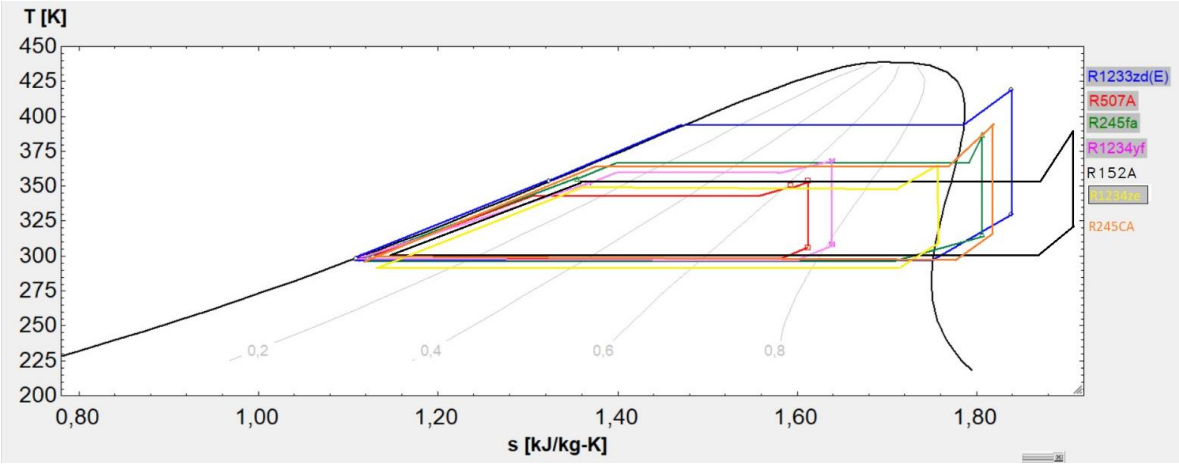


Figure 6.1. t-s diagrams of all working fluids used in this thesis

These diagrams in Figure 6.1 and Figure 6.2 can also be taken as guidelines to choose the best efficient working fluid. Thus, this innovative diagrams are also the originality of the outputs of this multigeneration study. Observing the area under these t-s and p-v diagrams which demonstrate the Wnet, R1233zd has the biggest area among the other working fluids in both Figures 6.1 and 6.2. Thus, R1233zd is selected as the most thermal efficient fluid comparing with other working fluids.

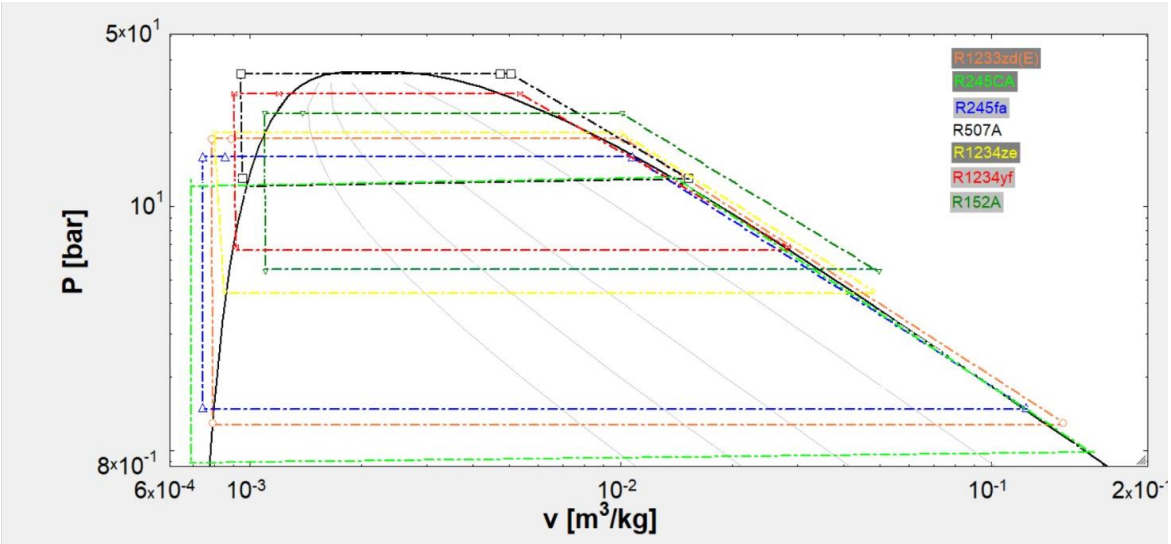


Figure 6.2. p-v diagrams of all working fluids used in this thesis

Considering all the parameters we evaluated R1233zd(E) is the most suitable fluid for this ORC. R1233zd(E) has the highest thermal and second law efficiency besides the reasonable cost. This makes this fluid is the optimal choice for both performance and long-term financial

benefits. Apart from thermodynamic and financial reasons, the environmental effects of this fluid is also appropriate. It has low global warming and ozone depletion potential, it does not last long in nature when it is compared to other fluids.

This study opens avenues for further research. Future investigations could focus on long-term system monitoring, reliability assessments, and additional cost optimization strategies to refine the system. Moreover, these multigeneration system will assist other system designers and this dissertation should prove a useful tool for future research. This thesis is expected to serve as a valuable resource for future work.

REFERENCES

[1] Lecompte, S. 2015. “Review of organic Rankine cycle (ORC) architectures for waste heat recovery”, Renewable and Sustainable Energy Reviews, 47, 448-461

[2] Imran, M., Haglind, F., Asim, M., Alvid J. January 2018. “Recent research trends in organic Rankine cycle technology: A bibliometric approach”, 81, Part 1, 552-562

[3] Tartière T., Astolfi M. 2017. “A World Overview of the Organic Rankine Cycle Market”, Energy Procedia Energy Procedia, Volume 129, 2-9

[4] Tchanche, B. 2014. “Heat resources and organic Rankine cycle machines”, Renewable and Sustainable Energy Reviews, 39, 1185-1199

[5] Sung T., Kim K. 2017. “An organic Rankine cycle for two different heat sources: steam and hot water”, Energy Procedia, 129, 883-890

[6] http://www.turboden.eu/en/rankine/rankine-advantages.php

[7] Capata, R. 2014. “Preliminary design and simulation of a turbo expander for small rated power organic Rankine cycle (ORC)”, Energies, 7, 7067-7093

[8] Rahbar, K., Mahmoud, S., Al-Dadah, R., Moazami, N. 2015. “Modelling and optimization of organic Rankine cycle based on a small-scale radial inflow turbine”, Energy Conversion and Management, 91, 186-198

[9] Rahbar, K., Mahmoud, S., Al-Dadah, R., Moazami, N., Mirhadizadeh S. 2017. “Review of organic Rankine cycle for small-scale applications”, Energy Conversion and Management, Volume 134, 135-155

[10] Eyidogan, M. 2016. “Investigation of Organic Rankine Cycle (ORC) technologies in Turkey from the technical and economic point of view”, Renewable and Sustainable Energy Reviews, 58, 885-895

[11] http://www.infinityturbine.com/general-info.html

[12] Lei B., Wu Y., Ma C., Wang W., Zhi R. 2017. “Theoretical analyses of pressure losses in organic rankine cycles”, Energy Conversion and Management, 153, 157–162

[13] Quoilin, S., Lemort, V., Lebrun, J. 2010. “Experimental study and modeling of an Organic Rankine Cycle using scroll expander”, Applied Energy, 87, 1260–1268

[14] Miao Z., Xu J., Zhang K. 2017. “Experimental and modeling investigation of an organic Rankine cycle system based on the scroll expander”, Energy, 134, 35-49

[15] Ameri, M. 2016. “Performance assessment and multi-objective optimization of an integrated organic Rankine cycle and multi-effect desalination system”, Desalination, 392, 34-45

[16] Eyerer, S. 2016. “Experimental study of an ORC (Organic Rankine Cycle) and analysis of R1233zd-E as a drop-in replacement for R245fa for low temperature heat utilization”, Energy, 103, 660-671

[17] Chen, H., Goswami, Y., Stefanakos, E. 2010. “A review of thermodynamic cycles and working fluids for the conversion of low-grade heat”, Renewable and Sustainable Energy Reviews, 14, 3059–3067

[18] Pezzuolo, A. 2016. “The ORC-PD: A versatile tool for fluid selection and Organic Rankine Cycle unit design”, Energy, 102, 605-620

[19] Hærvig, J. 2016. “Guidelines for optimal selection of working fluid for an organic Rankine cycle in relation to waste heat recovery”, Energy, 96, 592-602

[20] Drescher, U., Bruggemann, D. 2007. “Fluid selection for the Organic Rankine Cycle (ORC) in biomass power and heat plants”, Applied Thermal Engineering, 27, 223–228

[21] Desai, N. 2016. “Thermo-economic analysis and selection of working fluid for solar organic Rankine cycle”, Applied Thermal Engineering, Volume 95, 471-481

[22] Xu, H. 2016. “Investigation on the fluid selection and evaporation parametric optimization for sub- and supercritical organic Rankine cycle”, Energy, 96, 59-68

[23] Aslan A. (2010) Gönen Jeotermal Bölgesel Isıtma Sisteminin Enerji ve Termoekonomik Verimliliğinin İncelenmesi. Doktora Tezi, Balıkesir Üniversitesi Fen Bilimleri Enstitüsü, Balıkesir, Türkiye, 77-79.

[24] Jung, H., Taylor, L., Krumdieck, S. 2015. “An experimental and modelling study of a 1 kW organic Rankine cycle unit with mixture working fluid”, Energy, 81, 601-614

[25] Li, J. 2016. “Effect of working fluids on the performance of a novel direct vapor generation solar organic Rankine cycle system”, Applied Thermal Engineering, 98, 786-797

[26] Zhai, H. 2016. “Analysis of the quantitative correlation between the heat source temperature and the critical temperature of the optimal pure working fluid for subcritical organic Rankine cycles”, Applied Thermal Engineering, 99, 383-391

[27] Collings, P. 2016. “A dynamic organic Rankine cycle using a zeotropic mixture as the working fluid with composition tuning to match changing ambient conditions”, Applied Energy, 171, 581-591

[28] Chen H., Goswami D., Rahman M., Stefanakos, E. 2011. “A supercritical Rankine cycle using zeotropic mixture working fluids for the conversion of low-grade heat into power”, Energy, 36, 549-555

[29] Rajabloo T., Iora P., Invernizzi, C. 2016. “Mixture of working fluids in ORC plants with pool boiler evaporator”, Applied Thermal Engineering, 98, 1-9

[30] Feng Y., Hung T., Greg K., Zhang Y., Li B., Yang J., 2015. “Thermoeconomic comparison between pure and mixture working fluids of organic Rankine cycles (ORCs) for low temperature waste heat recovery”, Energy Conversion and Management, 106, 859-872

[31] Barse K. A., Mann M. D., 2016. “Maximizing ORC performance with optimal match of working fluid with system design”, Applied Thermal Engineering, 100, 11-19

[32] Desideri, A. 2016. “Experimental comparison of organic fluids for low temperature ORC (organic Rankine cycle) systems for waste heat recovery applications”, Energy, 97, 460-469

[33] Mondejar, M., Andreasen J., Regidor, M., Riva, S., Kontogeorgis, G., Persico, G., and Haglind, F. 2017. “Prospects of the use of nanofluids as working fluids for organic Rankine cycle power systems”, Energy Procedia, 129, 160–167

[34] Liu L., Zhu T., Ma J. 2017. “Working fluid charge oriented off-design modeling of a small scale Organic Rankine Cycle system” Energy Conversion and Management, 148, 944-953

[35] Shu G., Yu G, Tian H., Wei H., Liang X., Huang Z., 2016. “Multi-approach evaluations of a cascade-Organic Rankine Cycle (C-ORC) system driven by diesel engine waste heat: Part A – Thermodynamic evaluations”, Energy Conversion and Management, 108, 579–595

[36] Sung, T. 2016. “Thermodynamic analysis of a novel dual-loop organic Rankine cycle for engine waste heat and LNG cold”, Applied Thermal Engineering, 100, 1031-1041

[37] Karapekmez A., Dincer I. 2021. “Development of a multigenerational energy system for clean hydrogen generation”, Journal of Cleaner Production, 299, 126909

[38] Dincer, I. Bicer, Y. 2020. “Integration of renewable energy systems for multigeneration”, Integrated Energy Systems for Multigeneration

[39] Li, M. 2016. “Analytical thermal efficiency of medium-low temperature organic Rankine cycles derived from entropy-generation analysis”, Energy, 106, 121-130

[40] Yue C., You F., Huang Y., 2016. “Thermal and economic analysis of an energy system of an ORC coupled with vehicle air conditioning”, International Journal of Refrigeration, 64, 152–167

[41] Panesar A., Morgan R., Kennaird D. 2017. “Organic Rankine cycle thermal architecture – From concept to demonstration”, Applied Thermal Engineering, 126, 419-428

[42] Wei, D. 2008. “Dynamic modeling and simulation of an Organic Rankine Cycle (ORC) system for waste heat recovery”, Applied Thermal Engineering, 28, 1216–1224

[43] Nasri, F., Chaouki, A., Bacha, H. 2011. “Electricity production system from solar-heated rankine cycle: modeling and simulation”, IJRRAS 8 (2), 176-183

[44] Karellas S., Braimakis K., 2016. “Energy–exergy analysis and economic investigation of a cogeneration and trigeneration ORC–VCC hybrid system utilizing biomass fuel and solar power”, Energy Conversion and Management, 107, 103–113

[45] Paanu, T., Niemi, S., Rantanen, P. 2012. “Waste Heat Recovery – Bottoming Cycle Alternatives”, Proceedings of the University of Vaasa, Reports 175

[46] Rahbar, K. 2015. “Parametric analysis and optimization of a small-scale radial turbine for organic Rankine cycle”, Energy, 1-16

[47] Li, G. 2016. “Organic Rankine cycle performance evaluation and thermoeconomic assessment with various applications part I: Energy and exergy performance evaluation”, Renewable and Sustainable Energy Reviews, 53, 477-499

[48] Desai, N., Bandyopadhyay, S. 2009. “Process integration of organic Rankine cycle”, Energy 34, 1674–1686

[49] Li, Y. 2016. “Investigation of the organic Rankine cycle (ORC) system and the radial-inflow turbine design”, Applied Thermal Engineering, 96, 547-554

[50] Bürki, T., Börrnert, T. 2010. “Save 20% electricity by converting low temperature waste heat into electricity”, Asean Federation of Cement Manufacturers, FCM 22nd Technical Symposium&Exhibition, 28-34

[51] Proctor, M. 2016. “Dynamic modelling and validation of a commercial scale geothermal organic rankine cycle power plant”, Geothermics, 61, 63-74

[52] Yamamoto, T., Furuhata, T., Arai, N., Mori, K. 2001. “Design and testing of the Organic Rankine Cycle”, Energy 26, 239–251

[53] Landelle A., Tauveron N., Haberschill P., Revellin R., Colasson S. 2017. “Organic Rankine cycle design and performance comparison based on experimental database”, Applied Energy, 204, 1172–1187

[54] Fu, B. 2015. “Design, construction, and preliminary results of a 250-kW organic Rankine cycle system, Applied Thermal Engineering”, 80, 339-346

[55] Mahfuz M. H., Anisur M. R., Kibria M. A., Saidur R., Metselaar I. H. S. C. 2014. “Performance investigation of thermal energy storage system with Phase Change Material (PCM) for solar water heating application”, International Communications in Heat and Mass Transfer 57, 132–139

[56] Dong, S. 2016. “Optimum design method of Organic Rankine Cycle system based on semi-empirical model and experimental validation”, Energy Conversion and Management, 108, 85-95

[57] Kaygusuz K., Sarı A. 2003. “Renewable energy potential and utilization in Turkey”, Energy Conversion and Management, vol. 44, 3, 459-478

[58] Eroglu H. 2022. “Development of a Novel Solar Energy Need Index for Identifying Priority Investment Regions: A Case Study and Current Status in Turkey”, Environment Development and Sustainability, vol. 24, 10, 1007

[59] Ozgur M. A. 2008. “Review of Turkey's renewable energy potential”, Renewable Energy, 33, 2345–2356

[60] Imran, M. 2016. “Comparative assessment of Organic Rankine Cycle integration for low temperature geothermal heat source applications”, Energy, 102, 473-490

[61] Ahmed A., Esmaeil K., Irfan M., Al-Mufadi F. January 2018. “Design methodology of organic Rankine cycle for waste heat recovery in cement plants”, Applied Thermal Engineering, 129, 421-430

[62] Zhai H., An Q., Shi L. 2018. “Zeotropic mixture active design method for organic rankine cycle”, Applied Thermal Engineering, 129, 1171–1180

[63] Wu Q., Ren H., Gao W., Weng P., Ren J. 2018. “Design and operation optimization of organic Rankine cycle coupled trigeneration systems”, Energy 142, 666-677

[64] Alsharif M. H., Jahid A., Kannadasan R., Kim M. 2024. “Unleashing the potential of sixth generation (6G) wireless networks in smart energy grid management: A comprehensive review”, Energy Reports, 11, 1376–1398

[65] Mohammadi K., Khanmohammadi S., Khorasanizadeh H., Powell K. 2020. “A comprehensive review of solar only and hybrid solar driven multigeneration systems: Classifications, benefits, design and prospective”, Applied Energy 268, 114940

[66] Lykas P., Georgousis N., Bellos E., Tzivanidis C. 2023 “A comprehensive review of solar-driven multigeneration systems with hydrogen production”, International Journal of Hydrogen Energy 48, 2, 437-477

[67] Mukhtar M., Adebayo V., Yimen N., Bamisile O., Osei-Mensah E., Adun H., Zhang Q. and Luo G. “Towards Global Cleaner Energy and Hydrogen Production: A Review and Application ORC Integrality with Multigeneration Systems”, Sustainability 2022, 14(9), 5415

[68] Hassan A. A., Elwardany A., Ookawara S., Ahmed M., El-Sharkawy I. I. 2020. “Integrated adsorption-based multigeneration systems: A critical review and future trends”, International Journal of Refrigeration 116, 129-145

[69] Tiktas A. (2024) Güneş enerjisi, organik Rankine çevrimi ve absorpsiyon etkisi destekli özgün bir kojenerasyon sistemin tasarımı, simülasyonu ve performans değerlendirmesi, Doctorate Thesis, Ege University, Izmir, Turkey, 65-70

[70] Arslan M., Yilmaz C. 2024. Development of models for green hydrogen production of Turkey geothermal Resources: A case study demonstration of thermodynamics and thermoeconomics analyses, 359, 130430

[71] Rahbari H. R., Mandø M., Arabkoohsar A. 2023. “A review study of various High-Temperature thermodynamic cycles for multigeneration applications”, Sustainable Energy Technologies and Assessments 57, 103286

[72] Olsen D., Abdelouadoud Y., Liem P., Wellig B. 2017. “The Role of Pinch Analysis for Industrial ORC Integration”, Energy Procedia, 129, September 2017, 74-81

[73] Mahmoudan A., Esmaeilion F.,Hoseinzadeh S., Soltani M., Ahmadi P. , Rosen M. (2022) A geothermal and solar-based multigeneration system integrated with a TEG unit: Development, 3E analyses, and multi-objective optimization, Applied Energy, 308, 118399

[74] Ozbay H., Karafil A. (2019) Cost Analysis of PV Power Plant for Bilecik City, Journal of BŞEÜ Physical Sciences, 6, 2

[75] Azizi N., Esmaeilion F., Moosavian S., Yaghoubirad M., Ahmadi A., Aliehyaei M., Soltani M. (2022) Critical review of multigeneration system powered by geothermal energy resource from the energy, exergy, and economic point of views, 4859-4889

[76] Forghani A., Solghar A., Hajabdollahi H. (2024), Optimal design of a multi-generation system based on solar and geothermal energy integrated with multi-effect distillatory, Applied Thermal Engineering, 236 (A), 121381

[77] Almehmadi F., Elattar H., Fouda A., Alqaed S., Alharthi M. and Refaey H. (2022) Towards an Efficient Multi-Generation System Providing Power, Cooling, Heating, and Freshwater for Residential Buildings Operated with Solar-Driven ORC, Appl. Sci., 12(21), 11157

[78] Islam S., Dincer I. (May 2017) Development, analysis and performance assessment of a combined solar and geothermal energy-based integrated system for multigeneration Solar Energy 147(1):328-343

[79] Sen O. and Yilmaz C. (April 2020), Thermodynamic performance analysis of geothermal and solar energy assisted power generation and residential cooling system, International Advanced Researches and Engineering Journal 4(1): 41-47

[80] Şeker, U. Energy, Exergy And Environmental Assessment Of A Novel Multigeneration System Fed By Biomass And Geothermal Energy Sources, A Thesis Master Of Science in Energy Engineering

[81] Buker M. S., Riffat S. B. 2016. "Solar assisted heat pump systems for low temperature water heating applications: A systematic review", Renewable and Sustainable Energy Reviews, 55, 399-413

[82] Maali R., Khir T, Arici M. (2023) Energy and exergy optimization of a combined solar/geothermal organic Rankine cycle power, Journal of Central South University, 30, 3601–3616

[83] Aryanfar Y., El Haj Assad M., Khosravi A., Atiqure R. S. M., Sharma S., A. J. L. García, Alayi R. (2022) Energy, exergy and economic analysis of combined solar ORC-VCC power plant, International Journal of Low-Carbon Technologies, 17, 196–205

[84] Mollahüseyinoğlu O., Onat A., Onar İ. F., Okuyan C. (2005) Gönen ve simav jeotermal ısıtma sistemlerinin karşılaştırılması, Geothermal Energy Seminar

[85] "Atlas Of Solar Energy Potential" [Online]. Available: https://gepa.enerji.gov.tr/mycalculator/pages/10.aspx

[86] Habibzadeha A., Abbasalizadeha M., Mirzaeea I., Jafarmadara S., Shirvanib H. (2023) Thermodynamic evaluation of a novel geothermal and solar-driven multigeneration system for hydrogen and freshwater production, Hydrogen, Fuel Cell & Energy Storage, 10, 51-67

[87] Ghasemi, Sheu E., Tizzanini A., Paci M., Mitsos A. (2014) Hybrid solar–geothermal power generation: Optimal retrofitting, Applied Energy, 131, 158-170

[88] A. Habibzadeh, M. Abbasalizadeh, I. Mirzaee, S. Jafarmadar, H. Shirvani (2023) Thermodynamic Modeling and Analysis of a Solar and Geothermal-driven Multigeneration System Using TiO2 and SiO2 Nanoparticles, Iranian (Iranica) Journal of Energy and Environment 14(2), 127-138

[89] Sharifishourabi M., Dincer I., Mohany A. (2024) Advancing Energy Transition with Novel Biomass-Solar Based Multigeneration Energy System Using Hydrogen and Storage Options for Sustainable Cities, Sustainable Cities and Society, Elsevier, 108, 105457

[90] Capik M., Yılmaz A. O., Çavuşoğlu I. (2012) Present situation and potential role of renewable energy in Turkey, Renewable Energy, 46, 1-13

[91] Toklu E. (2013) Overview of potential and utilization of renewable energy sources in Turkey, Renewable Energy, 50, 456-463

[92] Okonkwo E.C., Adedeji M.J., Abid M., Ratlamwala T. (2019) Thermodynamic analysis of energy storage supported multigeneration system, Energy Storage, 1-33

[93] Sabbaghi M., Soltani M., Rosen M. A. (2024) A comprehensive 6E analysis of a novel multigeneration system powered by solar-biomass energies, Energy, 297, 131209

[94] Zhang Y., Aldosky A. J., Goyal V., Meqdad M. N., Nutakki T. U. K., Alsenani T. R., Nguyen V. N., Dahari M., Nguyen P., Ali H. E. (2024) A machine learning study on a municipal solid waste-to-energy system for environmental sustainability in a multi-generation energy system for hydrogen production, Process Safety and Environmental Protection, 182, 1171-1184

[95] Ghiyami M., Bahramian A., Sedae B. (2024) Development and performance assessment of a novel multigeneration clean energy system based on biomass-LNG using a dynamic model and supervised learning algorithms, International Journal of Hydrogen Energy, 66, 10-23

[96] Assareh E., Asl S. S. M., Ahmadinejad M., Parvaz M., Ghodrat M. (2024) Optimization of a solar energy system integrating cooling, hot water, and power units in Australian cities: A climate-based analysis and cost-efficiency investigation, International Journal of Hydrogen Energy, 49, Part C, 353-375

[97] Sami S., Gholizadeh M., Deymi-Dashtebayaz M. (2024) An applicable multi-generation system for different climates from energy, exergy, exergoeconomic,

economic, and environmental (5E) perspectives, Sustainable Cities and Society, 100, 105057

[98] Sharifishourabi M., Dincer I., Mohany A. (2024) Advancing energy transition with novel biomass-solar based multigeneration energy system using hydrogen and storage options for sustainable cities, Sustainable Cities and Society, 108, 105457

[99] Meke A. S., Dincer I. (2024) Design and assessment of a novel solar-based sustainable energy system with energy storage, Journal of Energy Storage, 88

[100] Bamisile O., Cai D., Adedeji M., Dagbasi M., Hu Y., Huang Q. (2024) Environmental impact and thermodynamic comparative optimization of CO2-based multi-energy systems powered with geothermal energy, Science of The Total Environment, 908, 168459

[101] El-Emam R. S., Constantin A., Bhattacharyya R., Ishaq H., Ricotti M. E. (2024) Nuclear and renewables in multipurpose integrated energy systems: A critical review, Renewable and Sustainable Energy Reviews, 192, 114157

[102] Taheri M. H., Seker U., Akkurt G. G., Mohammadpourfard M. (2024) Design, evaluation, and optimization of an integrated proton exchange membrane and double flash geothermal based organic Rankine cycle multi-generation system fed by a biomass-fueled gasifier, Sustainable Cities and Society, 101, 105126

[103] Pang T., Gao L., Wu W., Chi F. (2024) Eco-friendly multi-heat recovery applied to an innovative integration of flue gas-driven multigeneration process and geothermal power plant: Feasibility characterization from thermo-economic-environmental aspect, Journal of Cleaner Production, 449, 141750

[104] Bahrami A., Soltanifar F., Fallahi P., Meschi S. S. And Sohani A. (2024) Energy and Economic Advantages of Using Solar Stills for Renewable Energy-Based Multi-Generation of Power and Hydrogen for Residential Buildings, Buildings, 14(4), 1041

[105] Cai D., Acen C., Hu Y., Adedeji M., Dagbasi M., Staffell I., Bamisile O. (2024) Cost and thermodynamic analysis of wind-hydrogen production via multi-energy systems, Energy Conversion and Management, 306, 118286

[106] Ding X., Yang L., Zheng N., Duan L., Zhou Y. (2024) Dynamic response characteristics and economic analyses of two solar-assisted multi-generation systems, Applied Thermal Engineering, 241, 122339

[107] Sabbaghi M. A., Sefid M. (2024) Risk, sensitive analysis, and optimization of a new multi-generation system activated by solar and biomass energies, Energy Reports, 11, 1006-1018

[108] Shabani M. J., Babaelahi M. (2024) Innovative solar-based multi-generation system for sustainable power generation, desalination, hydrogen production, and refrigeration in a novel configuration, International Journal of Hydrogen Energy, 59, 1115-1131

[109] Zahedi R., Yousefi H., Aslani A., Ahmadi R. (2024) Numerical analysis of water, energy, and environment in the hybrid thermal and solar multigeneration power plants, Energy Sci. Eng., 1–15

[110] Forghani A. H., Solghar A. A., Hajabdollahi H. (2024) Optimal design of a multi-generation system based on solar and geothermal energy integrated with multi-effect distillatory, Applied Thermal Engineering, 236, Part A, 121381

[111] Yan M., Zhang Y., Chauhan B. S., Siddiqui M. R., Albani A., Tian R. A comprehensive thermo-economic-environmental study of an eco-friendly process incorporated with a natural gas-fed combined power plant for a novel multigeneration application, Journal of Cleaner Production, 434, 139959

[112] Zhu C., Wang M., Guo M., Deng J., Du Q., Wei W., Zhang Y., Talesh S. S. A. (2024) Optimizing solar-driven multi-generation systems: A cascade heat recovery approach for power, cooling, and freshwater production, Applied Thermal Engineering, 240, 122214

[113] Qing X. (2024) Solar-driven multi-generation system: Thermoeconomic and environmental optimization for power, cooling, and liquefied hydrogen production, Energy, 293, 130409

[114] Prajapati M., Shah M. (2024) Geothermal-solar hybrid systems for hydrogen production: A systematic review, International Journal of Hydrogen Energy, 67, 842-851

[115] Zheng J. (2024) Integrated renewable-based multi-generation system with environmental and economic optimization, Energy, 294, 130762

[116] Oluah C. K., Kerr S., Maroto-Valer M. M. (2024) Applicable models for upscaling of smart local energy systems: An overview, Smart Energy, 13, 100133

[117] Gao J., Zhang Y., Li X., Zhou X., Kilburn Z. J. (2024) Thermodynamic and thermoeconomic analysis and optimization of a renewable-based hybrid system for power, hydrogen, and freshwater production, Energy, 295, 131002

[118] Wu Y., Xu Y. (2024) A comprehensive evaluation of an environmentally friendly multi-heat recovery system using biogas energy source from thermodynamic, economic, and environmental perspectives, Journal of Environmental Chemical Engineering, 12, Issue 3, 112783

[119] Tchanche B. F., Papadakis G., Lambrinos G., Frangoudakis A., Fluid selection for a low-temperature solar organic Rankine cycle, (2009) Applied Thermal Engineering, vol. 29, issues 11–12, pp. 2468-2476

[120] Bao J., Zhao L. (2013) A review of working fluid and expander selections for organic Rankine cycle, Renewable and Sustainable Energy Reviews, vol. 24, 325-342

[121] Wang S., Liu C., Li Q., Liu L., Huo E. , Zhang C. (2020) Selection principle of working fluid for organic Rankine cycle based on environmental benefits and economic performance, Applied Thermal Engineering, vol. 178, 115598

[122] Braimakis K., Roumpedakis T. C., Leontaritis A. D., Karellas S. (2017) Comparison of Environmentally Friendly Working Fluids for Organic Rankine Cycles Chapter by Advances in New Heat Transfer Fluids, CRC Press, p. 50

[123] El-Sadi H. (2018) Using engineering equation solver (EES) to solve engineering problems in mechanical engineering, Proceedings of the ASME 2018 International Mechanical Engineering Congress and Exposition, vol. 5, Engineering Education, Pittsburgh, USA, November 9–15, 2018, V005T07A040

[124] Zhao P. (2015) A Computer Program for the Exergoeconomic Analysis of Energy Conversion Plants, Technische Universitaet Berlin (Germany), ProQuest Dissertations & Theses, 27610468

[125] Swat S. (2021) Introduction to the simulation of power plants for EBSILON® Professional Version 15, Google books

[126] Świerzewski M., Kalina J. (2019) Modelling of commercial biomass-fired orc system using ebsilon professional® software, 5th International Seminar on ORC Power Systems, September 9 - 11, 2019, Athens, Greece

[127] Hassboun T., El Bahır L., Aite Driss Y., El Adnani Mustapha (2016) Solar irradiation estimator based on a self-calibrated reference solar cell, Turkish Journal of Electrical Engineering and Computer Sciences, vol. 24, no. 6, article 26

[128] Somayaji, C, Mago, PJ, & Chamra, LM. (2006) Second law analysis and optimization of organic rankine cycle, Proceedings of the ASME 2006 Power Conference,. Atlanta, Georgia, USA. May 2–4, 2006. pp. 591-596

[129] Hai T., El-Shafay A. S., Chaturvedi R., Marjan R. K., Almujibah H., Rajab H., Almojil S. F., Almohana A. I. (2024) Quantitative assessment of hydrogen blending in a gas turbine-based plant for supplying residential electricity, water, and cooling load: A techno-economic-environmental optimization, Process Safety and Environmental Protection, 184, 428-444

[130] Wang D., Ali M. A., Alizadeh A., Singh P. K., Almojil S. F., Alali A. F., Almoalimi K. T., Almohana A. I. (2024) Thermoeconomic appraisal of a novel power and hydrogen cogeneration plant with integration of biomass and geothermal energies, International Journal of Hydrogen Energy, 52, Part C, 385-400

[131] Korpeh M., Asadbagi P., Afshari R., Rashidi A., Lotfollahi A. (2024) A comprehensive analysis and multi-objective optimization of a sustainable production system based on renewable energies, Applied Thermal Engineering, 242

[132] Dehghan M., Akbari G., Montazerin N., Maroufi A. (2024) Energetic/exergetic study of Kalina and refrigeration bottoming cycles on different solar‐driven organicRankine cycles, Energy Sci. Eng., 12, 1614–1637

[133] Zhang X., Cao M., Yang X., Guo H. and Wang J. (2019) Economic Analysis of Organic Rankine Cycle Using R123 and R245fa as Working Fluids and a Demonstration Project Report, Appl. Sci., 9, 288

[134] Küçük E. Ö. (2022) Organik Rankin Çevriminin Termodinamik Analizi Ve Termoekonomik Optimizasyonu, Doctorate Thesis, Bursa Uludag University

[135] Akkurt, F. (2024). Exergoeconomic Analysis of a Solar-Geothermal Hybrid Organic Rankine System. *Scientia Iranica*, doi: 10.24200/sci.2024.63354.8352

[136] Wang Y., Shi L., Song M., Jia M., Li B. (2024) Evaluating the energy-exergy-economy-environment performance of the biomass-photovoltaic-hydrogen integrated energy system based on hybrid multi-criterion decision-making model, Renewable Energy, 224, 120220

[137] Yang M. H., Yeh R. H. (2015) Thermo-economic optimization of an organic Rankine cycle system for large marine diesel engine waste heat recovery, Energy 82, 256-268

[138] Turton R, Bailie RC, Whiting WB. Analysis, synthesis and design of chemical processes. 4th ed. New Jersey: Prentice Hall PTR; 2013.

[139] Newnan D. G., Eschenbach T. G., Lavelle J. P., Engineering economic analysis, Oxford University Press, 2004

[140] Farr J. V., Faber I. J., Engineering Economics of Life Cycle Cost Analysis, CRC Press, 2018

[141] Sciubba E. (2004) From Engineering Economics to Extended Exergy Accounting: A Possible Path from Monetary to Resource-Based Costing, Journal of Industrial Ecology, vol. 8, Issue 4, 1-226

APPENDIX A

A.1 EES coding for energetic thermodynamic analysis of the system with R507A

```
m_dot=3,4[kg/s]
n_pump=0,8
P1=13[bar]
P[1]=13[bar]
T1=25,514+273
T[1]=25,514+273
h1=enthalpy(R507A;T=T1;P=P1)
s1=entropy(R507A;T=T1;P=P1)
s[1]=entropy(R507A;T=T1;P=P1)
v[1]=volume(R507A;T=T1;P=P1)

P2=35[bar]
P[2]=35[bar]
h2_s=enthalpy(R507A;s=s1;P=P2)
h2_a=((h2_s-h1)/n_pump)+h1
s2_a=entropy(R507A;h=h2_a;P=P2)
s[2]=entropy(R507A;h=h2_a;P=P2)
T[2]=temperature(R507A;P=P2;h=h2_a)
v[2]=volume(R507A;h=h2_a;P=P2)

T3=77,748+273
T[3]=77,748+273
P[3]=P2
h3=enthalpy(R507A;T=T3;P=P2)
s3=entropy(R507A;T=T3;P=P2)
s[3]=entropy(R507A;T=T3;P=P2)
v[3]=volume(R507A;T=T3;P=P2)

T4=81,331+273

T[4]=81,331+273

Q_solar=22,795[kW]
h4=((Q_solar/m_dot)+h3)
P[4]=P2
s4=entropy(R507A;T=T4;P=P2)
s[4]=entropy(R507A;T=T4;P=P2)
h4=enthalpy(R507A;T=T4;P=P2)
v[4]=volume(R507A;T=T4;P=P2)

P[5]=P1
h5=enthalpy(R507A;s=s4;P=P1)
s[5]=s4
```

T[5]=temperature(R507A;P=P1;s=s4)
v[5]=volume(R507A;s=s4;P=P1)

m_hot=8,3[kg/s]
T6=367[K]
P6=2,13[bar]

h6=enthalpy(Water;T=T6;P=P6)
s6=entropy(Water;T=T6;P=P6)

T7=351,943[K]
s7=entropy(Water;T=T7;P=P6)
h7=enthalpy(Water;T=T7;P=P6)
x_hot=m_hot*((h6-h7)-(T_0*(s6-s7)))
Q_jeo=m_hot*(h6-h7)
x_heat_67=(1-(T_0/T_h_1))*Q_jeo
x_heat_solar=(1-(T_0/T_h_2))*Qin_34
x_expended=x_heat_67+x_heat_solar+W_in
x_kazanilan=W_out
n_sec=(x_kazanilan)/(x_expended)

W_out=m_dot*(h4-h5)
wout=(h4-h5)
Q_out=m_dot*(h5-h1)
qout51=(h5-h1)
W_in=m_dot*(h2_a-h1)
win=(h2_a-h1)
Qin_23=m_dot*(h3-h2_a)

qin23=h3-h2_a
Qin_34=m_dot*(h4-h3)
qin34=h4-h3
Q_in=Qin_23+Qin_34
n_th=(W_out-W_in)/(Q_in)
T_0=293[K]
T_h_1=367[K]

A.2 EES coding for exergetic thermodynamic analysis of multigenerational system with R507A

x_mass_23=((h2_a-h3)-(T_0*(s2_a-s3)))
x_heat_23=(1-(T_0/T_h_1))*qin23
x_dest23=x_heat_23+x_mass_23
x_dest_23=T_0*(s3-s2_a-(qin23/T_h_1))
T_h_2=390[K]
x_mass_34=((h3-h4)-(T_0*(s3-s4)))
x_heat_34=(1-(T_0/T_h_2))*qin34
x_dest34=x_heat_34+x_mass_34
x_dest_34=T_0*(s4-s3-(qin34/T_h_2))

T_l=293[K]
x_mass_51=((h5-h1)-(T_0*(s4-s1)))
x_heat_51=(1-(T_0/T_l))*qout51
x_dest51=x_mass_51-x_heat_51
x_exp=x_heat_23+x_heat_34+win
x_recovered=wout

n_ii=(x_recovered)/(x_exp)
n_ii_jeo=((m_dot*(((h3-h2_a)-(T_0*(s3-s2_a)))))/((m_hot*((h6-h7)-(T_0*(s6-s7))))))

A.3 EES coding for energetic thermodynamic analysis of the system with R1234yf

m_dot=5.5[kg/s]
n_pump=0.8
P1=6.8[bar]
P[1]=6.8[bar]
T1=24.865+273
T[1]=24.865+273
h1=enthalpy(*R1234yf*,*T*=T1,*P*=P1)
s1=entropy(*R1234yf*,*T*=T1,*P*=P1)
s[1]=entropy(*R1234yf*,*T*=T1,*P*=P1),
v[1]=volume(*R1234yf*,*T*=T1,*P*=P1)

P2=29[bar]
P[2]=29[bar]
h2_s=enthalpy(*R1234yf*,*s*=s1,*P*=P2)
h2_a=((h2_s-h1)/n_pump)+h1
s2_a=entropy(*R1234yf*,*h*=h2_a,*P*=P2)
T2=temperature(*R1234yf*,*P*=P2,*h*=h2_a)
T[2]=temperature(*R1234yf*,*P*=P2,*h*=h2_a)
s[2]=s2_a
v[2]=volume(*R1234yf*,*s*=s2_a,*P*=P2)

P[3]=P2
P[4]=P2
T3=79.405+273 [K]
T[3]=79.405+273 [K]
h3=enthalpy(*R1234yf*,*T*=T3,*P*=P2)
s3=entropy(*R1234yf*,*T*=T3,*P*=P2)
s[3]=entropy(*R1234yf*,*T*=T3,*P*=P2)
v[3]=volume(*R1234yf*,*T*=T3,*P*=P2)
T4=95+273[K]
T[4]=95+273[K]

Q_solar=538,729[kW]
h4=((Q_solar/m_dot)+h3)
s4=entropy(*R1234yf*,*T*=T4,*P*=P2)
s[4]=entropy(*R1234yf*,*T*=T4,*P*=P2)
h4=enthalpy(*R1234yf*,*T*=T4,*P*=P2)

```
v[4]=volume(R1234yf,T=T4,P=P2)
h5=enthalpy(R1234yf,s=s4,P=P1)
s[5]=s4
T5=temperature(R1234yf,P=P1,s=s4)
T[5]=temperature(R1234yf,P=P1,s=s4)

v[5]=volume(R1234yf,s=s4,P=P1)
P[5]=P1
W_out=m_dot*(h4-h5)
Q_out=m_dot*(h5-h1)
qout51=(h5-h1)
W_in=m_dot*(h2_a-h1)
Qin_23=m_dot*(h3-h2_a)
qin23=h3-h2_a
Qin_34=m_dot*(h4-h3)
qin34=h4-h3
Q_in=Qin_23+Qin_34
n_th=(W_out-W_in)/(Q_in)
T_0=298[K]
T_h_1=367[K]
```

A.4 EES coding for exergetic thermodynamic analysis of multigenerational system with R1234yf

```
x_mass_23=((h2_a-h3)-(T_0*(s2_a-s3)))
x_heat_23=(1-(T_0/T_h_1))*qin23
x_dest23=x_heat_23+x_mass_23
x_dest_23=T_0*(s3-s2_a-(qin23/T_h_1))
T_h_2=408[K]

x_mass_34=((h3-h4)-(T_0*(s3-s4)))
x_heat_34=(1-(T_0/T_h_2))*qin34

x_dest34=x_heat_34+x_mass_34
x_dest_34=T_0*(s4-s3-(qin34/T_h_2))
T_l=293[K]
x_mass_51=((h5-h1)-(T_0*(s4-s1)))
x_heat_51=(1-(T_0/T_l))*qout51
x_dest51=x_mass_51-x_heat_51
x_dest_51=T_0*(s1-s4+(qout51/T_l))
win=(h2_a-h1)
wout=(h4-h5)
x_exp=x_heat_23+x_heat_34+win
x_recovered=wout
n_ii=(x_recovered)/(x_exp)
```

A.5 EES coding for energetic thermodynamic analysis of the system with R245fa

```
m_dot=4[kg/s]
n_pump=0,8
P1=1,5[bar]
P[1]=1,5[bar]
T1=25,317+273

T[1]=25,317+273
h1=enthalpy(R245fa;T=T1;P=P1)
s1=entropy(R245fa;T=T1;P=P1)
s[1]=entropy(R245fa;T=T1;P=P1)
v[1]=volume(R245fa;T=T1;P=P1)

P2=16[bar]
P[2]=16[bar]
h2_s=enthalpy(R245fa;s=s1;P=P2)
h2_a=((h2_s-h1)/n_pump)+h1
s2_a=entropy(R245fa;h=h2_a;P=P2)
s[2]=entropy(R245fa;h=h2_a;P=P2)

T[2]=temperature(R245fa;P=P2;h=h2_a)
T2=temperature(R245fa;P=P2;h=h2_a)
v[2]=volume(R245fa;h=h2_a;P=P2)

T3=82,301+273
T[3]=82,301+273
P[3]=P2
h3=enthalpy(R245fa;T=T3;P=P2)
s3=entropy(R245fa;T=T3;P=P2)
s[3]=entropy(R245fa;T=T3;P=P2)
v[3]=volume(R245fa;T=T3;P=P2)

 Q_solar=686,637[kW]
h4=((Q_solar/m_dot)+h3)
T4=113,670+273
T[4]=113,670+273
P[4]=P2
s4=entropy(R245fa;T=T4;P=P2)
s[4]=entropy(R245fa;T=T4;P=P2)
h4=enthalpy(R245fa;T=T4;P=P2)
v[4]=volume(R245fa;T=T4;P=P2)

P[5]=P1
h5=enthalpy(R245fa;s=s4;P=P1)
s[5]=s4
T[5]=temperature(R245fa;P=P1;s=s4)
T5=temperature(R245fa;P=P1;s=s4)
v[5]=volume(R245fa;s=s4;P=P1)

m_hot=8,3[kg/s]
```

```
T6=367[K]
P6=2,13[bar]
h6=enthalpy(Water;T=T6;P=P6)
s6=entropy(Water;T=T6;P=P6)

T7=358,02[K]

s7=entropy(Water;T=T7;P=P6)
h7=enthalpy(Water;T=T7;P=P6)

x_hot=m_hot*((h6-h7)-(T_0*(s6-s7)))
Q_jeo=m_hot*(h6-h7)
x_heat_67=(1-(T_0/T_h_1))*Q_jeo
x_heat34=(1-(T_0/T_h_2))*Qin_34
x_expended=x_heat_67+x_heat34+W_in
x_kazanilan=W_out
n_sec=(x_kazanilan)/(x_expended)

W_out=m_dot*(h4-h5)
wout=(h4-h5)
Q_out=m_dot*(h5-h1)
qout51=(h5-h1)
W_in=m_dot*(h2_a-h1)
win=(h2_a-h1)
Qin_23=m_dot*(h3-h2_a)
qin23=h3-h2_a
Qin_34=m_dot*(h4-h3)
qin34=h4-h3
Q_in=Qin_23+Qin_34
n_th=(W_out-W_in)/(Q_in)
T_0=293[K]
T_h_1=367[K]
```

A.6 EES coding for exergetic thermodynamic analysis of multigenerational system with R245fa

```
x_mass_23=((h2_a-h3)-(T_0*(s2_a-s3)))
x_heat_23=(1-(T_0/T_h_1))*qin23
x_dest23=x_heat_23+x_mass_23
x_dest_23=T_0*(s3-s2_a-(qin23/T_h_1))
T_h_2=448[K]

x_mass_34=((h3-h4)-(T_0*(s3-s4)))
x_heat_34=(1-(T_0/T_h_2))*qin34
x_dest34=x_heat_34+x_mass_34
x_dest_34=T_0*(s4-s3-(qin34/T_h_2))

T_l=293[K]
x_mass_51=((h5-h1)-(T_0*(s4-s1)))
x_heat_51=(1-(T_0/T_l))*qout51
x_dest51=x_mass_51-x_heat_51
x_exp=x_heat_23+x_heat_34+win
```

```
x_recovered=wout
n_ii=(x_recovered)/(x_exp)
```

A.7 EES coding for energetic thermodynamic analysis of the system with R1233zd

```
m_dot=3[kg/s]
P1=1,3[bar]
T1=25,075+273
h1=enthalpy(R1233zd(E);T=T1;P=P1)
s1=entropy(R1233zd(E);T=T1;P=P1)
P2=19[bar]
h2=enthalpy(R1233zd(E);s=s1;P=P2)
T3=80,783+273
h3=enthalpy(R1233zd(E);T=T3;P=P2)
s3=entropy(R1233zd(E);T=T3;P=P2)

Q_solar=610,623[kW]
h4=((Q_solar/m_dot)+h3)
T4=146,452+273
s4=entropy(R1233zd(E);T=T4;P=P2)
h4=enthalpy(R1233zd(E);T=T4;P=P2)
h5=enthalpy(R1233zd(E);s=s4;P=P1)
W_out=m_dot*(h4-h5)
Q_out=m_dot*(h5-h1)
qout51=(h5-h1)

W_in=m_dot*(h2-h1)
Qin_23=m_dot*(h3-h2)
qin23=h3-h2
Qin_34=m_dot*(h4-h3)
qin34=h4-h3

Q_in=Qin_23+Qin_34
n_th=(W_out-W_in)/(Q_in)
T_0=298[K]
T_h_1=383[K]
```

A.8 EES coding for exergetic thermodynamic analysis of multigenerational system with R1233zd

```
x_mass_34=((h3-h4)-(T_0*(s3-s4)))
x_heat_34=(1-(T_0/T_h_2))*qin34
x_dest34=x_heat_34+x_mass_34
x_dest_34=T_0*(s4-s3-(qin34/T_h_2))
T_l=T_0

x_mass_51=((h5-h1)-(T_0*(s4-s1)))
x_heat_51=(1-(T_0/T_l))*qout51
x_dest51=x_mass_51-x_heat_51
x_dest_51=T_0*(s1-s4+(qout51/T_l))
```

A.9 EES coding for energetic thermodynamic analysis of the system with R1234ze

```
m_dot=4[kg/s]
n_pump=0,8

P1=4,5[bar]
P[1]=1,009[bar]
T1=21,656+273[K]
T[1]=21,656+273[K]
h1=229,177[kJ/kg]
s1=1,1021[(kJ)/(kg*K)]
P2=20[bar]
P[2]=20[bar]

h2_a=230,830[kJ/kg]
s2=1,1032[(kJ)/(kg*K)]
s[2]=1,1032
T2=22,680+273[K]
T[2]=22,680+273[K]
Q_in_1=464,575[kW]
h3=346,974[kJ/kg]
T3=79,823+273[K]
s3=1,4535[(kJ)/(kg*K)]
Q_in_2=439,800[kW]
h4=456,924[kJ/kg]
s[4]=1,7626[(kJ)/(kg*K)]
s[5]=s4
h5=425,052[kJ/kg]

W_out=m_dot*(h4-h5)
Q_out=m_dot*(h5-h1)
W_in=m_dot*(h2_a-h1)
Qin_23=m_dot*(h3-h2_a)
Qin_34=m_dot*(h4-h3)
Q_in=Qin_23+Qin_34
n_th=(W_out-W_in)/(Q_in)
T_0=293[K]
T_h_1=367[K]
T_h_2=398[K]
```

A.10 EES coding for exergetic thermodynamic analysis of multigenerational system with R1234ze

```
x_heat_23=(1-(T_0/T_h_1))*Qin_23
x_heat_34=(1-(T_0/T_h_2))*Qin_34
x_exp=x_heat_23+x_heat_34+W_in
x_recovered=W_out
n_ii=(x_recovered)/(x_exp)
x_mass_34=((h3-h4)-(T_0*(s3-s4)))
x_dest34=x_heat_34+x_mass_34
```

```
x_dest_34=T_0*(s4-s3-(qin34/T_h_2))
T_l=T_0

x_mass_51=((h5-h1)-(T_0*(s4-s1)))
x_heat_51=(1-(T_0/T_l))*qout51
x_dest51=x_mass_51-x_heat_51
x_dest_51=T_0*(s1-s4+(qout51/T_l))
```

A.11 EES coding for energetic thermodynamic analysis of the system with R152A

```
m_dot=2[kg/s]
n_pump=0,8
P1=5,4[bar]
P[1]=5,4[bar]
T1=21,686+273[K]
T[1]=21,686+273[K]
h1=enthalpy(R152a;T=T1;P=P1)
s1=entropy(R152a;T=T1;P=P1)
P2=24[bar]
P[2]=24[bar]
h2_s=enthalpy(R152a;s=s1;P=P2)
h2_a=((h2_s-h1)/(n_pump))+h1
s2=entropy(R152a;h=h2_a;P=P2)
s[2]=entropy(R152a;h=h2_a;P=P2)
T2=temperature(R152a;P=P2;h=h2_a)
T[2]=temperature(R152a;P=P2;h=h2_a)
Q_in_1=404,233[kW]
h3=(Q_in_1/m_dot)+h2_a
T3=temperature(R152a;P=P2;h=h3)
s3=entropy(R152a;h=h3;P=P2)
s[3]=entropy(R152a;h=h3;P=P2)
Q_in_2=311,278[kW]
h4=(Q_in_2/m_dot)+h3
s4=entropy(R152a;h=h4;P=P2)
s[4]=entropy(R152a;h=h4;P=P2)
s5=s4

s[5]=s4
h5=enthalpy(R152a;s=s4;P=P1)

W_out=m_dot*(h4-h5)
Q_out=m_dot*(h5-h1)
W_in=m_dot*(h2_a-h1)
Qin_23=m_dot*(h3-h2_a)
Qin_34=m_dot*(h4-h3)
Q_in=Qin_23+Qin_34
n_th=(W_out-W_in)/(Q_in)
T_0=293[K]
T_h_1=367[K]
T_h_2=404[K]
```

A.12 EES coding for exergetic thermodynamic analysis of multigenerational system with R152A

```
x_heat_23=(1-(T_0/T_h_1))*Qin_23
x_heat_34=(1-(T_0/T_h_2))*Qin_34
x_exp=x_heat_23+x_heat_34+W_in
x_recovered=W_out

n_ii=(x_recovered)/(x_exp)

x_mass_34=((h3-h4)-(T_0*(s3-s4)))
x_dest34=x_heat_34+x_mass_34
x_dest_34=T_0*(s4-s3-(qin34/T_h_2))
T_l=T_0
x_mass_51=((h5-h1)-(T_0*(s4-s1)))
x_heat_51=(1-(T_0/T_l))*qout51
x_dest51=x_mass_51-x_heat_51
x_dest_51=T_0*(s1-s4+(qout51/T_l))
```

A.13 EES coding for energetic thermodynamic analysis of the system with R245CA

```
m_dot=3[kg/s]
n_pump=0,8
P1=1,009[bar]

P[1]=1,009[bar]
T1=25,153+273[K]
T[1]=25,153+273[K]
h1=234,281[kJ/kg]
s1=1,1199
P2=13,051[bar]
P[2]=13,051[bar]
h2_a=235,366[kJ/kg]
s2=1,1206[(kJ)/(kg*K)]
s[2]=1,1206
T2=25,650+273[K]
T[2]=25,650+273[K]
Q_in_1=256,537[kW]
h3=320,878[kJ/kg]
T3=85,368+273[K]
s3=1,381[(kJ)/(kg*K)]
Q_in_2=572,960[kW]
h4=511,865[kJ/kg]
s4=1,878[(kJ)/(kg*K)]
s5=s4
s[5]=s4
h5=461,250[kJ/kg]

W_out=m_dot*(h4-h5)
```

```
Q_out=m_dot*(h5-h1)
W_in=m_dot*(h2_a-h1)
Qin_23=m_dot*(h3-h2_a)

Qin_34=m_dot*(h4-h3)
Q_in=Qin_23+Qin_34
n_th=(W_out-W_in)/(Q_in)
T_0=293[K]
T_h_1=367[K]
T_h_2=417[K]
```

A.14 EES coding for exergetic thermodynamic analysis of multigenerational system with R245CA

```
x_heat_23=(1-(T_0/T_h_1))*Qin_23
x_heat_34=(1-(T_0/T_h_2))*Qin_34
x_exp=x_heat_23+x_heat_34+W_in
x_recovered=W_out
n_ii=(x_recovered)/(x_exp)
x_mass_34=((h3-h4)-(T_0*(s3-s4)))
x_dest34=x_heat_34+x_mass_34
x_dest_34=T_0*(s4-s3-(qin34/T_h_2))
T_l=T_0
x_mass_51=((h5-h1)-(T_0*(s4-s1)))
x_heat_51=(1-(T_0/T_l))*qout51
x_dest51=x_mass_51-x_heat_51
x_dest_51=T_0*(s1-s4+(qout51/T_l))
```

A.15 EES coding for cost analysis of multigenerational system with R245fa

```
Cp_t=10^((2,7051)+(1,4398*(log10(W_out)))-(0,1776*((log10(W_out))^2)))
Bare_t=Cp_t*(3,4*(0,90625))
M_turbine= (Bare_t/341635,5165)*80500[$]
Cp_p=10^(3,3892+(0,0536*(log10(W_in)))+(0,1538*((log10(W_in))^2)))
Bare_p=Cp_p*(1,89+(1,35*1,6*9,66667))
M_pump=(Bare_p/73913,6084)*17500[$]

p=0,185[$/(kW*h)]
t_s=24[h]
M_electricity=(W_out-W_in)(p)(t_s)*(360)[$]
M_condenser=(700)*(Q_out/828)
M_geothermal=(700)*(Qin_23/313,366)
M_solar=(3000)*(Qin_34/686,637)
M_collector=(350000)*(Qin_34/686,637)
M_initial_investment=M_turbine+M_pump+M_condenser+M_geothermal+M_sol
ar+M_collector
M_install=0,1*M_initial_investment
M_total=M_install+M_initial_investment
```

A.16 EES coding for cost analysis of multigenerational system with R1234yf

```
Cp_t=10^((2,7051)+(1,4398*(log10(W_out)))-(0,1776*((log10(W_out))^2)))
Bare_t=Cp_t*(3,4*(0,7655))
M_turbine= (Bare_t/341635,5165)*80500[$]
```

Cp_p=10^(3,3892+(0,0536*(log10(W_in)))+(0,1538*((log10(W_in))^2)))
Bare_p=Cp_p*(1,89+(1,35*1,6*3,265))
M_pump=(Bare_p/73913,6084)*17500[$]
p=0,185[$/(kW*h)]
t_s=24[h]
M_electricity=(W_out-W_in)*(p)*(t_s)*(360)[$]
M_condenser=(700)*(Q_out/828)
M_geothermal=(700)*(Qin_23/313,366)
M_solar=(3000)*(Qin_34/686,637)
M_collector=(350000)*(Qin_34/686,637)
M_initial_investment=M_turbine+M_pump+M_condenser+M_geothermal+M_solar+M_collector
M_install=0,1*M_initial_investment
M_total=M_install+M_initial_investment

A.17 EES coding for cost analysis of multigenerational system with R507A

Cp_t=10^((2,7051)+(1,4398*(log10(W_out)))-(0,1776*((log10(W_out))^2)))
Bare_t=Cp_t*(3,4*(0,63))
M_turbine= (Bare_t/341635,5165)*80500[$]

Cp_p=10^(3,3892+(0,0536*(log10(W_in)))+(0,1538*((log10(W_in))^2)))
Bare_p=Cp_p*(1,89+(1,35*1,6*1,69))
M_pump=(Bare_p/73913,6084)*17500[$]
p=0,185[$/(kW*h)]
t_s=24[h]
M_electricity=(W_out-W_in)(p)(t_s)*(360)[$]
M_condenser=(700)*(Q_out/828)
M_geothermal=(700)*(Qin_23/313,366)
M_solar=(3000)*(Qin_34/686,637)
M_collector=(350000)*(Qin_34/686,637)
M_initial_investment=M_turbine+M_pump+M_condenser+M_geothermal+M_solar+M_collector

M_install=0,1*M_initial_investment
M_total=M_install+M_initial_investment

A.18 EES coding for cost analysis of multigenerational system with R1233zd

Cp_t=10^((2,7051)+(1,4398*(log10(W_out)))-(0,1776*((log10(W_out))^2)))
Bare_t=Cp_t*(3,4*(0,9316))
M_turbine= (Bare_t/341635,5165)*80500[$]
Cp_p=10^(3,3892+(0,0536*(log10(W_in)))+(0,1538*((log10(W_in))^2)))
Bare_p=Cp_p*(1,89+(1,35*1,6*13,6154))
M_pump=(Bare_p/73913,6084)*17500[$]
p=0,185[$/(kW*h)]
t_s=24[h]
M_electricity=(W_out-W_in)(p)(t_s)*(360)[$]
M_condenser=(700)*(Q_out/828)
M_geothermal=(700)*(Qin_23/313,366)
M_solar=(3000)*(Qin_34/686,637)
M_collector=(350000)*(Qin_34/686,637)

M_initial_investment=M_turbine+M_pump+M_condenser+M_geothermal+M_sol
ar+M_collector
M_install=0,1*M_initial_investment
M_total=M_install+M_initial_investment

A.19 EES coding for cost analysis of multigenerational system with R152A

Cp_t=10^((2,7051)+(1,4398*(log10(W_out)))-(0,1776*((log10(W_out))^2)))
Bare_t=Cp_t*(3,4*(0,9316))
M_turbine= (Bare_t/341635,5165)*80500[$]
Cp_p=10^(3,3892+(0,0536*(log10(W_in)))+(0,1538*((log10(W_in))^2)))
Bare_p=Cp_p*(1,89+(1,35*1,6*13,6154))
M_pump=(Bare_p/73913,6084)*17500[$]

p=0,185[$/(kW*h)]
t_s=24[h]
M_electricity=(W_out-W_in)(p)(t_s)*(360)[$]
M_condenser=(700)*(Q_out/828)
M_geothermal=(700)*(Qin_23/313,366)

M_solar=(3000)*(Qin_34/686,637)
M_collector=(350000)*(Qin_34/686,637)
M_initial_investment=M_turbine+M_pump+M_condenser+M_geothermal+M_sol
ar+M_collector
M_install=0,1*M_initial_investment
M_total=M_install+M_initial_investment

A.20 EES coding for cost analysis of multigenerational system with R245CA

Cp_t=10^((2,7051)+(1,4398*(log10(W_out)))-(0,1776*((log10(W_out))^2)))
Bare_t=Cp_t*(3,4*(0,9316))
M_turbine= (Bare_t/341635,5165)*80500[$]
Cp_p=10^(3,3892+(0,0536*(log10(W_in)))+(0,1538*((log10(W_in))^2)))
Bare_p=Cp_p*(1,89+(1,35*1,6*13,6154))
M_pump=(Bare_p/73913,6084)*17500[$]
p=0,185[$/(kW*h)]
t_s=24[h]
M_electricity=(W_out-W_in)(p)(t_s)*(360)[$]
M_condenser=(700)*(Q_out/828)
M_geothermal=(700)*(Qin_23/313,366)
M_solar=(3000)*(Qin_34/686,637)
M_collector=(350000)*(Qin_34/686,637)
M_initial_investment=M_turbine+M_pump+M_condenser+M_geothermal+M_sol
ar+M_collector
M_install=0,1*M_initial_investment
M_total=M_install+M_initial_investment

A.21 EES coding for cost analysis of multigenerational system with R1234ze

Cp_t=10^((2,7051)+(1,4398*(log10(W_out)))-(0,1776*((log10(W_out))^2)))
Bare_t=Cp_t*(3,4*(0,9316))
M_turbine= (Bare_t/341635,5165)*80500[$]
Cp_p=10^(3,3892+(0,0536*(log10(W_in)))+(0,1538*((log10(W_in))^2)))
Bare_p=Cp_p*(1,89+(1,35*1,6*13,6154))

M_pump=(Bare_p/73913,6084)*17500[$]
p=0,185[$/(kW*h)]
t_s=24[h]
M_electricity=(W_out-W_in)(p)(t_s)*(360)[$]

M_condenser=(700)*(Q_out/828)
M_geothermal=(700)*(Qin_23/313,366)
M_solar=(3000)*(Qin_34/686,637)
M_collector=(350000)*(Qin_34/686,637)
M_initial_investment=M_turbine+M_pump+M_condenser+M_geothermal+M_solar+M_collector
M_install=0,1*M_initial_investment
M_total=M_install+M_initial_investment

RESUME

Ozlem Boydak graduated from Yıldız Technical University both Mechanical Engineering and Electrical Engineering with double major. She then received her master's degree in Mechanical Engineering from Boğaziçi University, where she studied on the thermal simulation of high-pressure die casting. After five years of work experience in the automotive, manufacturing, and transportation sectors at the companies Ford Otosan, Gedik Holding, and Ulaşım A.Ş., she continues to work as a lecturer at Istanbul Medeniyet University. Her international publications can be listed as follows:

1. Thermodynamic investigation of organic Rankine cycle energy recovery system and recent studies, O Boydak, I Ekmekci, M Yilmaz, H Koten, Thermal science 22 (6 Part A), 2679-2690, 2018.
2. A Thermodynamic Analysis And Comparison Of An Organic Rankine Cycled (ORC) System With Six Different Wet, Dry And Isentropic Working Fluids, O Boydak, I Ekmekçi, M Yilmaz, Journal of New Results in Engineering and Natural Sciences, 1-8, 2022.
3. Environment Friendly Technology: Organic Rankine Cycle (ORC) Energy Recovery System Based On A Eco-Friendly Working Fluid, O Boydak, I Ekmekci, M Yilmaz, H Koten, Advisor In Chief 4, 26, 2018.